GIS METHODS TO IMPLEMENT SEDIMENT BEST MANAGEMENT PRACTICES AND LOCATE EPHEMERAL GULLIES

by

NAGA PRASAD DAGGUPATI

B.S., ANGR AGRICULTURAL UNIVERSITY, 2004
M.S., KANSAS STATE UNIVERSITY, 2007

AN ABSTRACT OF A DISSERTATION

submitted in partial fulfillment of the requirements for the degree

DOCTOR OF PHILOSOPHY

Department of Biological & Agricultural Engineering
College of Engineering

KANSAS STATE UNIVERSITY
Manhattan, Kansas

2012

Abstract

Soil erosion is one of the most important of today's global environmental problems. Over the past few decades, soil conservation practices were implemented to reduce soil erosion in the United States. However, excessive sediment still remains among the most prevalent water quality problems. Agricultural fields and in particular ephemeral gullies (EGs) are considered to be a major contributor of sediment. The overall goal of this study was to improve modeling utility to identify and quantify sources of sediment. Specific objectives were: (1) to develop and demonstrate a method of field-scale targeting using Soil and Water Assessment Tool (SWAT) and to use this method as a targeted, flexible approach to pay explicitly for sediment-yield reductions; (2) to evaluate topographic index models (Slope Area [SA], Compound Topographic Index [CTI], Slope Area Power [SAP] and Wetness Topographic Index [WTI]) and a physical-based model (Overland Flow Turbulent [OFT]) in predicting spatial EG location and lengths.

Black Kettle Creek watershed was the focus of an innovative project to pay for modeled field sediment reductions. An Arc-Geographical Information System (GIS) tool bar was developed that post processed SWAT hydrologic response unit output to field boundaries and prepared maps of high-priority fields by sediment, total nitrogen, and total phosphorus and was demonstrated to be useful for field-scale targeting. Calibrated SWAT model was used to establish baseline sediment yields. Various Best Management Practices (BMPs) were simulated and payments to implement each BMP for a given field were calculated. This study helped to guide determination of appropriate farmer support payments and quantified the important influence of BMP type and site-specific conditions for use in targeting conservation practice funding to achieve maximum soil-loss reductions per dollar spent. Extreme care should be used in selecting the source of spatial model input data when using SWAT for field-level targeting.

Automated geospatial models were developed in a GIS environment to spatially locate and derive length of EGs using topographic index and physical based models. EG predictions were better for the SA model among the four topographic index models tested. Individual calibration of topographic index model threshold for each application site was needed. An OFT model (physical based model), which utilized topography, precipitation, soil, landuse/landcover and SWAT-based runoff estimates, did not need individual site calibration, and may have broader applicability than empirical based models.

GIS METHODS TO IMPLEMENT SEDIMENT BEST MANAGEMENT PRACTICES AND LOCATE EPHEMERAL GULLIES

by

NAGA PRASAD DAGGUPATI

B.S., ANGR AGRICULTURAL UNIVERSITY, 2004
M.S., KANSAS STATE UNIVERSITY, 2007

A DISSERTATION

submitted in partial fulfillment of the requirements for the degree

DOCTOR OF PHILOSOPHY

Department of Biological & Agricultural Engineering
College of Engineering

KANSAS STATE UNIVERSITY
Manhattan, Kansas

2012

Approved by:

Major Professor
Kyle Douglas-Mankin

Copyright

Abstract

Soil erosion is one of the most important of today's global environmental problems. Over the past few decades, soil conservation practices were implemented to reduce soil erosion in the United States. However, excessive sediment still remains among the most prevalent water quality problems. Agricultural fields and in particular ephemeral gullies (EGs) are considered to be a major contributor of sediment. The overall goal of this study was to improve modeling utility to identify and quantify sources of sediment. Specific objectives were: (1) to develop and demonstrate a method of field-scale targeting using Soil and Water Assessment Tool (SWAT) and to use this method as a targeted, flexible approach to pay explicitly for sediment-yield reductions; (2) to evaluate topographic index models (Slope Area [SA], Compound Topographic Index [CTI], Slope Area Power [SAP] and Wetness Topographic Index [WTI]) and a physical-based model (Overland Flow Turbulent [OFT]) in predicting spatial EG location and lengths.

Black Kettle Creek watershed was the focus of an innovative project to pay for modeled field sediment reductions. An Arc-Geographical Information System (GIS) tool bar was developed that post processed SWAT hydrologic response unit output to field boundaries and prepared maps of high-priority fields by sediment, total nitrogen, and total phosphorus and was demonstrated to be useful for field-scale targeting. Calibrated SWAT model was used to establish baseline sediment yields. Various Best Management Practices (BMPs) were simulated and payments to implement each BMP for a given field were calculated. This study helped to guide determination of appropriate farmer support payments and quantified the important influence of BMP type and site-specific conditions for use in targeting conservation practice funding to achieve maximum soil-loss reductions per dollar spent. Extreme care should be used in selecting the source of spatial model input data when using SWAT for field-level targeting.

Automated geospatial models were developed in a GIS environment to spatially locate and derive length of EGs using topographic index and physical based models. EG predictions were better for the SA model among the four topographic index models tested. Individual calibration of topographic index model threshold for each application site was needed. An OFT model (physical based model), which utilized topography, precipitation, soil, landuse/landcover and SWAT-based runoff estimates, did not need individual site calibration, and may have broader applicability than empirical based models.

Table of Contents

List of Figures

List of Tables

Acknowledgements

I have been fortunate enough to have wonderfully supportive people encouraging me throughout this journey. I would like to take this opportunity to offer these people my sincere gratitude.

I owe my deepest gratitude to my professor, advisor, supervisor and esteemed mentor Dr. Kyle Douglas Mankin, for his constructive guidance from the beginning to the end. His mentorship is paramount in providing extraordinary experience towards my long-term career goals. I appreciate all his contributions of time, ideas, and funding to make my Ph.D. experience productive and stimulating.

I am grateful to Dr. Phil Barnes for sharing his field experiences and valuable suggestions. My sincere thank goes to my committee members Dr. Stacy Hutchinson and Dr. Marcellus Caldas for their advice and valuable suggestions that ultimately helped to improve this work. I would like to thank Dr. Aleksey Shesukov, who as a good friend was always willing to help and give his best suggestions. I would also like to thank my fellow graduate student Sumathy for her endless support and encouragement.

My deepest gratitude goes to my dad, mom and brother for all their unflagging love and support throughout my life; this dissertation is simply impossible without them. Lastly I would like to thank my wife for always cheering me up and stood by me.

Dedication

I would like to dedicate this Doctoral dissertation to my father, Dr. Sreenivasulu Daggupati. There is no doubt in my mind that without his continued support and counsel I could not have completed this process.

Abbreviations and Symbols

A	Upstream contributing area or upstream drainage area or drainage area (m^2)
ACR	ArcCN-Runoff
a_{cr}	Critial drainage area per unit contour length (m^2/m)
AGRL	General Agriculture
ALFA	Alfalfa
ALFA_BF	Baseflow recession constant (days)
ALFA_BNK	Baseflow factor for bank storage (days)
AnnAGNPS	Annualized Agricultural Nonpoint Source
ArcSWAT	ArcMap Integrated Soil and Water Assessment Tool (river basin model)
ARS	Agricultural Research Service (USDA)
As	Drainage area per unit contour length (m^2/m)
ASR	Aquifer Storage and Recovery
AWiFS	Advanced Wide Field Sensor
BASINS	Better Assessment Science Integrating Point and Nonpoint Sources (U.S. EPA)
BMP	Best Management Practice
c	Constant
CEAP	Conservation Effects Assessment Project
CF	Contour Farming
CH_Cov	Channel cover factor
CH_EROD	Channel erodibility factor
Ch_K2	Channel hydraulic conductivity (mm/hr)
CH_N(2)	Channel Manning's roughness coefficient
CLU	Common Landuse Unit
CN	Curve Number
CN_2	Curve Number II
CORN	Corn
CPNM	Crope Code (SWAT)
CSAs	Critical Source Areas
CTI	Compound Topographic Index
DEM	Digital Elevation Model
DEPTIL	Depth of mixing caused by tillage operation (mm)

E_{BMP}	BMP efficiency
EFTMIX	Mixing efficiency of tillage
EG	Ephemeral Gully
EGEM	Ephemeral Gully Erosion Model
EPA	Environmental Protection Agency
EPCO	Plant uptake compensation factor
ESCO	Soil evaporation compensation coefficient (SWAT)
ESRI	Environmental Systems Research Institute
FILTERW	Width of edge of field filter strip (m)
FullHRU	Shapefile with all HRUs included
GAP	Gap Analysis Program
GIS	Geographical Information System
GPS	Global Positioning Systems
GRSG	Grain Sorghum
GRWY	Grassed waterway
Gw_Revap	Groundwater revap coefficient
GWQMIN	Depth of water in shallow aquifer require for return flow (mm)
h	Flow depth (m)
HRU	Hydrological Response Unit
I	Uniform infiltration capacity (mm/hr)
IRS	Indian Remote Seining
KDHE	Kansas Department of Health and Environment
L	Length of the Ephemeral gully (m)
LAT_SED	Sediment concentration in lateral flow (mg/L)
LIDAR	Light Detection and Ranging
LULC	Land Use/Land Cover
Mgmt	Management operations
MUSLE	Modified Universal Soil Loss Equation
n	Manning's resistance coefficient (second/$m^{1/3}$)
NASS	National Agricultural Statistics Service
NEXRAD	Next Generation Weather Radar
NLCD	National Land Cover Dataset
NPS	Non-Point Source pollution
NRCS	Natural Resources Conservation Service (USDA)

NRI	National Resources Inventory
NSE	Nash-Sutcliffe Efficiency
NT	No-till
OFT	Overland Flow Turbulent
P	Steady-state precipitation intensity (mm/hr)
PBIAS	Percent bias (%)
Pc	Percent clay (%)
PLANC	Plan of curvature (m/100)
q	Discharge per unit contour length (m^3/m)
q_{cr}	Critical discharge (m^3)
R	Hydraulic radius (m)
R^2	Coefficient of determination
RB	Riparian Buffer
REGEM	Revised Ephemeral Gully Erosion Model
RMSE	Root mean square error
RNGE	Rangeland
RSR	RMSE to standard deviation ratio
RUSLE	Revised Universal Soil Loss Equation
S	Local slope (m/m)
S1	Study area 1
S2	Study area 2
SA	Slope-Area
SAP	Slope-Area-Power
SHALLST	Initial depth of shallow aquifer (mm)
SLSUBBSN	Average slope length
SMTMP	Snow melt base temperature (ºC)
SOYB	Soybean
SPCON	Linear parameter for channel sediment routing
SPEXP	Exponent factor for channel sediment routing
SSURGO	Soil Survey Geographic Database
STATSGO	State Geographic Database
SURLAG	Surface runoff lag coefficient
S_v	Valley Slope gradient (m/m)
SWAT	Soil and Water Assessment Tool (river basin model)

t	Topographic EG index value
T	Critical threshold for t values
T_c	Time of concentration (min)
T-d	tillage (disc)
T-f	Tillage (Field cultivator)
TILL	Tillage
TM	Thematic Mapper
T-m	Tillage (disc primary)
TR	Terraces
U.S.	United States
URLD	Urban lands
USDA	United States Department of Agriculture
USGS	United States Geological Survey
USLE	Universal Soil Loss Equation
V	Volume of Ephemeral gully (m^3)
v	Flow velocity (m/s)
WATR	Water
WETF	Forested wetlands
WH	Wheat harvested
WP	Wheat Planted
WTI	Wetness Topographic Index
WWHT	Winter Wheat
γ	Weight per unit volume of water (kg/m^3)
κ	Kappa
ρ	Density of water (kg/m^3)
τ	Shear stress indicator
τ_{cr}	Soil critical shear stress (N/m^2)
τ_s	Soil shear strength (N/m^2)

Chapter 1 - Introduction

1.1 General Background

"The threat of nuclear weapons and man's ability to destroy the environment are really alarming. And yet there are other almost imperceptible changes - I am thinking of the exhaustion of our natural resources, and especially of soil erosion - and these are perhaps more dangerous still, because once we begin to feel their repercussions it will be too late." (p. 144, The Dalai Lama's Little Book of Inner Peace: 2002, Element Books, London).

Soil erosion affects both agricultural areas and natural environment, and is one of the most important of today's global environmental problems. Annual soil losses are in excess of 50 Mg/ha in a few areas around the world, and are up to 100 times faster than the rate of soil formation, indicating that soil is lost nearly a half-centimeter layer every year (Banwart, 2011). David Montgomery (2007a) reported that agriculture is a major source of soil erosion (Figure 1.1). The location of the agricultural field and the farming practice implemented determine the magnitude of soil losses. Many countries including top four crop-producing areas (United States [U.S.], China, India and Brazil) are losing topsoil at an alarming rate (Figure 1.2). Reduction in top soil results in reduction of soil quality and thereby soil's suitability for agriculture or other vegetation. Projection in future show that global growth of human population and wealth requires a major intensification of agricultural production to meet expected 50% increase in demand for food in 2030 and possibly a doubling by 2050 (Godfray et al., 2010). Meeting the demands of food with decreasing top soil due to soil erosion is a challenge.

Soil erosion's main off-site effect is the movement of sediment and agricultural pollutants into streams and reservoirs. This is generally referred to as non-point source (NPS) pollution. NPS pollution results in sedimentation and eutrophication of our streams and reservoirs and poses a significant threat. It also impacts natural ecosystems, and negatively affects the use of water for drinking, household needs, recreation, fishing, agriculture, transportation and commerce. Hargrove et al. (2010) emphasized the need to reduce NPS pollution by reducing soil erosion, which is considered a high-priority issue for many states in the U.S. and is crucial to the future quality of life for our citizens.

Figure 1.1 Comparison of rates of soil erosion from agricultural fields under conventional agriculture (*n* = 448) and geologic erosion rates from low-gradient continental cratons (*n* = 218), soil-mantled landscapes (*n* = 663), and alpine terrain (*n* = 44). Shaded area represents range of the USDA. *T* values (0.4–1.0 mm/yr) were used to define tolerable soil loss (Source: Montgomery, 2007b).

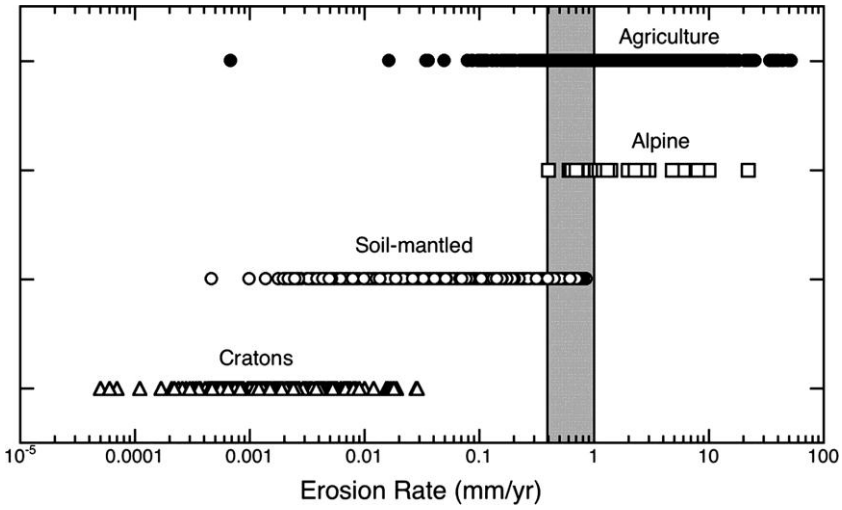

Figure 1.2 Soil degradation around world (Source: P Rekacewicz, UNEP/GRID-Arendal).

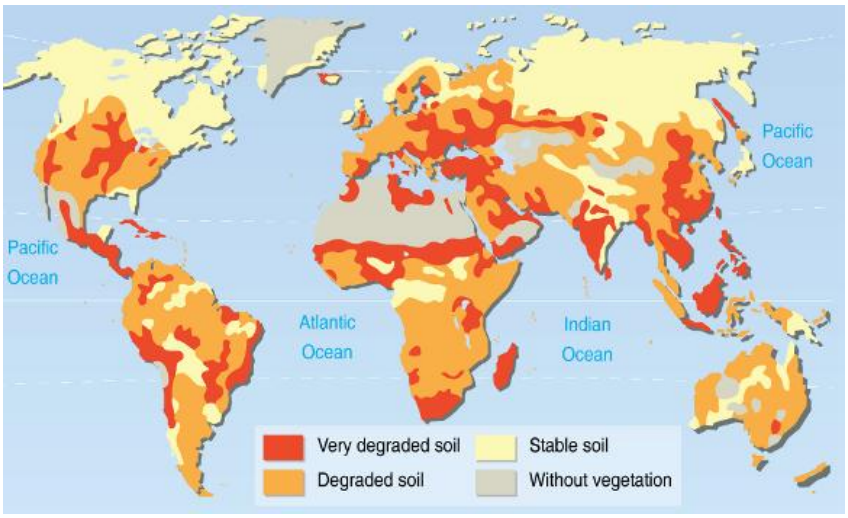

Clean Water Act, established in 1972, led to state and federal agencies making great strides in reducing total levels of water pollution. Pollution from NPSs, such as agricultural fields, remained a major concern. Section 319 of the Water Quality Act in 1987 authorized the U.S. Environment Protection Agency (EPA) to cooperate with other agencies and institutions to

establish the NPS program, in which funds were provided to each state, territory and tribe to implement NPS pollution controls, such as soil conservation practices or best management practices (BMPs). The BMPs help in reducing NPS pollution depending on the type of practice and location of implementation. Figure 1.3 shows that soil erosion rates can approach those under native conditions when BMPs are implemented.

Figure 1.3 Probability plots of rates of soil erosion from agricultural fields under conventional (e.g., tillage) and conservation agriculture (e.g., terracing and no-till methods), with erosion rates from areas and plots under native vegetation, rates of soil production, and geologic rates of erosion (Source: Montgomery, 2007b).

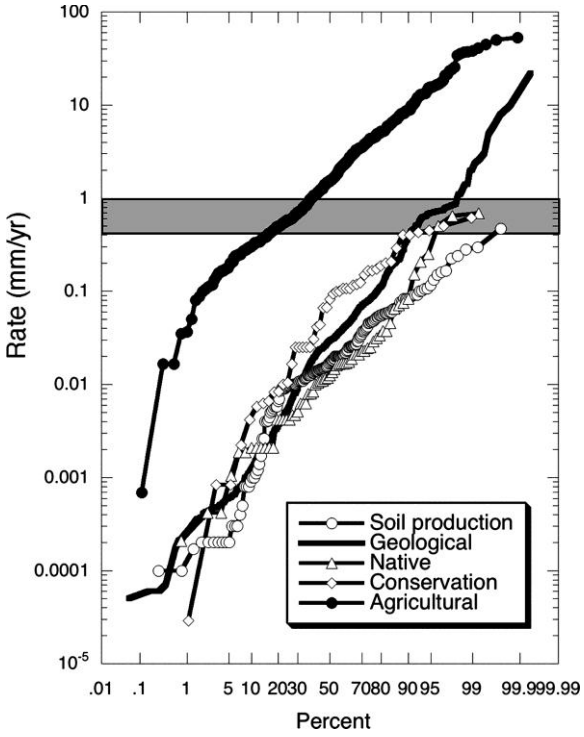

Over the past few decades in the U.S., BMPs of various kinds were implemented in agricultural fields to reduce NPS. Hargrove et al. (2010) reported that the soil erosion in agricultural landscapes has generally decreased, especially over the past 50 years due to implementation of BMPs. However, excessive sediment and pollutants remain among the most prevalent water quality problems. This could be due to not implementing the BMPs in highest sediment-producing agricultural fields, and also due to not addressing fields with ephemeral gully (EG) erosion. Summarizing the conclusions of a national conference on issues that threaten sustainability of federal reservoirs, Hargrove et al. (2010) concluded that improved

understanding of sources and rates of sedimentation was one of the three greatest needs for research:

"One of the biggest research needs is to identify and quantify the significant sediment sources and their delivery rates to reservoirs for a range of ecosystem types and climatic zones. All potential sources need to be considered, including uplands, riparian areas, streambanks, and stream channels. The contribution of ephemeral gullies to upland erosion needs to be quantified. Simulation models need to be developed that account for all sources of sediment and that predict the impact of management practices." (pp. 15A-16A)

Watershed models play an important role in water quality and assessment and improvement programs. Results from watershed models such as Soil and Water Assessment Tool (SWAT) have been used to target general areas where soil conservation measures were needed, but they have been less effective at making field-level recommendations. Also, little progress has been made in applying these theoretical model results to the practical challenge of allocating conservation practice funding to meet specific soil-loss objectives. Currently available watershed models fail to locate or simulate EGs, even though they are considered to be a major source of sediment. There is a need to spatially locate and derive length of EGs so that estimates of EG sediment load can be achieved using process based models or regression equations.

1.2 Study Goals and Objectives

This study focused on improving the SWAT model capability to target specific agricultural fields with the greatest soil erosion potential and demonstrate a better method to allocate conservation practice funding. This study also attempted to predict spatial location and length of EGs using topographic and physical-based models.

Four chapters were organized to support the purpose of this study. The goals and objectives of each chapter are described below.

Chapter 2 - Field-Level Targeting using SWAT: Mapping Outputs from HRUs to Fields and Assessing Limitations of GIS Input Data

The goal was to demonstrate a method of field-scale targeting using ArcSWAT. Specific objectives are as follows:

(1) Demonstrate the use of ArcSWAT output mapped at the field scale for conservation practice targeting; and

(2) Assess the impact of topography, soil, land use, and land management source data on field-scale targeting results.

Chapter 3 - Field-Scale Conservation Practice Targeting, Funding, and Assessment using SWAT

The goal was to develop a targeted, flexible method to ensure attainment of sediment-reduction objectives by paying farmers explicitly for sediment-yield reductions using watershed modeling. Specific objectives were to:

1) Identify cropland fields with the highest soil erosion potential, and accurately quantify baseline sediment yields;

2) Simulate and evaluate the effectiveness of various BMPs for each identified field using a calibrated SWAT model; and

3) Design a farmer friendly in-field sign-up sheet that calculates field-specific payments.

Chapter 4 - Predicting Ephemeral Gully Location and Length using Topographic Models

The goal was to evaluate existing topographic index models (SA, CTI, SAP and WTI) in predicting EG location within agricultural fields according to two metrics: occurrence (presence or absence within a given area) and length (total accumulated length within a given area). Specific objectives were to:

(1) Develop a GIS-based methodology to locate and derive length of EGs using existing topographic index models;

(2) Compare and evaluate the impacts of DEM resolution (2 m, 10 m, 30 m) and landuse data source (NASS, field reconnaissance) on EG occurrence and length predictions; and

(3) Evaluate the impacts of topographic index thresholds (T) on EG occurrence and length predictions.

Chapter 5 - Predicting Ephemeral Gully Length using Physical Model

The goal in this study was to develop a model in a geographic information system (GIS) environment to predict length of EGs utilizing a physical-based Overland Flow Turbulent (OFT)

equation developed by Montgomery and Dietrich (1994), which makes use of topography, soil, landuse/landcover, and precipitation factors. The specific objective was to:

(1) Compare and evaluate performance of the OFT and SA models in predicting EG length.

1.3 References

Banwart, S. 2011. Save our soils. *Nature* 474: 151-152.

Godfray, B., J. R. Crute, I. R. Haddad, L. Lawrence, D. Muir, J. F. Pretty, J. Robinson, S. Thomas and C. Toulmin. 2010. Food security: The challenge of feeding 9 billion people. *Science*. 327(5967): 812-818.

Hargrove, W. L., D. Johnson, D. Snethen, and J. Middendorf. 2010. From Dust Bowl to Mud Bowl: Sedimentation, conservation measures, and the future of reservoirs. *J. Soil Water Conserv.* 65(1): 14A-17A.

Montgomery, D. R., and W.E. Dietrich. 1994. Landscape Dissection and Drainage Area-Slope Thresholds. Process Models and Theoretical Geomorphology, M. J. Kirby, ed., Wiley, New York, 221-246.

Montgomery, D. R. 2007a. *Dirt: Erosion of Civilizations*. University of California Press, 296 pp.

Montgomery, D. R. 2007b. Soil erosion and agricultural sustainability. In Proc. National Academy of Sciences, USA 104. 13268-13272.

Chapter 2 - Field-Level Targeting using SWAT: Mapping Outputs from HRUs to Fields and Assessing Limitations of GIS Input Data[1]

Abstract

Soil erosion from agricultural fields is a fundamental water quality and quantity concern throughout the United States (US). Watershed models can help target general areas where soil conservation measures are needed, but they have been less effective at making field-level recommendations. The objectives of this study were to demonstrate a method of field-scale targeting using Arc-Soil and Water Assessment Tool (SWAT) and to assess the impact of topography, soil, land use, and land management source data on field-scale targeting results. The study was implemented in Black Kettle Creek watershed (7,818 ha) in south-central Kansas. An Arc-Geographical Information System (GIS) toolbar was developed to post-process SWAT hydrologic response unit (HRU) output to generate sediment yields for individual fields.

The relative impact of each input data source on field-level targeting was assessed by comparing ranked lists of fields on the basis of modeled sediment-yield density (Mg ha^{-1}) from each data-source scenario. Baseline data of field-reconnaissance land use and management were compared to National Agricultural Statistics Service (NASS) and National Land Cover Dataset (NLCD) data, 10 m Digital Elevation Model (DEM) topography were compared to 30 m, and Soil Survey Geographic Database (SSURGO) soil data were compared to State Geographic Database (STATSGO).

Misclassification of cropland as pasture by NASS and aggregation of all cropland types to a single category by NLCD led to as much as 75% and 82% disagreement, respectively, in fields identified as having the greatest sediment-yield densities. Neither NASS nor NLCD data include land management data (such as terraces, contour farming, or no-till), but such inclusion changed targeted fields by as much as 71%. Impacts of 10 m versus 30 m DEM topographic data and STATSGO versus SSURGO soil data altered the fields targeted as having the highest

[1] This chapter was published in *Transactions of the ASABE*: Daggupati, P., K. R. Douglas-Mankin, A. Y. Sheshukov, P. L. Barnes, and D. L. Devlin. 2011. Field-level targeting using SWAT: Mapping output from HRUs to fields and assessing limitations of GIS input data. *Trans. ASABE* 54(2):501–514. A copy of granted permission to reprint the journal article is presented in Appendix C.

sediment-yield densities to a lesser extent (about 10% to 25%). SWAT results post-processed to field boundaries were demonstrated to be useful for field-scale targeting. However, use of incorrect source data directly translated into incorrect field-level sediment-yield ranking, and thus incorrect field targeting. Sensitivity was greatest for land use data source, followed closely by inclusion of land management practices, with less sensitivity to topographic and soil data sources.

2.1 Introduction

Soil erosion and sedimentation are fundamental water quality and quantity concerns throughout the U.S. Soil erosion from agricultural fields is a major contributor of sediment yields into surface waters. Watershed models, both empirical and process-based, are used for watershed management, planning, development, and best management practice (BMP) implementation. Process-based models, such as the Soil and Water Assessment Tool (SWAT; Arnold et al., 1998), have been used widely to assess the extent of soil erosion as affected by agricultural land use and management practices at both field and watershed scales (Pandey et al., 2007).

Strategic targeting and prioritization of areas that need BMP implementation is the key to effective watershed management (Mankin et al., 2004; Diebel et al., 2008). Identifying fields or critical source areas (CSAs) with the greatest sediment-yield potential and targeting these fields or areas for educational and implementation efforts would efficiently allocate time, money, and educational resources (Pionke et al., 2000; Strauss et al., 2007; White et al., 2009; Busteed et al., 2009; Tuppad et al., 2010). Targeting can be separated into two phases: (1) an assessment phase, in which BMPs and/or source areas are identified and prioritized, and (2) a planning phase, in which a stakeholder group considers BMPs and source areas targeted by the assessment process along with other information to target actions, such as educational efforts or financial support. In Kansas, watershed modeling has been widely used in the assessment targeting phase to quantify and prioritize pollutant yields from BMPs and source areas (Devlin et al., 2005; Nejadhashemi et al., 2011). In this study, the term "targeting" generally refers to this assessment-phase targeting.

Over the past few decades, empirical-based and process-based models have been used widely to identify CSAs. Tim et al. (1992) integrated simulation modeling with a geographic information system (GIS) to identify CSAs in Nomini Creek watershed in Virginia. Sivertun et al. (1998), Sivertun and Prange (2003), and Barnes et al. (2009) used GIS and a Revised

Universal Soil Loss Equation (RUSLE) (Renard et al., 1991) based model to identify CSAs in which to implement conservation practices. Tripathi et al. (2003), White et al. (2009), and Busteed et al. (2009) used the SWAT model to identify and prioritize CSAs.

The SWAT model can be effective for identifying CSAs because it uses a distributed hydrologic modeling approach that utilizes spatially distributed climate, topography, soils, land use, and land management practices (Gassman et al., 2007; White et al., 2009). SWAT subdivides the watershed into subwatersheds and further into hydrologic response units (HRUs), areas within a subwatershed that have unique combinations of land use, soil, and slope. The HRU-level output can be referenced to the original land areas having the specific characteristics of each HRU and thus can be used to identify CSAs that exceed a threshold pollutant yield value (Busteed et al., 2009; Ghebremichael et al., 2010). HRUs may spread across several fields, or a given field may contain several HRUs, each with different pollutant yield potential (Figure 2.1). However, the management unit for crop BMP implementation typically is the field, not the HRU, because the entire area within a field receives the same crop type, tillage, and management practices. Farmers or landowners typically are not willing to manage field subareas differently. Therefore, HRU-level output must be aggregated or disaggregated to produce field-level output when the intention is to use the modeled information for practical targeting of BMP implementation.

Figure 2.1 Locations of HRU areas (in red) with the greatest SWAT-estimated sediment yield in relation to field boundaries

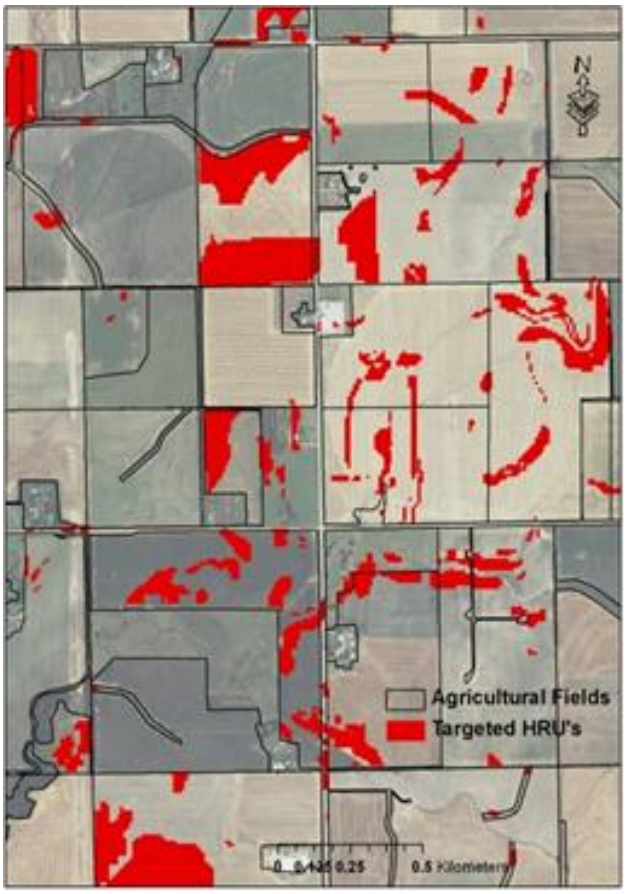

The SWAT model requires input data and parameters that describe the characteristics and distribution of topography, soils, land cover, and weather within the watershed. Watershed modelers can readily download these input data from various data sources. The SWAT model is sensitive to the quality of land use, topographic, and soil data and the preprocessing techniques used to prepare and input these data (Romanowicz et al., 2005). Inamdar and Naumov (2006) used SWAT to determine annual sediment yields and identified CSAs of erosion for the Buffalo River watershed. They used a land use/land cover (LULC) layer downloaded from the EPA BASINS website and manually updated the LULC layer by using 2002 digital ortho quarter quads. They concluded that the accuracy and resolution of the cropland areas delineated on the LULC layers are critical for reliable sediment predictions. Zhan et al. (2009) used the SWAT model to simulate runoff and sediment yield by changing LULC layers (from 1990 and 2000) in the Chao River catchment in China. Their results showed that the LULC change had little influence on runoff but had more influence on sediment yield.

Chaubey et al. (2005) evaluated the effect of digital elevation model (DEM) resolution (from 30 to 1000 m) on SWAT model predictions. They found that the DEM resolution affected the watershed delineation, stream network and subbasin classification, and the model predictions. Dixon and Earls (2009) used the SWAT model to test the sensitivity of DEM resolution (30, 90, and 300 m) and resampling techniques in predicting streamflow. They concluded that model predictions were sensitive to DEM resolution, and resampling may not be an adequate technique for modeling streamflow using the distributed watershed model. Chaplot (2005) determined the impact of DEM resolution (20 to 500 m) and soil map scale (1:25,000; 1:250,000; and 1:500,000 scale) by using SWAT to simulate runoff, sediment, and NO_3-N loads. They concluded that a DEM resolution of 50 m was required to simulate watershed loads, and decreasing the DEM resolution beyond 50 m affected the predictions of nitrogen and sediment yields. They also concluded that the detailed soil map needed to be considered to accurately estimate the watershed loads. Wang and Melesse (2006) and Peschel et al. (2006) evaluated the effects of soil layer (SSURGO and STATSGO) on modeling predictions and found that the SSURGO soil layer predicted streamflow better than the STATSGO soil layer.

Heathman et al. (2009) used SWAT to evaluate the impact of different combinations of GIS-based soil data (SSURGO and STATSGO) and land use data (GAP and NASS) on streamflow prediction. The two land use layers studied resulted in greater differences in predicted streamflow than the two soil layers studied. Veith et al. (2008) used SWAT to assess high and low resolution land use management data on flow, sediment concentration, and P concentration at the outlet of a small watershed (<100 ha). Their results showed that the high-resolution data can enable the model to provide valuable water quality information, while the low-resolution data can be used for initial problem-solving efforts. Research has evaluated the difference in modeled watershed-scale yields of flow, sediment, and nutrients resulting from input data having a range of spatial resolutions. In these studies, changes in spatial representation of topography, soils, and land use were assessed by comparing impacts on watershed-scale yields. However, very few studies have assessed the impact of spatial data resolution on the representation or modeling accuracy of watershed models at the individual field scale.

Therefore, objectives of this study were to (1) demonstrate the use of ArcSWAT output mapped at the field scale for conservation practice targeting, and (2) assess the impact of topography, soil, land use, and land management source data on field-scale targeting results. This

study focused on evaluating common datasets that were readily downloadable from the internet or manually prepared.

2.2 Project Area and Project Setting

The city of Wichita in south-central Kansas undertook the Equus Beds Aquifer Storage and Recovery (ASR) project, which diverted water from the Little Arkansas River watershed through bank storage (diversion) wells during high flows. In 2007, approximately 1.3 million m^3 (350 million gal) of water was injected into the Equus Beds aquifer. However, for every 3,800 m^3 (1 million gal) of water injected, an average of 6.4 Mg (7 tons) of sediment needed to be removed prior to injection (Steele, 2006), representing a substantial treatment expense. Steele (2006) conducted a water quality monitoring study and concluded that the Black Kettle Creek subwatershed of the Little Arkansas River watershed delivered the greatest sediment yields compared with other subwatersheds. This led to initiation of a project with the goal of reducing sediment yields from Black Kettle Creek watershed by cost-sharing implementation of targeted conservation practices in agricultural fields with the greatest soil erosion potential.

Black Kettle Creek watershed is a 7,818 ha (19,295 acres) subwatershed of the Little Arkansas River watershed (360,000 ha) located within McPherson and Harvey counties in south-central Kansas (Figure 2.2). Primary land uses in the watershed are cropland (84% of total area) followed by rangeland (12%), urban area (2%), and forests (2%). The cropland is predominantly wheat, followed by sorghum, soybeans and corn. The major pollutant concerns in this watershed are sediment and phosphorus (Steele, 2006).

Figure 2.2 Field boundaries and stream network for Black Kettle Creek watershed.

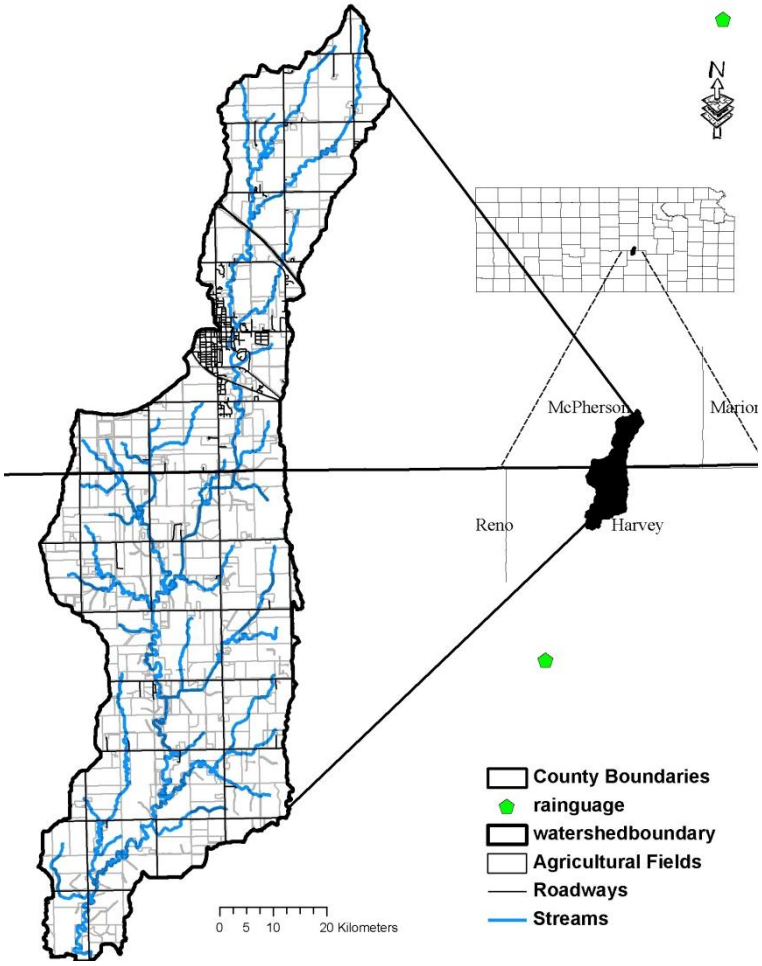

2.3 Methods

The Soil and Water Assessment Tool (SWAT), a widely used, watershed-scale, process-based model developed by the USDA Agricultural Research Service (ARS) (Arnold et al., 1998; Neitsch et al., 2005; Gassman et al., 2007; Douglas-Mankin et al., 2010), was used to identify and target the specific fields with the greatest soil erosion potential.

2.3.1 SWAT input data

Watershed and subwatershed boundaries were delineated with U.S. Geological Survey 10 m × 10 m DEM (USGS, 1999) or 30 m × 30 m DEM (USGS, 1999) depending on the modeling scenario. Watershed and subwatershed boundaries for all model runs were set using a minimum stream-definition area of 500 ha, which defined nine subbasins with the 10 m DEM and seven subbasins with the 30 m DEM. Slope categories of 0% to 2%, 2% to 4%, and >4% were used for

all the modeling scenarios to capture low, medium, and high slopes in the watershed (Figure 2.3). Relative to the 10 m DEM, the 30 m DEM overestimated the watershed area in the 0% to 2% slope class by 2.1% but underestimated the area in the 2% to 4% class by 1.9% and underestimated the area in the >4% class by 49.8%, although the total area in the >4% class was less than 5% of the watershed area in both DEM cases (Table 2.1)

Figure 2.3 Slope classifications (10 m and 30 m DEM) for Black Kettle Creek watershed.

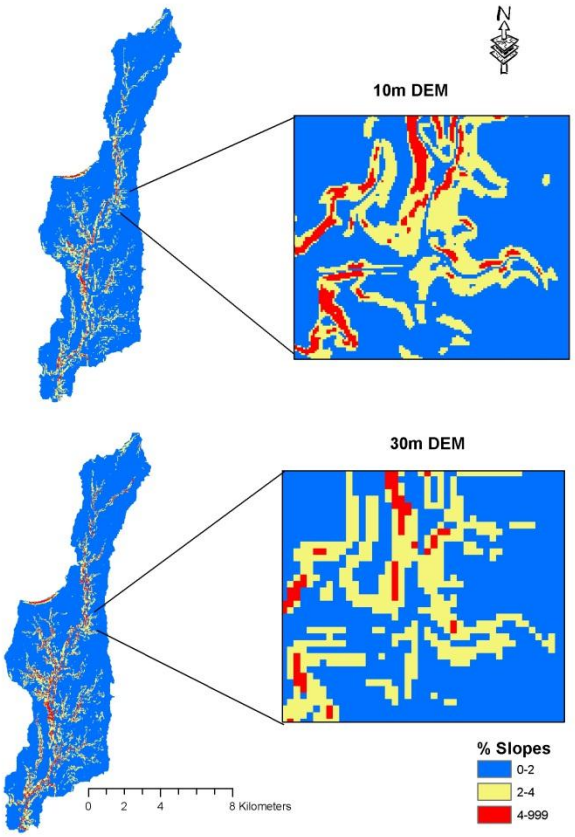

Table 2.1 Characteristics of 10 m and 30 m DEM data for Black Kettle Creek watershed

Slope Category (%)	10 m DEM Area (ha)	10 m DEM Mean Slope (%)	10 m DEM Overall Slope (%)	30 m DEM Area (ha)	30 m DEM Mean Slope (%)	30 m DEM Overall Slope (%)
>4	281	5.17		141	4.89	
2-4	1027	2.7	2.58	1007	2.6	2.18
0-2	6487	0.96		6620	0.97	

Soil data were derived from either the Soil Survey Geographic (SSURGO) database (USDA-NRCS, 2005) or the State Soil Geographic (STATSGO) database (USDA-NRCS, 1994) depending on the modeling scenario (Figure 2.4). The SSURGO soil layer was prepared using a SSURGO processing tool (Sheshukov et al., 2009) that converted the SSURGO data to a format compatible with ArcSWAT. The soil series in the SSURGO database for the Black Kettle Creek watershed included a broader range of hydrologic soil groups and USLE K values than the soil associations in the STATSGO database. The STATSGO soil data overestimated the watershed areas in the higher-runoff hydrologic soil groups (C and D) and in the highest erosivity class (K of 0.37) relative to the SSURGO data (Table 2.2).

Figure 2.4 Soil classifications (SSURGO and STATSGO) for Black Kettle Creek watershed.

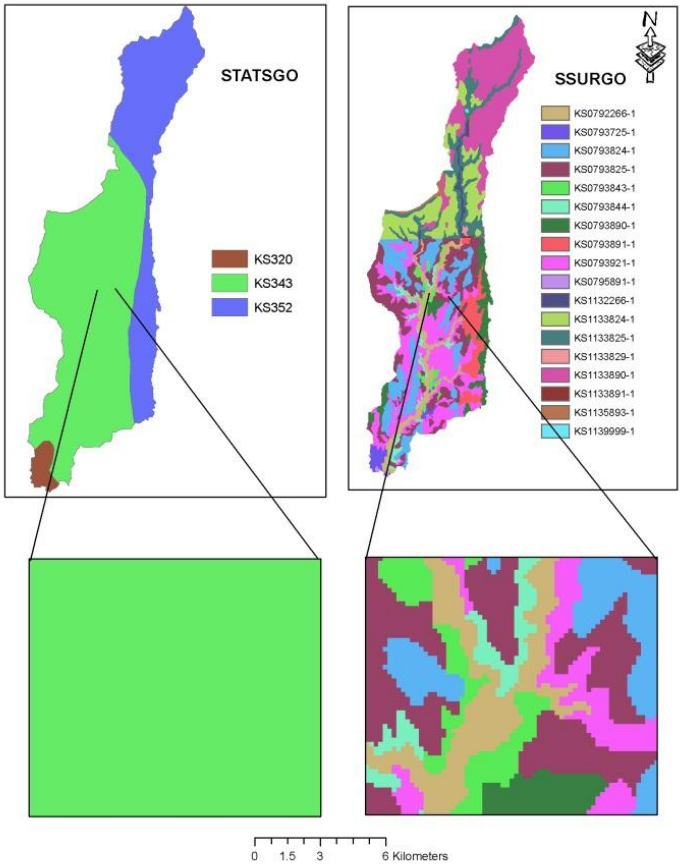

Table 2.2 Characteristics of SSURGO and STATSGO soil data for Black Kettle Creek watershed

Parameter		Area (ha)	
		SSURGO	STATSGO
Hydrologic soil group	A	2.8	0
	B	841.5	0
	C	4778.1	5265.3
	D	2186.4	2504.4
ULSE K	0.37	6965.8	7796.4
	0.32	768.8	0
	0.28	50.1	0
	0.20	22.2	0
	0.01	2.8	0

The LULC data were derived from the 2001 National Land Cover Dataset (2001) (Homer et al., 2004), the USDA National Agricultural Statistical Service (USDA-NASS, 2008), or from field reconnaissance survey data depending on the modeling scenario (Figure 2.5). The NLCD land cover was compiled for all 50 states utilizing Landsat 5 and Landsat 7 imagery centered on a nominal collection year of 2001 (Yang, 2008). The NASS land cover was produced for each state utilizing the Thematic Mapper (TM) instrument on Landsat 5, Landsat 7 ETM gap-filled data, and Indian Remote Sensing (IRS) Advanced Wide Field Sensor (AWiFS) on Resourcesat-1. The NASS land cover was developed based on satellite imagery taken during mid-July of each year (Mueller and Seffrin, 2006). The NASS land cover data are assessed mostly for agricultural areas, and NLCD land cover data are suggested for use in non-agricultural areas (www.nass.usda.gov/research/Cropland/metadata/metadata_ks08.htm). The metadata of the NASS land cover (USDA-NASS, 2008) used in this study reported classification errors (omission and commission errors) of 9.68% and 12.52% for sorghum, 8.74% and 6.93% for soybeans, and 4.48% and 4.48% for winter wheat. The NLCD land cover data distinguished 21 different data classes, while the NASS land cover data distinguished 84 classes; however, the non-agricultural classes (e.g., rangeland, pasture, woody wetlands) in the NASS land cover data are derived from the NLCD land cover data.

In the case of field reconnaissance survey data, the field data were developed using the common land use unit (CLU) field boundary shapefile, obtained from the USDA Natural Resource Conservation Service online geospatial data gateway (USDA-NRCS, 2004). Each field's land cover was manually edited based on a field-by-field reconnaissance survey conducted

by the authors in November 2008 and October 2009. The difference in the total cropland area in the NLCD land use layer and the field layer was minimal, which indicates that there was not much of a temporal difference of cropland from 2001 to 2009 in this watershed (Table 2.3). However, the three LULC data sources produced different estimates of total area in each land use category (Table 2.3) as well as spatial location of land uses (Figure 2.5). For example, Figure 2.5 shows that a field identified as grain sorghum (GRSG) by the field reconnaissance was identified largely as rangeland (RNGE) by NASS and general agriculture (AGRL) by NLCD. Similar disagreement was observed at numerous locations in the study watershed. As a result, over the watershed as a whole, NASS underestimated cropland by 1076 ha relative to field reconnaissance and overestimated rangeland by a similar area (1109 ha) (Table 2.3).SWAT parameters ALPHA_BF, EPCO, and ESCO were adjusted from the default SWAT parameters for all the scenarios in this study. ALPHA_BF was set to 0.028 based on the baseflow filter program (Arnold and Allen, 1999; Nathan and McMahon, 1990), while EPCO of 0.8 and ESCO of 0.2 were used based on experience in a nearby watershed (Gali, 2010).

Figure 2.5 Land use/land cover classifications (field reconnaissance, NASS, and NLCD) for Black Kettle Creek watershed.

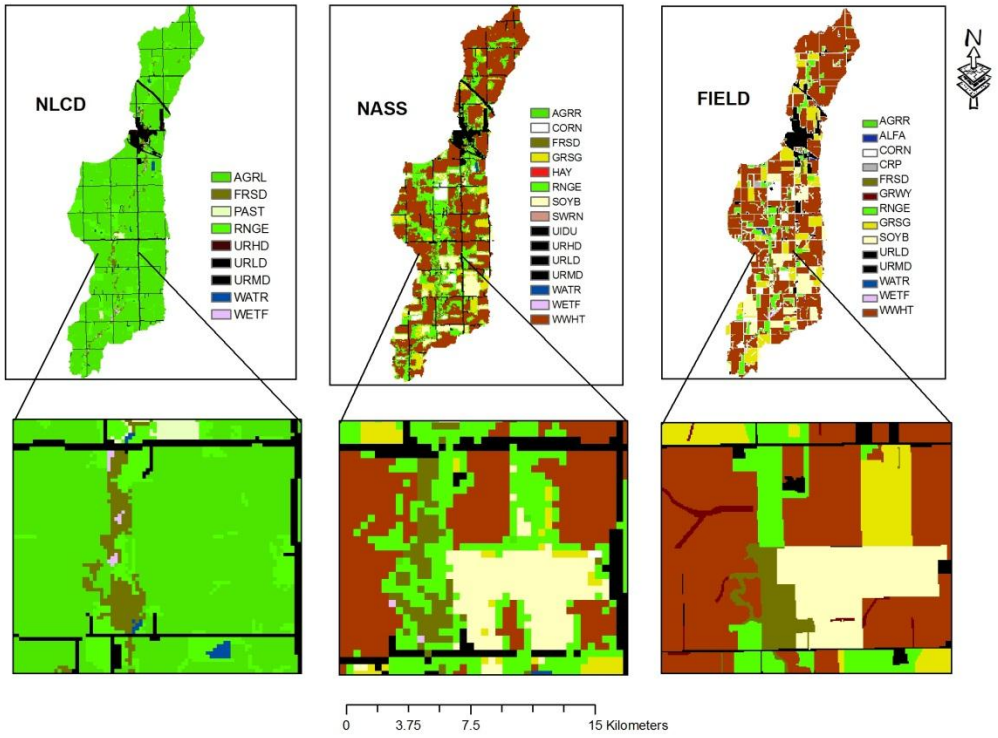

Table 2.3 Characteristics of field reconnaissance, NASS, and NLCD land use/land cover data for Black Kettle Creek watershed

Land Use Category	SWAT Abbreviation	Land Use Data Source		
		Field (ha)	NASS (ha)	NLCD (ha)
Winter wheat	WWHT	4529	3917	0
Soybean	SOYB	609	518	0
Grain sorghum	GRSG	801	424	0
Corn	CORN	210	197	0
General agriculture	AGRL, AGRR	1	18	6060
Sum of cropland	--	6149	5073	6060
Rangeland	RNGE	685	1794	912
Forest	FRSD	156	166	157
Forested wetlands	WETF	26	10	30
CRP	CRPP[a]	25	0	0
Alfalfa	ALFA	23	0	0
Grassed waterway	GRWY[a]	72	0	0
Urban	URLD, URMD, URHD	658	733	604
Water	WATR	2	18	30

[a] Created crop parameters in land cover/plant growth database

2.3.2 Representation of Hydrological Response Units (HRUs)

HRUs in SWAT do not have spatial reference. However, this limitation was overcome by redefining the topographic, soil, and land use thresholds to 0%, which retained all combinations of topography, soil, and land use in the model output and allowed reconnection of HRU output back to its original position in the landscape (Gitau et al., 2006). Another method was used by Ghebremichael et al. (2010), who defined HRUs according to field boundaries to maintain the spatial location of crop fields. In contrast to the Ghebremichael et al. (2010) approach, this study set the topographic, soil, and land use thresholds to 0% so that all slope, soil, and land use combinations in the watershed were captured and then post-processed HRU results to represent field-level results, as described below. A summary of input data sources used in each modeled scenario is presented in Table 2.4. The number of HRUs varied from 1456 to 216 depending on the scenario (Table 2.4).

Table 2.4 Source data used for each modeled scenario

			Source Data Designations				
Scenario	No. of HRUs	No. of Sub-basins	Soils[a]	Topo-graphy[b]	Land Use[c]	Land Mgmt.[d]	Tillage Mgmt.[e]
0	1456	9	S	10	F	T	R
1	1112	7	S	30	F	T	R
2	1169	9	S	10	F	N	C
3	1133	9	S	10	A	N	C
4	800	9	S	10	L	N	C
5	319	9	O	10	F	N	C
6	344	9	O	10	A	N	C
7	216	9	O	10	L	N	C
8	1338	9	S	10	F	T	C
9	1292	9	S	10	F	N	R

[a] S = SSURGO, and O = STATSGO.
[b] 10 = 10 m DEM, and 30 = 30 m DEM.
[c] F = field reconnaissance of land uses/crop types, A = NASS (USDA-NASS, 2008), and L = NLCD (Homer et al., 2004).
[d] T = digitized satellite image of terraced areas, and N = assume no terraces.
[e] R = field reconnaissance of no-till or high-residue fields, contour farming, and C = assume conventional tillage only.

2.3.3 Representation of conservation practices in SWAT

The fields with conservation practices (e.g., terraces, contour farming, no-till) were identified from either the field reconnaissance survey or analysis of the digital ortho imagery (KGS, 2002; USDA-NRCS, 2004). Combinations of land cover, conservation structures, and

tillage practices (e.g., wheat crop with terraces and conventional tillage) were created in the SWAT database by copying the data from its original land cover (e.g., wheat) and assigning a new land cover name (e.g., wheat with terrace) and crop code (CPNM) (e.g., TWHT). The terrace structural practice (12% of cropland area), assumed to be coupled with contour farming, was simulated by reducing the curve number (CN) by six units (USDA-SCS, 1972; Neitsch et al., 2005; Arabi et al., 2008) and reducing USLE practice factor values to 0.1 (Wischmeier and Smith, 1978; Arabi et al., 2008). The contour farming practice alone (0.02% of cropland area) was simulated by reducing the CN by five units and reducing USLE practice factor values to 0.5 (Arabi et al., 2008). The no-tillage or residue management practice (5% of cropland area; no overlap with terrace practice fields) was simulated by reducing the CN by two units (Arabi et al., 2008) and increasing Manning's roughness coefficient for overland flow (OV_N) to 0.14 for no residue, to 0.20 for 0.5 to 1.0 Mg ha^{-1} residue, and to 0.30 for 2 to 9 Mg ha^{-1} residue (Neitsch et al., 2005; Arabi et al., 2008). Arabi et al. (2008) used a procedure that adjusted the USLE practice factor (USLE_P) and minimum USLE cover factor (USLE_C0) to incorporate the impact of residue biomass on erosion and transport of nutrients from upland areas because the current version of SWAT does not incorporate the impact of residue biomass on erosion. The residue biomass left on the surface in all no-till fields was assumed to be 500 kg ha^{-1} (Arabi et al., 2008), based on experience by the authors in the study watershed.

The baseline scenario (scenario 0, Table 2.4) represented the best resolution and most accurate data available from each source: HRU slopes from 10 m × 10 m DEM data, soil distribution and characteristics from the SSURGO database, land use and crop types from the field reconnaissance data, structural land management (terrace) locations by the digital ortho imagery, and tillage management practices (no-till, contour farming) from the field reconnaissance data. Other scenarios were developed by varying the input data source, as shown in Table 2.4, and comparing the output results.

Daily precipitation data for the watershed were obtained from the Hesston weather station (Harvey County) located about 10 km northeast of the watershed and the Goessel weather station (McPherson County) located about 15 km east of the watershed. Temperature, solar radiation, wind speed, and relative humidity data were obtained from the Newton (Harvey County) weather station located about 25 km south of the watershed. Missing data were adjusted by using SWAT's weather generator. Each SWAT scenario was simulated for the period from 1992 to

2009 (18 years). Annual average precipitation and temperature over the study period were 795 mm (31.2 in.) and 13.9°C (57°F). Data from 2006 to 2009 were used for model validation, and data from 1995 to 2006 (12 years) were used for all field targeting analyses. The HRU, Subbasin, and Reach outputs files were exported and written as tables in the Access database (SWATOutput.mdb).

2.3.4 Model validation

Modeled streamflow for the baseline condition and selected scenarios was evaluated using measured flow data collected from 1 January 2006 to 31 July 2009 at the outlet of Black Kettle Creek watershed. Stream stage was recorded at 15 min intervals using an automated stage recorder (6700 water sampler, 730 bubbler flow module, Isco, Inc., Lincoln, Neb.) and averaged for each 24 h period (midnight to midnight). Average daily water depth was used with surveyed stream cross-sectional area, surveyed longitudinal channel slope, and estimated channel roughness coefficient (Cowan, 1956) to estimate average daily streamflow using Manning's equation (Grant and Dawson, 2001).

The statistical parameters used to evaluate the relationship between the observed and simulated streamflow were coefficient of determination (R^2), Nash-Sutcliffe model efficiency (NSE) (Nash and Sutcliffe, 1970), and percent bias (PBIAS), as recommended by Moriasi et al. (2007). The R^2 value indicates the consistency with which measured versus predicted values follow a best fit line, with 1.0 being optimal (Santhi et al., 2001). The NSE has been widely used to evaluate the performance of hydrologic models (Wilcox et al., 1990). The NSE value can range from 1 to $-\infty$, where a value of 1 indicates perfect model fit. PBIAS measures the average tendency of the simulated data to be larger or smaller than their observed counterparts. The optimal value of PBIAS is 0.0%, with positive values indicating model underestimation bias and negative values indicating model overestimation bias (Gupta et al., 1999).

For the baseline (scenario 0), the model agreement with observed flow data was satisfactory to good for monthly statistics of R^2 (0.75), NSE (0.66), and PBIAS (-18.1%) (Table 2.5) using performance ratings proposed by Moriasi et al. (2007). The annual average observed and simulated flows were also in good agreement. For the other selected scenarios, the model agreement with monthly observed flow data was satisfactory based on NSE (0.50 to 0.65) but more variable based on PBIAS (very good for two scenarios $<\pm 10\%$, good for one scenario

<±15%, satisfactory for one scenario <±25%, and unsatisfactory for two scenarios) depending on the modeling scenario (Table 2.5). The annual average observed and simulated flows for other scenarios were in close agreement. Further detailed calibration was not done in this study to avoid site-specific empiricism and bias of parameters, as the goal of this study was to compare different scenarios with different data sources.

Table 2.5 Monthly model validation statistics for selected scenarios

Scenario[a]	R^2	NSE	PBIAS (%)	Annual Avg. Flow (m^3 s^{-1})
Observed	--	--	--	0.29
0	0.75	0.66	-18.1	0.30
2	0.68	0.64	-6.9	0.31
3	0.55	0.48	-12.4	0.34
4	0.59	0.52	-3.0	0.31
5	0.62	0.60	-24.6	0.36
6	0.53	0.45	-31.8	0.38
7	0.56	0.48	-26.1	0.39

[a] 0 = S10FTR, 1 = S30FTR, 2 = S10FNC, 3 = S10ANC, 4 = S10LNC, 5 = O10FNC, 6 = O10ANC, 7 = O10LNC, 8 = S10FTC, 9 = S10FNR, where S = SSURGO, O = STATSGO, 10 = 10 m DEM, 30 = 30 m DEM, F = field reconnaissance of land uses/crop types, A = NASS (USDA-NASS, 2008), L = NLCD (Homer et al., 2004), T = digitized satellite image of terraced areas, N = assume no terraces, R = field reconnaissance of no-till or high residue fields, and C = assume conventional tillage only.

Stream sediment data were not available for calibration. Model results were validated using published measurements of sediment yields from small cropland drainage areas in Kansas (Holland, 1971). According to Holland, cropland areas in the Black Kettle Creek watershed area had sediment yields ranging from 2.78 to 5.86 Mg ha^{-1} $year^{-1}$ (1.24 to 2.48 ton $acre^{-1}$ $year^{-1}$). Before 1971, typical cropland areas in this region had minimal implementation of conservation practices and few terraces. Modeling results for the top 25 fields, also with no conservation practices or terraces, ranged from 2.83 to 5.50 Mg ha^{-1} $year^{-1}$ (1.14 to 2.26 ton $acre^{-1}$ $year^{-1}$), in good agreement with measured sediment yields. Further sediment calibration was not considered to be warranted for this study.

2.3.5 Tool to map HRU to field boundaries

To identify specific fields for targeting, the SWAT HRU output had to be mapped to the actual field boundaries. Converting SWAT HRU output to field-level results and identifying the fields that produced the greatest sediment yields involved several steps after running SWAT: (1) calculate average annual sediment for HRUs from SWATOutput tables, (2) join to FullHRU shapefile, (3) process FullHRU shapefile, (4) convert FullHRU shapefile to Grid, and (5) use zonal statistics to get pollutant yields for each field. These steps are time consuming and labor intensive. Therefore, an ArcGIS-based SWAT Targeting Toolbar (Figure 2.6) was developed with ArcGIS-Visual Basic to post-process the SWAT output and prepare maps of sediment, total phosphorus, and total nitrogen yields for a user-defined land-area boundary. The toolbar was divided into two menu items: the SWAT Output Processing tool, and the Watershed Targeting tool.

Figure 2.6 Overview of SWAT targeting toolbar.

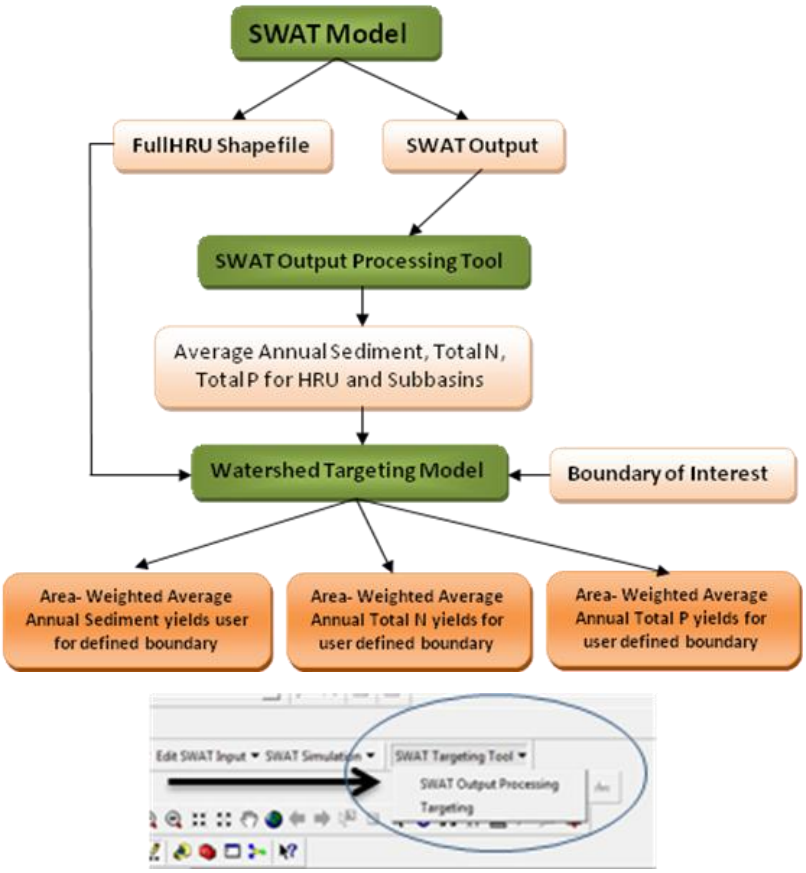

The SWAT Output Processing menu opened the Excel spreadsheet-based SWAT Output Processing tool. This tool read the SWAT output tables that were stored in an Access database (SWATOutput.mdb) and exported average annual sediment, total nitrogen, and total phosphorus yields for HRUs and subbasins.

The Targeting menu opened the Watershed Targeting tool that was built with Model Builder in the ArcGIS environment. This tool needed output from the SWAT Output Processing tool, FullHRU shapefile (generated in SWAT model run), and boundary of interest (e.g., fields, subbasins, counties). Once the inputs were satisfied, the tool produced maps of area-weighted average annual pollutant yields (sediment, total phosphorus, and total nitrogen yields) for the user-defined boundary. In this study, the CLU field boundary shapefile was used. Because this project involved identifying and targeting the fields producing the greatest sediment yields, we used only the sediment-yield analyses in this study. Using these tools and procedures, area-weighted average annual sediment yields were developed for each field for each scenario.

2.3.6 Data resolution assessment

The area within each CLU field boundary was calculated using GIS. A substantial number of small parcels in the CLU field boundary represented windbreaks, field borders, grassed waterways, and other small (<1 acre) areas that were less than a typical farm field-management unit. Since the focus of this study was on field-level targeting, these sub-field units were not relevant. Therefore, a threshold of 0.4 ha (1 acre) was applied, which reduced the number of field parcels included in analyses for this study from 677 to 593.

For each modeling scenario, field-scale sediment-yield density (Mg ha^{-1}) for each of 593 fields in the watershed was ranked from high to low. We used four subsets of fields in this ranking for comparison: the top 10% of fields (60 fields), top 20% of fields (118 fields), fields that summed to equal the top 10% of total field sediment yields (Mg), and fields that summed to equal the top 20% of sediment yields. The number of fields that contributed to the top 10% or 20% of sediment yields varied by scenario. These methods were referred to as the top 10% of fields, 20% of fields, 10% of yields, and 20% of yields, respectively. The ranking thresholds selected in this study were chosen for two reasons. First, project funding was available to pay for management practices on about 10% to 20% of the watershed's land area. Second, previous studies (Parajuli et al., 2008; Tuppad et al., 2010) have shown that the benefit of targeting

(relative to random placement) diminishes substantially after practices have been implemented on the "most critical" ~20% of land area.

The individual fields identified as in the top percentage of fields and top percentage of yields were compared among modeling scenarios. Scenario 0, or S10FTR (abbreviations described in Table 2.4), was considered to be the baseline scenario because SSURGO soils data, 10 m DEM, field-by-field land use reconnaissance assessment, and inclusion of terraces and no-till practices were considered to constitute the available input data that best represented actual conditions of the watershed. Comparisons were conducted by spatially overlapping two different scenarios in the GIS framework. For example, the shapefile of scenario 1 was overlapped with the shapefile of scenario 0 to obtain a new shapefile that showed fields that were in agreement between both scenarios.

The goal in this study was to identify the specific fields that should be targeted for conservation practice implementation and cost-share funding. If a given scenario produced a ranked list with the same fields as the comparison scenario, it was considered to be in agreement. Agreement between each pair of scenarios was assessed by reporting the percentage of fields that appeared in corresponding ranked subsets for both scenarios as a percentage of the number of fields in the scenario that best represented actual conditions (as stated above).

2.4 Results and Discussion

2.4.1 Impact of data source on characteristics of top-ranked fields

Source of soil, slope, land use, and land management data impacted the field-scale sediment yields simulated by SWAT, and these changes were not uniform across fields in the study watershed. In many cases, the ranking of field-scale sediment-yield densities (Mg ha^{-1}) changed as a result.

Characteristics of the ten fields with the greatest field-scale sediment-yield density for each scenario are summarized in Table 2.6. Modeled HRUs within a field that were not identified as cropland were labeled "noise." Even scenarios based on field reconnaissance LULC data (scenarios 0, 1, 2, 5, 8, and 9) had 1.1% to 3.0% of field area incorrectly modeled as non-cropland ("noise") area. The source of this noise was in the conversion of the field reconnaissance data shapefile (based on CLU field boundaries) into raster format during input to SWAT. Greater noise was observed in fields using NLCD LULC data (scenario 4 with 7.2%;

scenario 7 with 7.3%) and NASS LULC data (scenario 3 with 22.3%; scenario 6 with 28.6%). The NLCD and NASS data are already in raster form when input to SWAT, so noise from these data are directly caused by inaccurate land use assignment. The NASS data included more detailed categories of LULC than NLCD (Table 2.2) but more often incorrectly identified cropland as rangeland, which was the primary factor in causing 3 to 4 times more field area to be misclassified as cropland for NASS than NLCD on the top sediment-yielding fields (Table 2.6).

Table 2.6 Average characteristics for top 10 sediment-yielding fields from each scenario. HRUs within a field that were not identified as cropland were labeled "noise."

Scenario[a]	Avg. No. of HRUs per field	Total Ten-Field Area (m^2)	Noise Area (m^2)	Noise (%)	Average Slope (%)	Slope[b] (%)			Hydrologic Soil Group[b]			USLE K Factor[b]	
						0-2	2-4	4-10	B	C	D	0.32	0.37
0	13	236,116	2,652	1.1	2.5	66	25	9	15	80	5	15	85
1	11	117,009	3,542	3.0	2.2	65	30	4	17	78	6	15	85
2	17	101,172	1,735	1.7	2.5	58	35	7	19	72	9	15	85
3	15	175,215	39,076	22.3	2.4	75	24	2	11	75	14	1	99
4	12	47,711	3,455	7.2	3.0	23	43	37	24	76	0	16	84
5	12	134,224	2,326	1.7	2.7	48	38	14	0	90	10	0	100
6	12	202,800	57,932	28.6	2.4	69	28	3	0	97	3	0	100
7	8	66,337	4,825	7.3	3.2	26	45	29	0	100	0	0	100
8	16	123,559	2,167	1.8	2.3	89	33	5	15	45	40	15	85
9	18	181,652	3,308	1.8	2.7	55	38	7	25	52	24	25	76

[a] 0 = S10FTR, 1 = S30FTR, 2 = S10FNC, 3 = S10ANC, 4 = S10LNC, 5 = O10FNC, 6 = O10ANC, 7 = O10LNC, 8 = S10FTC, and 9 = S10FNR, where S = SSURGO, O = STATSGO, 10 = 10 m DEM, 30 = 30 m DEM, F = field reconnaissance of land uses/crop types, A = NASS (USDA-NASS, 2008), L = NLCD (Homer et al., 2004), T = digitized satellite image of terraced areas, N = assume no terraces, R = field reconnaissance of no-till or high residue fields,
and C = assume conventional tillage only.

[b] Percent of total ten-field area in slope, hydrologic soil group, or K-factor category for a given scenario.

Use of STATSGO data (scenarios 5, 6, and 7) forced all soils to have a K factor of 0.37 (Table 2.2), so obviously the same shift was observed in the top ten fields (Table 2.6). Similarly, STATSGO data only contained hydrologic soil groups C and D (Table 2.2), so these soil groups also would be expected to be more heavily represented in STATSGO scenarios. As a result, hydrologic soil groups for the top ten fields consistently shifted toward greater percentage of group C soils for the STATSGO scenarios (5, 6, and 7), with 90% or more of the targeted fields having group C soils compared to 80% in scenario 0 and 61% in the overall watershed (Table 2.2).

Compared to corresponding scenarios based on field LULC data (scenario 0) (Table 2.6), use of NLCD LULC data (scenario 4) had little influence on the percentage of field area having a given K factor (e.g., area with K = 0.37 changed from 85% to 84%), a small reduction in field

area having hydrologic soil groups C and D (e.g., area with group D changed from 5% to 0%), and a large increase in the field area with 2% to 4% and >4% slope classes (e.g., area with slope >4% changed from 9% to 37%). The NLCD data resulted in 29% (scenario 7: STATSGO) and 37% (scenario 4: SSURGO) of the area of the top ten fields falling within the >4% slope class, compared to 3.6% of the total watershed (Table 2.3), 10 m DEM), which was much greater than any other scenario (Table 2.6). We conclude that the net result of the use of NLCD data was the increasing importance of non-land-use factors for field selection.

Use of NASS LULC data (scenario 3) had almost the opposite effect of NLCD data (scenario 4). These data increased the K factor to 0.37 for almost all targeted field areas, shifted about 5% of both B and C group soils to hydrologic soil group D, and decreased the field areas with >4% slope classes compared to corresponding scenarios based on field LULC data (scenario 0) (Table 2.6). From a process perspective, the impact of the incorrect classifications of cropland as pasture decreased the influence of LULC on the highest ranked sediment-yielding fields and led to greater influence of soil factors (greater area of high K factor and hydrologic soil group D) on the ranking. For example, the top ten sediment-yielding fields in scenario 0, none of which contained pasture, were found to average 30.7% pasture area (range of 25 to 36%) based on NASS data used in scenario 3. By comparison, the top ten sediment-yielding fields in scenario 3, again based on NASS data, averaged 12.5% pasture area, but ranged from 0% to 31%. The reduced percentage of cropland area in scenario 3 fields led to the greater importance of soil factors in contributing to simulated sediment yield in the top-ranked fields.

2.4.2 Impact of data source on field sediment-yield Rank

Output maps showing the top 10% and 20% of fields and the top 10% and 20% of yields were prepared with GIS for all modeling scenarios. Examples in Figure 2.7 show maps of the top 10% and 20% of fields and yields for scenario 0 (baseline). The number of fields, percentage of total area, and spatial location of fields in the watershed varied between scenarios and methods (by field and by yield) (Table 2.7). Depending upon the data source scenario, different fields were identified as the greatest sediment yielders, as demonstrated in Figure 2.8 for the top 20% of sediment yields for all scenarios.

Figure 2.7 Top 10% and 20% of watershed fields and sediment yield for the baseline scenario 0.

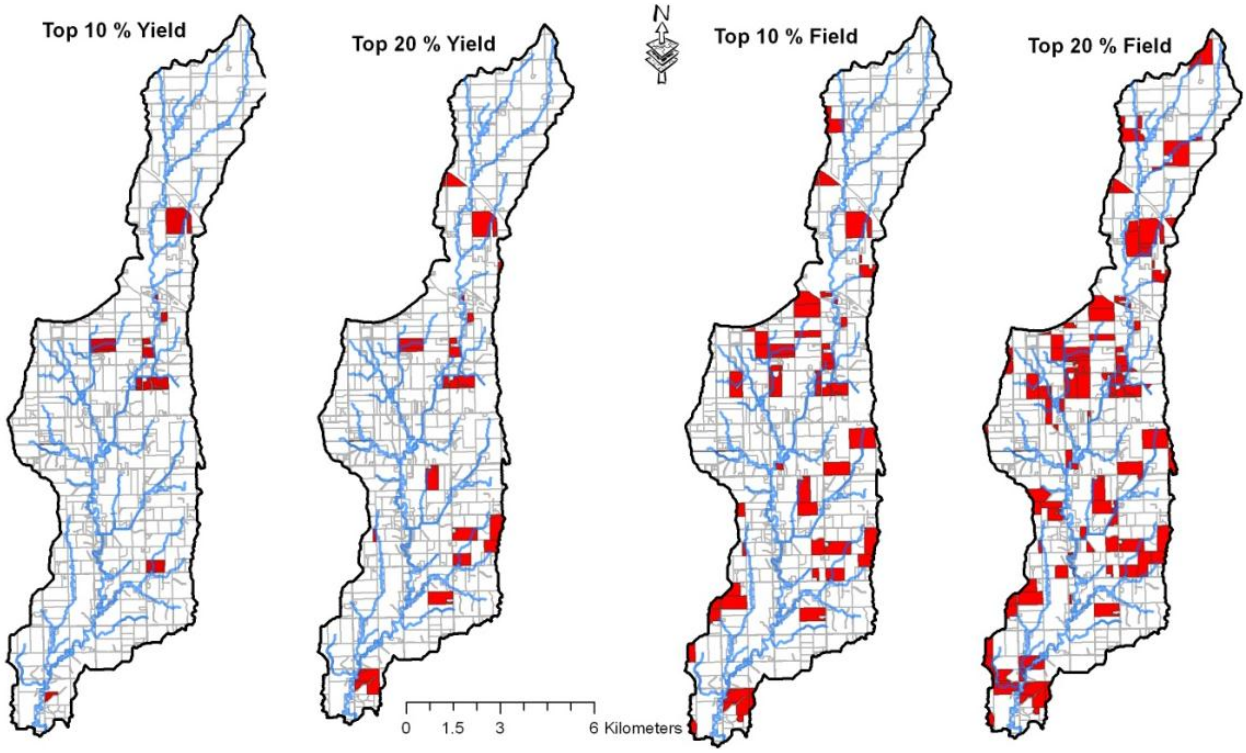

Figure 2.8 Number, percentage of watershed area and percentage of sediment yields of fields included in each ranking method for each modeled scenario.

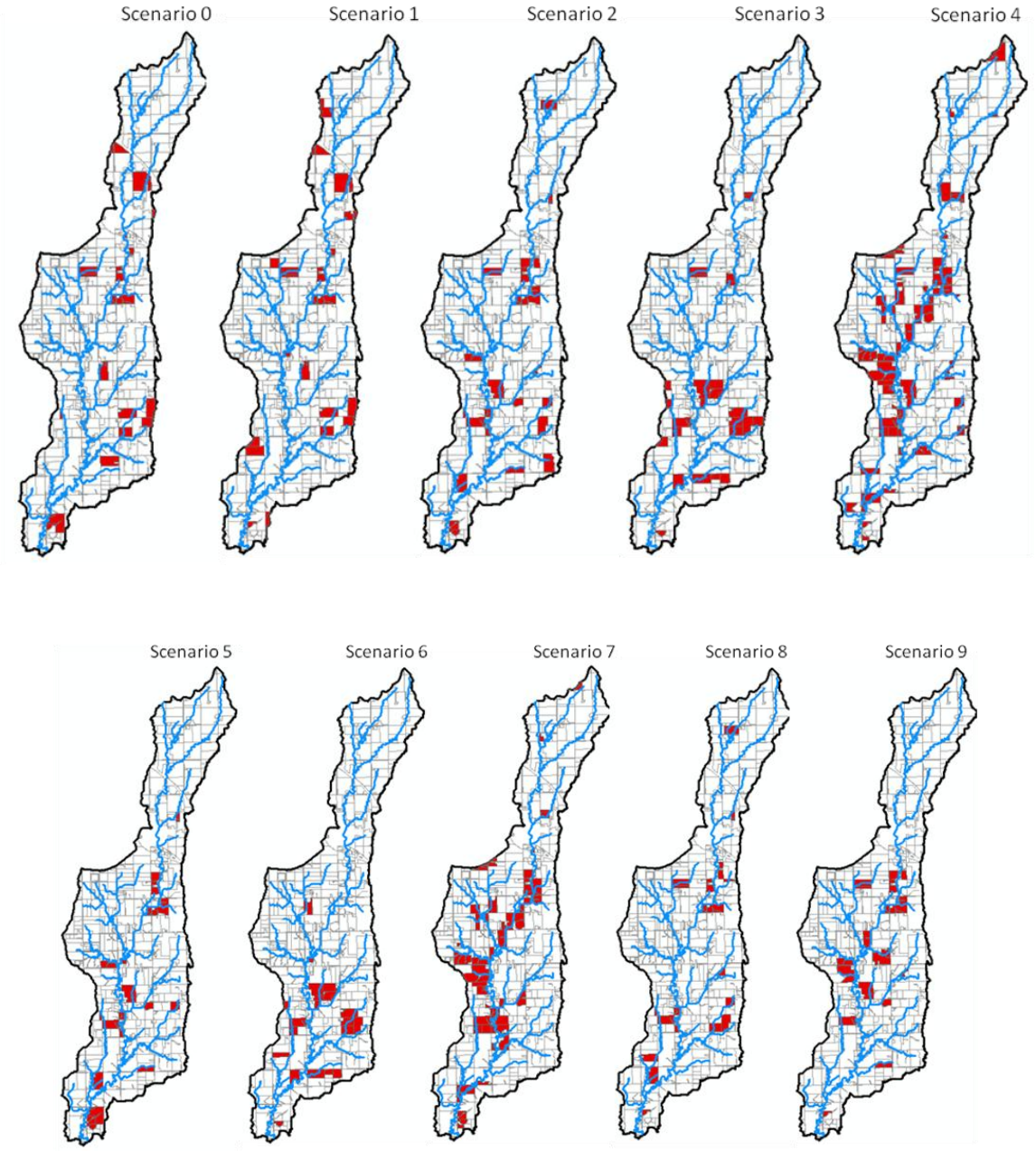

Table 2.7 Number, percentage of watershed area and percentage of sediment yields of fields included in each ranking method for each modeled scenario

		Ranking Method[b]			
	Scenario[a]	10%Y	20%Y	10%F	20%F
Number of fields	0	14	25	60	118
	1	16	26	60	118
	2	17	29	60	118
	3	11	25	60	118
	4 (AGRR)	45	82	60	118
	4 (WWHT)	46	81	60	118
	5	15	27	60	118
	6	10	20	60	118
	7 (AGRR)	37	75	60	118
	7 (WWHT)	39	79	60	118
	8	15	27	60	118
	9	12	22	60	118
Area (% of watershed)	0	2.5	5.4	12.3	20.0
	1	3.1	5.8	12.4	22.0
	2	2.6	6.0	13.5	23.6
	3	2.6	6.4	13.6	25.7
	4 (AGRR)	5.2	11.9	7.2	19.8
	4 (WWHT)	5.2	11.9	8.2	18.3
	5	2.2	4.9	13.2	23.4
	6	2.6	5.5	14.5	24.9
	7 (AGRR)	4.2	10.0	7.2	17.6
	7 (WWHT)	4.4	10.7	7.1	16.9
	8	2.0	4.7	12.5	21.0
	9	3.0	5.2	14.8	23.5
Sediment yield (% of total)	0	10	20	40.5	50.0
	1	10	20	38.4	52.4
	2	10	20	38.9	58.0
	3	10	20	33.7	48.2
	4 (AGRR)	10	20	13.3	31.3
	4 (WWHT)	10	20	13.7	28.5
	5	10	20	42.0	61.9
	6	10	20	39.1	52.9
	7 (AGRR)	10	20	15.2	30.0
	7 (WWHT)	10	20	15.6	31.2
	8	10	20	42.0	56.5
	9	10	20	41.5	57.9

[a] 0 = S10FTR, 1 = S30FTR, 2 = S10FNC, 3 = S10ANC, 4 = S10LNC, 5 = O10FNC, 6 = O10ANC, 7 = O10LNC, 8 = S10FTC, 9 = S10FNR, where S = SSURGO, O = STATSGO, 10 = 10 m DEM, 30 = 30 m DEM, F = field reconnaissance of land uses/crop types, A = NASS (USDA-NASS, 2008), L = NLCD (Homer et al., 2004), T = digitized satellite image of terraced areas, N = no terraces, R = field reconnaissance of no-till/high-residue fields, C = conventional tillage only; AGRR = general row crop for all cropland, WWHT = winter wheat for all cropland.

[b] 10%Y (20%Y) = fields with top 10% (20%) of watershed sediment yield (Mg) ranked by field sediment-yield density (Mg ha^{-1}), and 10%F (20%F) = top 10% (20%) of fields ranked by field sediment-yield density.

Depending upon the scenario, the top 10% of ranked fields (10%F; 60 fields) represented 7.2% to 14.8% of the total watershed area, and the top 20% of fields (20%F; 118 fields) represented 17.6% to 25.7% of the total watershed area (Table 2.7). Comparing the different scenarios for the same number of fields revealed that more area was accumulated for the top 60 or 118 fields when the highest-ranked fields were larger, as would be expected.

The number of fields required to accumulate a given threshold of the total sediment yield for all fields in the watershed varied by scenario (Table 2.7). The top 10% of sediment yield (10%Y) was simulated to come from as few as ten fields (scenario 6, O10ANC) and as many as 45 fields (scenario 4, S10LNC) and from as little as 2.0% of the watershed area (scenario 8, S10FTC) to as much as 5.2% (scenario 4). Estimates for the top 20% of yields ranged from 20 fields (scenario 6) to 82 fields (scenario 4) and from 4.7% of the watershed area (scenario 8) to 11.9% (scenario 4). The percentage of total watershed sediment yield from the top-ranked fields also varied among scenarios (Table 2.7). For example, the top 10% of sediment-yielding fields generated as little as 13.3% (scenario 4, S10LNC) to as much as 42.0% (scenario 5, O10FNC; and scenario 8, S10FTC) of the total field-scale sediment yield in the watershed.

The two scenarios using the NLCD LULC data (scenarios 4 and 7) required more fields to accumulate the 10% and 20% yield thresholds and accumulated a smaller percentage of the watershed area in the top 10% and 20% of fields compared to other scenarios (Table 2.7). The NLCD coverage assigned all cropland to a single land use category, in this case general agriculture (AGRR; Table 2.3), which assigned parameters according to a typical summer crop (Neitsch et al., 2005). This forced the NLCD scenarios (4 and 7) to model the fields that actually grew winter wheat (WWHT) as AGRR, which has a greater USLE Cmin factor (0.2 for AGRR vs. 0.02 for WWHT) and a different crop phenological cycle (summer vs. winter growing season). In this watershed, winter wheat fields were smaller (mean area 13 ha) than other crop fields (mean area 20 ha). Even though winter wheat land would have been expected to have less contribution to erosion than summer cropland, the small winter wheat fields were modeled to have a greater Cmin factor and thus greater sediment yields. Greater inclusion of these fields increased the number of smaller fields included in the top-ranked sediment-yielding fields.

To test the impact of the default crop assignment by NLCD, we ran additional scenarios identical to scenarios 4 and 7 except that all NLCD cropland was assigned parameters consistent with WWHT. The number of fields in each ranking method changed only minimally (Table 2.7),

and the specific fields identified between the two methods were largely in agreement (e.g., 78% agreement in fields identified in the top 20% of sediment yields).

The results summarized in Table 2.7 demonstrate a fairly consistent relationship among the top-ranked fields (with the greatest sediment-yield densities) between the number of fields and the percentage of watershed area covered by those fields. For the top 118 sediment-yielding fields analyzed in this study (Table 2.7), the relationship was linear, with a slope (expressed as fields per percentage of total watershed area) ranging from 4.6 to 6.9 and averaging 5.6 fields per percentage for eight of the ten scenarios. For model results using the NLCD data, however, slopes were much greater for both scenario 4 (9.3 fields per percentage) and scenario 7 (10.4 fields per percentage), because of the greater inclusion of WWHT fields, as discussed above. This indicates that all data sources, except NLCD, were fairly consistent in describing the relative distribution of sediment yields within the watershed.

The spatial distribution of top sediment-yielding fields was variable among the scenarios (Figure 2.8). Targeted fields for the baseline (scenario 0) were distributed throughout the watershed. This suggests that a dispersed targeted approach (Diebel et al., 2008), in which fields are targeted by specific characteristics but may be dispersed throughout the watershed, would be most effective for targeting fields for BMP implementation. This is contrary to the conclusions of Diebel et al. (2008), who suggested greater efficiency from an aggregated targeted approach, in which fields are targeted by specific characteristics but may be aggregated only from within a specific subwatershed. Although the aggregated approach might lead to more dramatic, localized impact from a given BMP implementation effort, results of this study show that it would miss fields in other subwatersheds with greater sediment-yield reduction potential.

2.4.3 Impact of data source on spatial field targeting

Some of the fields targeted by the baseline (scenario 0) also appeared in many of the other scenarios (Figure 2.8), but many did not. This study evaluated the importance of each data source in determining the spatial location of fields with the greatest sediment-yield densities by determining the percentage of agreement between paired scenarios in terms of fields above a given threshold ranked by sediment-yield density.

2.4.3.1 Topography

Varying DEM data resolution from 10 m (scenario 0, S10FTR) to 30 m (scenario 1, S30FTR) changed the top-ranked fields included in each analyzed subset (Table 2.8). Agreement ranged from 76% (for 20%Y) to 93% (for 10%F). However, differences in identified fields were greater for the top 14 to 25 fields (79% to 76%) than for the top 60 to 118 fields (93% to 90%). The relative lack of agreement for the highest-ranked fields probably related to the relative underestimation of fields in the highest slope class (>4%), which have the greatest potential for erosion (Table 2.1). Agreement between the 10 m and 30 m DEM scenarios was better than for other input data categories tested (Table 2.7), indicating that 30 m resolution was adequate to capture the gently rolling topography of this watershed.

Table 2.8 Targeting comparison: agreement of fields included in targeted lists between rankings by four methods. Paired scenario comparisons have different source data for only one category

Test Category	Scenario[a]		Agreement in Ranked Fields (%)[b]			
	From	To	10%Y	20%Y	10%F	20%F
Topography	0 (10)	1 (30)	79	76	93	90
Soils	2 (S)	5 (O)	71	79	80	90
	3 (S)	6 (O)	89	72	82	85
	4 (S)	7 (O)	60	73	73	81
Land use	2 (F)	3 (A)	35	31	25	43
	2 (F)	4 (L, AGRR)	60	59	40	58
	2 (F)	4 (L, WWHT)	35	34	18	45
Crop type	4 (AGRR)	4 (WWHT)	72	78	72	82
Land management	0 (TR)	8 (TC)	36	48	66	76
	0 (TR)	9 (NR)	36	48	61	76
	0 (TR)	2 (NC)	29	32	48	68

[a] 0 = S10FTR, 1 = S30FTR, 2 = S10FNC, 3 = S10ANC, 4 = S10LNC, 5 = O10FNC, 6 = O10ANC, 7 = O10LNC, 8 = S10FTC, 9 = S10FNR, where S = SSURGO, O = STATSGO, 10 = 10 m DEM, 30 = 30 m DEM, F = field reconnaissance of land uses/crop types, A = NASS (USDA-NASS, 2008), L = NLCD (Homer et al., 2004), T = digitized satellite image of terraced areas, N = assume no terraces, R = field reconnaissance of no-till or high residue fields, and C = assume conventional tillage only; AGRR = general row crop for all cropland, WWHT = winter wheat for all cropland.

[b] 10%Y (20%Y) = fields with top 10% (20%) of watershed sediment yield (Mg) ranked by field sediment-yield density (Mg ha^{-1}), and 10%F (20%F) = top 10% (20%) of fields ranked by field sediment-yield density.

2.4.3.2 Soils

Changing the input soil dataset from SSURGO (scenarios 2, 3, or 4) to STATSGO (scenarios 5, 6, or 7) changed the top-ranked fields included in each analyzed subset (Table 2.8). Agreement in field selection ranged from 60% (NLCD for 10%Y) to 90% (field for 20%F). Agreement tended to increase as the number of fields and targeted area included in the subset being compared increased. Simulations using the NLCD source data generally resulted in less agreement than using NASS or field data because the greater uniformity of LULC for the NLCD data reduced the influence of non-soil-related factors and increased the influence of soil-related factors on the field rankings. This result implies an interactive effect between soils and LULC in ranking fields by sediment-yield density.

In some scenarios, there was slightly less agreement between results from different soil data sources than between results from different topographic data sources. Generally, however, the agreement was similar, ranging from about 75% to 90% within the top 20% of ranked fields.

2.4.3.3 Land use

Changing land use data source from field (scenario 2, S10FNC) to NASS (scenario 3, S10ANC) or NLCD (scenario 4, S10LNC) had a major impact on field rankings (Table 2.8). Agreement with field scenario 2 was similar for NASS scenario 3 (25% to 43%) and NLCD scenario 4-WWHT (18% to 45%), and both were lower than NLCD scenario 4-AGRR (40% to 60%). In the case of NASS, the lower agreement was influenced by fact that the NASS land cover data often classified parcels of rangeland in the middle of agricultural fields and also occasionally had rangeland in place of agricultural crops. Greater agreement between scenario 2 (field) and scenario 4-AGRR (NLCD) than for scenario 4-WWHT (NLCD) indicated that many of the targeted fields actually grew summer crops, and imposing the WWHT crop type, with lower C_{min}, removed these fields from the top rankings and reduced agreement. This can be observed more directly with the comparison of scenario 4-AGRR and scenario 4-WWHT, which showed that 18% to 28% of the fields from one ranking did not agree with the other due to the change in crop designation from summer row crop to winter wheat.

Agreement between the pairs of land use data source comparisons ranged from 18% to 45% between scenario 2 (field) and scenario 3 (NASS) or scenario 4-WWHT (NLCD) and from 40% to 60% between scenario 2 and scenario 4-AGRR (NLCD). For these land use cases, agreements were less than for the topography and soil data source comparisons (ranging from

60% to 93%), indicating that having accurate land use designations was more critical than topography or soils in targeting the highest sediment-yielding fields in this watershed.

2.4.3.4 Terrace and tillage management

Changing the land management data from inclusion of terraces, contour farming, and tillage management (scenario 0, S10FTR) to inclusion of only terraces (scenario 8, S10FTC), only contour farming and tillage management (scenario 9, S10FNR), or neither (scenario 2, S10FNC) had a major effect on the top-ranked fields included in each analyzed subset (Table 2.8). Agreement ranged from 29% (scenario 2 for 10%Y) to 76% (either scenario 8 or 9 for 20%F).

These results confirmed the importance of including not only land use but also current practice in identifying fields for targeting. In this case, it is likely that inclusion in the model of management practices that had already been implemented on the fields with the greatest potential sediment-yield densities reduced sediment yields enough to remove many of those fields from the highest ranked (i.e., targeted) subsets. For many fields with the highest rankings in scenarios 2 through 7, modeling the implementation of terraces and/or contour farming and no-till resulted in sediment-yield density reductions adequate to remove those fields from the targeted list. This provides support that these practices (identified by field reconnaissance) appear to have been correctly placed in areas that otherwise would have been high-loss areas. Shifting from baseline (scenario 0) to the combination of terraces, contour farming, and no-till (scenario 2) resulted in less agreement in field selection than shifting to either terraces (scenario 8) or contour farming and no-till (scenario 9) alone. This modeling result indicated that, in some cases, multiple practices are needed to reduce sediment-yield potential enough to remove a field from the targeted list.

2.5 Conclusions

Agricultural fields with the greatest soil erosion potential were identified using ArcSWAT. An ArcGIS toolbar was developed to aggregate SWAT HRU output by field and prepare maps of high-priority fields by sediment, total nitrogen, and total phosphorus yields, although only sediment-yield rankings were assessed in this study.

The fields ranked by SWAT as having the greatest sediment-yield densities (Mg ha^{-1}) changed with resolution in topographic and soil data sources. Changing from 10 m to 30 m DEM

topographic data and from STATSGO to SSURGO soil data altered the fields identified as yielding the most sediment by about 10% to 25%, depending upon the areas of the included fields as well as interactive effects with other input data sources.

Land use and management data source had the greatest influence on fields identified as having the greatest sediment-yield densities. Changing from field reconnaissance to NASS or NLCD land use data altered the fields selected as yielding the most sediment by 40% to 70%. Changing just the management data by including terraces and/or contour farming and no-till independently altered the selected fields by 25% to 70%.

Results of this study clearly demonstrate that use of incorrect or improper resolution source data can directly translate into incorrect field-level sediment-yield ranking, and thus incorrect field targeting, when using SWAT. Fields with high sediment-yield density in this study appeared to be most sensitive to land use data source (field reconnaissance, NASS, or NLCD), followed closely by inclusion of land management practices (terraces, contour farming, and no-till). Both DEM (10 m or 30 m) and soil (SSURGO or STATSGO) data source also were very important, although to a lesser extent than other inputs.

2.6 References

Arabi, M., J. R. Frankenberger, B. A. Engel, and J. G. Arnold. 2008. Representation of agricultural conservation practices with SWAT. *J. Hydrol. Proc.* 22(16): 3042-3055.

Arnold, J. G., and P. M. Allen. 1999. Automated methods for estimating baseflow and ground water recharge from streamflow records. *J. American Water Resour. Assoc.* 35(2): 411-424.

Arnold, J. G., R. Srinivasan, R. S. Muttiah, and J. R. Williams. 1998. Large-area hydrologic modeling and assessment: Part I. Model development. *J. American Water Resour. Assoc.* 34(1): 73-89.

Barnes, P. L., T. Keane, D. Devlin, and K. Douglas-Mankin. 2009. Watershed assessment to target practice placement. ASABE Paper No. MC09302. St. Joseph, Mich.: ASABE.

Busteed, P. R., D. E. Storm, M. J. White, and S. H. Stoodley. 2009. Using SWAT to target critical source sediment and phosphorus areas in the Wister Lake basin, USA. *American J. Environ. Sci.* 5(2): 156-163.

Chaplot. V. 2005. Impact of DEM mesh size and soil map scale on SWAT runoff, sediment, and NO_3-N loads predictions. *J. Hydrol.* 312(1-4): 207-222.

Chaubey, I., A. S. Cotter, T. A. Costello, and T. Soerens. 2005. Effect of DEM data resolution on SWAT output uncertainty. *J. Hydrol. Proc.* 19(3): 621-628.

Cowan, W. L. 1956. Estimating hydraulic roughness coefficients. *Agric. Eng.* 37(7): 473-475.

Devlin, D. L., W. L. Hargrove, J. C. Leatherman, K. R. Mankin, and R. M. Wilson. 2005. Using WRAPS to implement TMDLs in Kansas. In *Proc. 3rd Conf. Watershed Mgmt. to Meet Water Quality Standards and Emerging TMDL.* ASABE Paper No. 701P0105. St. Joseph, Mich.: ASABE.

Diebel, M. W., J. T. Maxted, P. J. Nowak, and M. J. Vander Zanden. 2008. Landscape planning for agricultural nonpoint-source pollution reduction: I. A geographical allocation framework. *Environ. Mgmt.* 42(5): 789-802.

Dixon, B., and J. Earls. 2009. Resample or not?! Effects of resolution of DEMs in watershed modeling. *J. Hydrol. Proc.* 23(12): 1714-1724.

Douglas-Mankin, K. R., R. Srinivasan, and J. G. Arnold. 2010. Soil and Water Assessment Tool (SWAT) model: Current developments and applications. *Trans. ASABE* 53(5): 1423-1431.

Gali, R. 2010. Assessment of NEXRAD MPE and Stage III rainfall data on streamflow modeling using SWAT for Cheney Lake, KS watershed. Unpublished MS thesis. Manhattan, Kans.: Kansas State University, Department of Biological and Agricultural Engineering.

Gassman, P. W., M. R. Reyes, C. H. Green, and J. G. Arnold. 2007. The Soil and Water Assessment Tool: Historical development, applications, and future research directions. *Trans. ASABE* 50(4): 1211-1250.

Ghebremichael, L. T., T. L. Veith, and M. C. Watzin. 2010. Determination of critical source areas for phosphorus loss: Lake Champlain basin, Vermont. *Trans. ASABE* 53(5): 1595-1604.

Gitau, M. W., T. L. Veith, W. J. Gburek, and A. R. Jarrett. 2006. Watershed-level best management practice selection and placement in the Town Brook watershed, New York. *J. American Water Resour. Assoc.* 42(6): 1565-1581.

Grant, D. M., and B. D. Dawson. 2001. *Isco Open Channel Flow Measurement Handbook.* 5th ed. Lincoln, Neb.: Isco, Inc.

Gupta, H. V., S. Sorooshian, and P. O. Yapo. 1999. Status of automatic calibration for hydrologic models: Comparison with multi-level expert calibration. *J. Hydrol. Eng*. 4(2): 135-143.

Heathman, G. C., M. Larose, and J. C. Ascough. 2009. SWAT evaluation of soil and land use GIS data sets on simulated streamflow. *J. Soil Water Cons.* 64(1): 17-32.

Holland, D. D. 1971. Sediment yields from small drainage areas in Kansas. Bulletin No. 16. Topeka, Kans.: Kansas Water Resources Board.

Homer, C., C. Huang, L. Yang, B. Wylie, and M. Coan. 2004. Development of a 2001 National Landcover Database for the United States. *Photogrammetric Engineering and Remote Sensing*. 70(7): 829-840.

Inamdar, S., and A. Naumov. 2006. Assessment of sediment yields for a mixed-landuse Great Lakes watershed: Lessons from field measurements and modeling. *J. Great Lakes Res.* 32(3): 471-488.

KGS. 2002. Digital orthophoto quarter quadrangles. Lawrence, Kans.: University of Kansas, Kansas Geological Survey. Available at: www.kansasgis.org. Accessed January 2009.

Mankin, K. R., S. J. Bhuyan, and J. K. Koelliker. 2004. Effects of cell size on AGNPS inputs and predictions. *J. Environ. Hydrol.* 12(Dec.), Paper 22.

Moriasi, D. N., J. G. Arnold, M. W. Van Liew, R. L. Bingner, R. D. Harmel, and T. L. Veith. 2007. Model evaluation guidelines for systematic quantification of accuracy in watershed simulations. *Trans. ASABE* 50(3): 885-900.

Mueller, R., and R. Seffrin. 2006. New methods and satellites: A program update on the NASS cropland data layer acreage program. *Intl. Archives Photogrammetry, Remote Sensing, and Spatial Information Sci.*, Vol. XXXVI-8/W48. International Society for Photogrammetry and Remote Sensing (ISPRS).

Nash, J. E., and J. V. Sutcliffe. 1970. River flow forecasting through conceptual models: Part I. A discussion of principles. *J. Hydrol.* 10(3): 282-290.

Nathan, R. J., and T. A. McMahon. 1990. Evaluation of automated techniques for baseflow and recession analysis. *Water Resour. Res.* 26(7): 1465-1473.

Neitsch, S. L., J. G. Arnold, J. R. Kiniry, and J. R. Williams. 2005. Soil and Water Assessment Tool (SWAT), Theoretical documentation. Temple, Tex.: USDA-ARS Grassland Soil and Water Research Laboratory.

Nejadhashemi, A. P., S. A. Woznicki, and K. R. Douglas-Mankin. 2011. Comparison of four models (STEPL, PLOAD, L-THIA, SWAT) in simulating sediment, N, and P loads and source areas for watershed planning. *Trans. ASABE.* 54(3): 875-890.

Pandey, A., V. M. Chowdary, and B. C. Mal. 2007. Identification of critical erosion prone areas in the small agricultural watershed using USLE, GIS, and remote sensing. *Water Resour. Mgmt.* 21(4): 729-746.

Parajuli, P. B., K. R. Mankin, and P. L. Barnes. 2008. Applicability of targeting vegetative filter strips to abate fecal bacteria and sediment yield using SWAT. *J. Agric. Water Mgmt.* 95(10): 1189-1200.

Peschel, J. M., P. K. Haan, and R. E. Lacey. 2006. Influences of soil dataset resolution on hydrologic modeling. *J. American Water Resour. Assoc.* 42(5): 1371-1389.

Pionke, H. B., W. J. Gburek, and A. N. Sharpley. 2000. Critical source area controls on water quality in an agricultural watershed located in the Chesapeake basin. *Ecol. Eng*. 14(3): 255-265.

Renard, K. G., G. R. Foster, G. A. Weesies, and J. P. Porter. 1991. RUSLE, Revised Universal Soil Loss Equation. *J. Soil Water Cons*. 46(1): 30-33.

Romanowicz, A. A., M. Vanclooster, M. Rounsevell, and I. La Junesse. 2005. Sensitivity of the SWAT model to the soil and land use data parametrisation: A case study in the Thyle catchment, Belgium. *Ecol. Modeling* 187(1): 27-39.

Santhi, C., J. G. Arnold, J. R. Williams, L. M. Hauck, and W. A. Dugas. 2001. Application of a watershed model to evaluate management effects on point and nonpoint-source pollution. *Trans. ASAE* 44(6): 1559-1570.

Sheshukov, A., P. Daggupati, M. C. Lee, and K. R. Douglas-Mankin. 2009. ArcMap tool for pre-processing SSURGO soil database for ArcSWAT. In *Proc. 5th Intl. SWAT Conf.* College Station, Tex.: Texas A&M University, Texas Water Resources Institute.

Sivertun, A., and L. Prange. 2003. Nonpoint-source critical area analysis in the Gisselo watershed using GIS. *Environ. Modeling Software.* 18(10): 887-898.

Sivertun, A., L. E. Reinelt, and R. Castensson. 1998. A GIS method to aid in nonpoint-source critical area analysis. *Intl. J. Geogr. Inform. Sci*. 2(4): 365-378.

Steele, K. 2006. Atrazine best management practices: Impacts on water quality. Unpublished MS thesis. Manhattan, Kans.: Kansas State University, Department of Biological and Agricultural Engineering.

Strauss, P., A. Leone, M. N. Ripa, N. Turpin, J. M. Lescot, and R. Laplana. 2007. Using critical source areas for targeting cost-effective best management practices to mitigate phosphorus and sediment transfer at the watershed scale. *Soil Use Mgmt.* 23(1): 144-153.

Tim, U. S., S. Mostaghimi, and V. O. Shanholtz. 1992. Identification of critical nonpoint pollution source areas using geographic information systems and water quality modeling. *Water Res. Bull*. 28(5): 877-887.

Tripathi, M. P., R. K. Panda, and N. S. Raghuwanshi. 2003. Identification and prioritization of critical subwatersheds for soil conservation management using the SWAT model. *Biosyst. Eng*. 85(3): 365-379.

Tuppad, P., K. R. Douglas-Mankin, and K. A. McVay. 2010. Strategic targeting of cropland management using watershed modeling. *Agric. Eng. Intl.: CIGR J.* 12(3-4): 12-24.

USDA-NASS. 2008. Kansas agricultural statistics: Kansas county data. Washington, D.C.: USDA National Agricultural Statistics Service. Available at: http://www.nass.usda.gov/Statistics_by_State/Kansas/index.aspAccessed January 2009.

USDA-NRCS. 1994. State Soil Geographic (STATSGO) database. Washington, D.C.: USDA Natural Resources Conservation Service. Available at: http://soildatamart.nrcs.usda.gov/Default.aspx. Accessed January 2009.

USDA-NRCS. 2004. Geospatial data gateway. Fort Worth, Tex.: USDA Natural Resources Conservation Service. Available at: http://datagateway.nrcs.usda.gov. Accessed January 2009.

USDA-NRCS. 2005. Soil Survey Geographic (SSURGO) database. Washington, D.C.: USDA Natural Resources Conservation Service. Available at: http://soildatamart.nrcs.usda.gov/Default.aspx. Accessed January 2009.

USDA-SCS. 1972. *National Engineering Handbook*, Section 4. Washington, D.C.: USDA Soil Conservation Service.

USGS. 1999. DASC data catalog Lawrence, Kans.: Kansas Data Access and Support Center**.** Available at: www.kansasgis.org/catalog/catalog.cfm. Accessed January 2009.

Veith, T. L., A. N. Sharpley, and J. G. Arnold. 2008. Modeling a small, northeastern watershed with detailed, field-level data. *Trans. ASABE* 51(2): 471-483.

Wang, X., and A. M. Melesse. 2006. Effects of STATSGO and SSURGO as inputs on SWAT model's snowmelt simulation. *J. American Water Resour. Assoc.* 42(5): 1217-1236.

White, M. J., D. E. Storm, P. R. Busteed., S. H. Stoodley, and S. J. Phillips. 2009. Evaluating nonpoint-source critical source area contributions at the watershed scale. *J. Environ. Qual*. 38(4): 1654-1663.

Wilcox, B. P., W. J. Rawls, D. L. Brakensiek, and J. R. Wight. 1990. Predicting runoff from rangeland catchments: a comparison of two models. *Water Resour. Res.* 26:2401– 2410.

Wischmeier, W. H., and D. D. Smith. 1978. Predicting rainfall erosion losses: A guide to conservation planning. USDA Agricultural Handbook No. 537. Washington D.C.: USDA.

Yang. L. 2008. Development of the United States national land cover database: Experience from 1992 and 2001 implementation. *Intl. Archives Photogrammetry, Remote Sensing, and Spatial Information Sci.*, Vol. XXXVII, Part B4. International Society for Photogrammetry and Remote Sensing (ISPRS).

Zhan, C. H., Z. X. Xu, Y. D. Wu, and M. J. Xue. 2009. LUCC and its impact on runoff and soil erosion in Chao River catchment of Miyun reservoir basin. *J. Sichuan University (Eng. Sci. Edition)* 41(2): 148-153.

Chapter 3 - Field-Scale Conservation Practice Targeting, Funding, and Assessment using SWAT[2]

Abstract

Watershed models have been widely used to estimate soil erosion and evaluate the effectiveness of conservation practices at different temporal and spatial scales; however, little progress has been made in applying these theoretical model results to the practical challenge of allocating conservation practice funding to meet specific soil-loss objectives. Black Kettle Creek subwatershed (7,809 ha) of Little Arkansas River watershed (360,000 ha) in south central Kansas was the focus of an innovative project to target conservation practice funding and pay directly for modeled sediment reduction. Detailed data (10-m DEM topography, SSURGO soils, and a manually developed landuse/landcover layer) were input into the SWAT model, and the calibrated model was used to quantify soil-erosion for each field. Various BMPs (no-till, conservation till, contour farming, terraces, contour grass strips, riparian buffers, and permanent grass), both singly and in selected combinations, were simulated and the effectiveness for each field was determined.

The mean BMP effectiveness for top 250 fields ranged from 52% to 96% for single BMPs and 85% to 94% for selected combinations of BMPs. Permanent grass produced the greatest average single-BMP effectiveness (96%) followed by Terraces (with contour farming) (78%) and No-till (72%). No-till + Terrace (with contour farming) had the greatest combined-BMP effectiveness (94%). From these field-scale sediment-reduction estimates, payments to implement each BMP for a given field within the watershed were calculated. An in-field sign-up sheet was developed with field-specific sediment-loss-based payments calculated for each BMP option. Targeting of conservation practices based on payments scaled directly by project outcome (in this case, dollars per ton of sediment reduction) using a modeling approach allowed

[2] This chapter was modified from a manuscript draft submitted to *J. of Soil and Water Conervation*: Daggupati, P., K.R. Douglas-Mankin, A.Y. Sheshukov, and P.L. Barnes. (submitted 5/11/11). Paying for sediment: Field-scale conservation practice targeting, funding, and assessment using SWAT. *J. Soil Water Conserv.* JSWC-D-11-00053. This manuscript was still under review at the time of publication of this dissertation.

flexibility for both adopters (farmers) and funders (project staff) while assuring the project objective (i.e., sediment reduction) was met.

3.1 Introduction

Soil erosion from cropland can be reduced by strategic selection and placement of agricultural conservation practices in the highest sediment producing areas or critical source areas (CSAs) (Pionke et al., 2000; Strauss et al., 2007; Busteed et al., 2009; White et al.,2009; Tuppad et al., 2010a). Watershed models have been widely used to estimate soil erosion, identify CSAs, and evaluate effectiveness of best management practices (BMPs) at various temporal and spatial scales. Ability of watershed models to process spatially distributed input data (climate, topography, soils, landuse, and land management practices) has led to identification of the CSAs within a watershed in many studies (Tripathi et al., 2003; Busteed et al., 2009; White et al., 2009; Daggupati et al., 2011). In Bracmout et al. (2006), Arabi et al. (2008), and Tuppad et al. (2010b), alteration of input parameters within one watershed model, the Soil and Water Assessment Tool (SWAT), allowed simulation of BMPs and evaluation of the effectiveness at different scales. Douglas-Mankin et al. (2010a) and Tuppad et al. (2010b) showed that both structural BMPs (e.g., grassed waterways, terraces, filter strips) and non-structural BMPs (e.g., no-till, conservation till, strip till) could be assessed and targeted with SWAT.

Many modeling studies have quantified water-quality impacts of BMP implementation, focusing on sediment, nutrient, or bacteria loads; this study focused on sediment. The water quality benefits of crop rotation, riparian buffer, and strip-cropping practices in two watersheds in central Iowa resulted in a 15% to 60% decrease in median sediment loading at the watershed level (Vache et al., 2002). Benefits of using BMPs ranged from 5% to 99% sediment loss reduction at farm level (5% to 99% less sediment entering streams) and 1% to 2% reduction at the watershed level (1% to 2% less sediment exported at the watershed outlet) (Santhi et al., 2006). The lower reduction at the watershed level was due to very small implementation area compared to watershed area. Watershed level sediment loss reductions were greatest for terraces (over 60%), whereas other practices ranged from 30% to 40% (Gassman et al., 2006). Structural BMPs in good condition and in current conditions reduced average annual sediment yield by 16% to 23% and 7% to 10% at the watershed outlet (Bracmort et al., 2006). Conversions of 40%, 50%, 75%, and 100% of cropland from conventional tillage to conservation tillage resulted in

sediment loss reductions of 20%, 26%, 33%, and 40%, respectively, at the watershed outlet (Dalzell et al. 2004). The implementation of individual BMPs reduced sediment loads from 3% to 37% at the watershed level with even higher reductions at the subwatershed and field levels (Tuppad et al., 2010b).

Establishing, implementing, and maintaining environmentally effective BMPs can be costly (Gitau et al., 2004). Implementation of a BMP that costs less and gives more reduction in pollution load would be desirable. BMP optimization techniques (single and multiple objective functions) have been used to recommend the best possible BMP(s) among various different possibilities to achieve maximum pollutant reduction with minimum increase in cost from implementation and maintenance (Maringanti et al., 2009). BMP optimization techniques use heuristic search algorithms, such as genetic algorithms, to obtain an optimal solution (Gitau et al., 2004). Various studies have used BMP optimization techniques to select and place BMPs (Gitau et al., 2004; Arabi et al., 2006; Maringanti et al., 2009; Veith et al., 2008; Chaubey et al., 2010); however, none of these studies have demonstrated how to use model results to improve farmer BMP adoption. Published studies have used watershed models to develop hypothetical scenarios or best-case scenarios to achieve a particular water quality goal for making watershed management recommendations (e.g., sediment load reduction as a result of implementing a selected BMP in 20% of the highest priority area), but little progress has been made in applying theoretical model results to the practical challenge of allocating conservation practice funding to maximize soil-loss reductions.

The goal of this study was to use watershed modeling to meaningfully support targeting and funding of conservation practice implementation explicitly for sediment yield reductions. Specific objectives were to 1) identify cropland fields with the highest soil erosion potential, and accurately quantify baseline sediment yields; 2) simulate and evaluate the effectiveness of various BMPs for each identified field using a calibrated SWAT model; 3) Design a farmer friendly in-field sign-up sheet that calculates field-specific payments

3.2 Methods

3.2.1 Study area

Black Kettle Creek watershed is a 7,809 ha (19,295 ac) subwatershed of the Little Arkansas River watershed located within McPherson and Harvey counties in south central

Kansas (Figure 3.1). Primary land use in the watershed was cropland (84% of total area) followed by rangeland (12%), urban area (2%), and forest (2%). The cropland was predominantly wheat (58% of total cropland) followed by sorghum (10%), soybean (8%), and corn (3%). A water quality monitoring study conducted by Steele (2006) found that the Black Kettle Creek watershed delivered the greatest sediment yields in south central Kansas. This led to initiation of a project with the goal of reducing sediment yields from Black Kettle Creek watershed through cost-sharing implementation of targeted conservation practices in agricultural fields with greatest soil erosion potential. Many people in this watershed are aware of the water quality problems and are engaged in various educational programs and demonstration projects.

Figure 3.1 Little Arkansas watershed and Black Kettle Creek watershed.

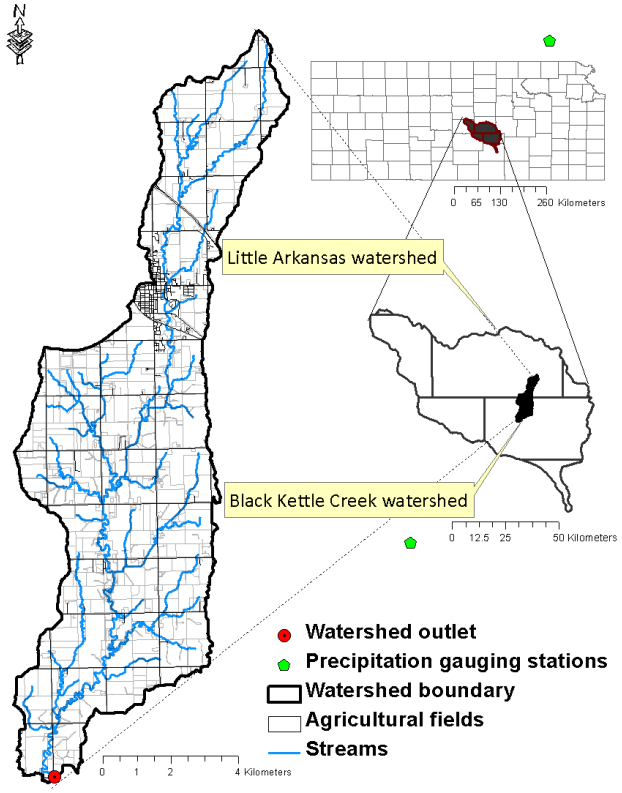

3.2.2 The Soil and Water Assessment Tool (SWAT) model

This study utilized the SWAT model, version 2005 (ArcSWAT 2.1.6), a widely used, watershed-scale, process-based model (Gassman et al., 2007; Douglas-Mankin et al., 2010b) developed by the USDA Agricultural Research Service (ARS) (Arnold et al., 1998; Neitsch et al., 2005). The SWAT model divides the watershed into a number of subwatersheds based on

topography. Each subwatershed wasfurther divided into hydrologic response units (HRUs), which are the smallest landscape component of SWAT used for computing hydrologic processes. Flow, sediment, nutrients, and other constituent yields are simulated at the HRU level, summed to the subwatershed level, and then routed through the channels, ponds, reservoirs and wetlands to the watershed outlet. The SWAT model uses the Modified Universal Soil Loss Equation (MUSLE) (Williams, 1975) to estimate sediment yield at the HRU level. In-stream sediment transport was modeled using a modified Bagnold's equation, which is a function of peak channel velocity. Sediment is either deposited or re-entrained through channel erosion depending on the sediment load entering into the channel. SWAT does not explicitly simulate ephemeral gully erosion.

3.2.3 Data input

Extreme care needs to be taken in selecting the model input data when using SWAT for field-level studies (Daggupati et al. 2011). The topographic dataset was prepared from the U.S. Geological Survey (USGS) 10 m × 10 m Digital Elevation Model (USGS, 1999). The soil dataset was developed from the Soil Survey Geographic (SSURGO) database (USDA-NRCS, 2005) with a processing utility (Sheshukov et al., 2011) that converted the SSURGO dataset into an ArcSWAT compatible format. Landuse/landcover (LULC) data were derived manually using the CLU (Common Landuse Unit) field boundary shapefile. Each field landcover in the LULC data was manually edited based on a field-by-field survey conducted by the authors in November 2008 and October 2009. Structural and non-structural management practices were derived from field surveys, whereas farming operations such as planting, harvesting, and manure application were derived by consulting extension specialists. Sets of unique combinations of landcover, conservation structures, and tillage practices (e.g., wheat crop with terraces and conventional tillage) were created in the SWAT database by copying data from its original landcover dataset (e.g., wheat) and assigning a new landcover name with a crop code parameter (CPNM) in SWAT (e.g., TWHT for wheat with terrace). The final LULC dataset was extensively checked to confirm that management practices were accurately represented for every field in the watershed.

Daily precipitation data for the watershed were obtained from the Hesston weather station (Harvey County) located about 10 km northeast of the watershed and the Goessel weather station (McPherson County) located about 15 km east of the watershed. Temperature, solar radiation,

wind speed, and relative humidity data were obtained from the Newton (Harvey County) weather station located about 25 km south of the watershed. Missing daily weather data (e.g., 94 days [Hesston] and 81 days [Goessel] over the 2006-2009 calibration period) occurred primarily during the winter (dry) season and were adjusted for both calibration and scenario runs using a stochastic weather generator embedded in SWAT. Each SWAT scenario was simulated for the period from January 1, 1990, to July 31, 2009.

3.2.4 SWAT model setup

During watershed delineation, a minimum subwatershed drainage area was set at 500 ha (1,235 ac), which resulted in 9 subwatersheds in the Black Kettle Creek watershed. Three slope categories (0-2%, 2-4%, and >4%) were used to identify areas of low, medium, and high slopes. The HRUs in SWAT do not have spatial reference, but this limitation was overcome by redefining the topographic, soil, and landuse thresholds to 0%, 0%, 0% (Gitau et al., 2006; Busteed et al., 2009; Daggupati et al., 2011), which forced simulation of every combination of slope category, soil type, and landuse type, resulting in 1,456 HRUs. Management practices (structural and non-structural) and farming operations were simulated by modifying SWAT management files for each HRU that represent individual farm fields within the watershed.

3.2.5 Model calibration and evaluation

Model predictions can be considered more reasonable and representative of hydrologic processes in a study area once a model is calibrated (Morasai et al., 2007). Flow calibration was performed for the period from 01/01/2006 to 07/31/2009 using daily measured stream flow recorded at the outlet of the watershed (Figure 3.1). An automated baseflow filter program (Arnold and Allen, 1999) was used to estimate the relative contributions of surface runoff and base-flow at the outlet of the watershed, and a baseflow recession constant (ALFA_BF, Table 3.1) was determined. Sediment calibration was performed for the period from 01/01/2006 to 01/31/2008 using total measured monthly sediment load at the watershed outlet. Daily calibration of sediment was not performed due to the lack of daily sediment data.

The SWAT model was first calibrated for flow and then for sediment. During flow calibration, the model was first run using baseline parameters. The daily hydrograph (time series plot) of observed and model simulated flows were plotted and model statistics were calculated. Based on the nature and shape of daily hydrograph, the corresponding baseline parameters

(affecting flow) were either increased or decreased from their respective baseline within the ranges shown in Table 3.1. (For example, if simulated surface flow was high compared to observed flow, then curve number (CN_2), soil available water (SOL_AWC), and soil evaporation, and compensation factor (ESCO) were decreased) After editing the parameters, the model was run again, and daily flow hydrograph and model statistics were evaluated to check improvements. Fine tuning of parameters were done until (1) shape (peaks and base flow) of observed and predicted hydrographs were reasonably similar, and (2) maximum Nash-Sutcliffe Efficiency (NSE) between observed and simulated stream flow was attained.

Table 3.1 SWAT model calibration parameters

Variable	Description	Model range	Value used
Hydrology			
CN_2	Curve number 2	±5	-3
ESCO	Soil evaporation compensation factor	0 to 1	0.8
EPCO	Plant uptake compensation factor	0 to 1	0.2
ALFA_BF	Baseflow recession constant (days)	0 to 1	0.2
ALFA_BNK	Baseflow factor for bank storage (days)	0 to 1	0.04
Gw_Revap	Groundwater revap coefficient	0.02 to 0.2	0.04
Ch_K2	Channel hydraulic conductivity (mm/hr)	-0.001 to 500	2
SURLAG	Surface runoff lag coefficient	1 to 24	2
SHALLST	Initial depth of shallow aquifer (mm)	0 to 1000	600
SMTMP	Snow melt base temperature (^oC)	-5 to 5	-3
GWQMIN	Depth of water in shallow aquifer require for return flow (mm)	0 to 5000	4
Sediment			
CH_EROD	Channel erodibility factor	0 to 1	0.4
CH_Cov	Channel cover factor	0 to 1	0.1
CH_N(2)	Channel Manning's roughness coefficient	0 to 1	0.014
SPEXP	Exponent factor for channel sediment routing	1 to 2	1
SPCON	Linear parameter for channel sediment routing	0.0001 to 0.001	0.0004
LAT_SED	Sediment concentration in lateral flow (mg/L)	0 to 5000	100
SLSUBBSN	Average slope length	10 to 150	multiplied by 1.5 from default

Once flow was calibrated, the model was calibrated for sediment using total measured monthly sediment load at the watershed outlet. Sediment calibration was also done by adjusting and fine tuning sediment related parameters as shown in Table 3.1 until maximum NSE between observed and simulated monthly sediment loads was attained.

The model statistics reported for flow and sediment calibration were coefficient of determination (R^2), Nash-Sutcliffe model efficiency (NSE) (Nash and Sutcliffe, 1970), percent bias (PBIAS), root mean square error (RMSE), and RMSE to standard deviation ratio (RSR) (Moriasi et al., 2007).

3.2.6 Targeting cropland with greatest soil erosion potential

Daggupati et al. (2011) reported that SWAT HRU output must be downscaled to the field level for practical simulation of BMP implementation. A similar approach was used in this study. Average annual sediment yields over a 12-year period (1995-2006) were calculated for each HRU from the calibrated SWAT model. A conversion utility within the SWAT HRU-to-Field Toolbar in ArcMap GIS (Daggupati et al., 2011) was used to convert an HRU-level output to area-weighted field-level output to identify the fields with greatest soil erosion potential. Total of 593 fields were ranked from highest to lowest based on average annual field-scale sediment yield density (Mg ha–1). The top 20% of fields with the highest sediment yields (118 fields) were identified and selected for preliminary targeting activities (Figure 3.2). During routine ground-truthing of model input data and results, project staff found that ephemeral gullies could also contribute significantly to land erosion. Thus, fields with ephemeral gullies were manually identified and added separately to the SWAT-generated targeting map (Figure 3.2). For each ephemeral gully, size and estimated sediment yield values were recorded based on visual observation by trained personnel. The combined SWAT and ephemeral gully targeting map was presented to farmers, which helped communicate project methods and kindle interest in participation in BMP implementation.

Figure 3.2 Top 20% fields by current sediment yield and fields with ephemeral gullies identified by field reconnaissance.

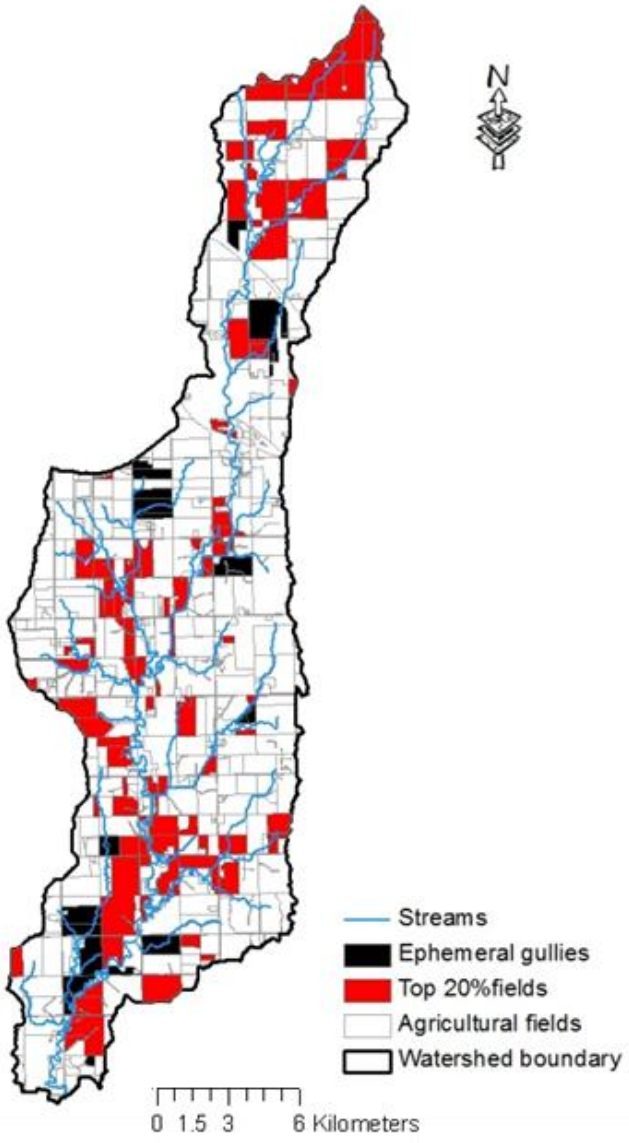

3.2.7 BMP simulation and effectiveness

Individual BMPs and combinations of BMPs were selected *a priori* by local extension personnel together with the Project team to be candidates for farmer adoption based on BMPs that were currently in the watershed and that would be effective in reducing sediment yields. Effectiveness of each BMP in the targeted fields was simulated using the calibrated SWAT model, similar to Gitau et al. (2006) and Tuppad et al. (2010 a, b). Baseline sediment yields were established for each CLU field using the SWAT HRU-to-Field Toolbar based on current field conditions. The list of BMPs that were simulated is given in Table 3.2.

Table 3.2 Selected BMPs

Single BMPs	**Combinations of BMPs**
No-till	No-till + Contour farming
Conservation till	No-till + Terraces (+ Contour farming)
Contour farming	No-till + Contour grass strips
Terraces (+ Contour farming)	No-till + Riparian vegetative buffer
Contour grass strips	Conservation till + Contour farming
Riparian vegetative buffer strip	Conservation till + Terraces (+ Contour farming)
Permanent grass	Conservation till + Contour grass strips
	Conservation till + Riparian vegetative buffer
	Contour grass strips + Riparian vegetative buffer strip

BMP descriptions and SWAT parameters modified to represent each BMP are given in Table 3.3**.** Combinations BMPs were represented simply by combining two single BMPs. For example, the No-till + Contour farming BMP was represented by modifying parameters of No-till and contour farming. The effectiveness, EBMP for each BMP in every field was calculated using Eq. 3.1:

$$E_{BMP} = \frac{(\text{Baseline sediment yield} - \text{New BMP sediment yield})}{\text{Baseline sediment yield}} \times 100 \qquad (3.1)$$

Table 3.3 SWAT model parameters changed to represent best management practices (BMPs)

BMP	SWAT variable	Initial parameter	Parameter used	Source
Riparian buffer (RB)	FILTERW	0 m	6 m	USDA NRCS recommends 6 m minimum RB width
				Bracmort et al. (2006), Arabi et al. (2008) used FILTERW for RB
No-till (NT)	Cmin	Row crop: 0.2	Row crop: 0.1	Maski et al. (2008) NT = 0.43 TILL
		Wheat: 0.03	Wheat: 0.03	SWAT default for close grown row crops, wheat
	CN_2	Varies	Reduce CN_2 by 2 units	Maski et al. (2008) Δ2-3 for TILL vs. NT Waidler et al. (2009) Δ2 for TILL vs. NT Arabi et al. (2008) reduce CN for NT
	Tillage	Chisel plow or Tandem disc (EFTMIX: 0.3; DEPTIL: 100 mm)	Generic no-till (EFTMIX: 0.05; DEPTIL: 25 mm)	Waidler et al. (2009)
Conservation tillage (CT)	Cmin	Row crop: 0.2 (SWAT default)	Row crop: 0.15	Maski et al. (2008) NT = 0.43 TILL
		Wheat: 0.03	Wheat: 0.03	SWAT default for close grown row crops, wheat
	CN_2	Varies	Reduce CN_2 by 2 units	Maski et al. (2008) Δ2-3 for TILL vs. NT Waidler et al. (2009) Δ2 for TILL vs. NT Arabi et al. (2008) reduce CN for NT
	Tillage	Chisel plow or Tandem disc (EFTMIX: 0.3; DEPTIL: 100 mm)	Generic conservation till (EFTMIX: 0.2; DEPTIL: 100 mm)	Waidler et al. (2009)
Terrace (Tr) + Contour farming (CF)	P factor	1	0.1	Wischmeier and Smith (1978) P factor range 0.1-0.18
	CN_2	Varies	Reduced by 6 units	Arabi et al. (2008) recommends 6 units for terraces
Contour farming (CF)	P factor	1	0.6	Wischmeier and Smith (1978) P factor range 0.5-0.6 (for 0-9% slope)
	CN_2	Varies	Reduced by 3 units	Arabi et al. (2008) recommends 3 units for contouring
Strip cropping or Contour grass strips	P factor	1	0.45	Wischmeier and Smith (1978) P factor range 0.38-0.45 (Type B: mostly crop/some grass strips, 0-9% slope)
	CN_2	Varies	Reduced by 3 units	Arabi et al. (2008) recommends 3 units for contouring
Permanent grass	C factor	Row crop: 0.2; Wheat: 0.03	Big bluestem: 0.003	Waidler et al. (2009)
	CN_2	Varies	Reduced by 5 units	
	Mgmt.	Varies	Management operation changed to Big bluestem	

3.2.8 Cost calculations

The payment to farmers for BMP implementation was based on simulated sediment yield reductions, which varied by field and by BMP implemented. The payment for a field to implement a particular BMP was calculated based on Eq. 3.2:

$$\mathrm{P}ayment(\$) = \left[Yield_{Baseline}\left(\frac{t}{ac}\right) - Yield_{BMP}\left(\frac{t}{ac}\right)\right] \times Area(ac) \times 100.00\left(\frac{\$}{t}\right) \quad (3.2)$$

For example, if field #525 (3.11 ac, Appendix A) produced a baseline sediment yield of 2.76 t/ac, and if the farmer of that field decided to implement the no-till practice, then we would pay the farmer according to the simulated sediment yield after implementing no-till practice, in this case 0.87 t/ac. The payment that the farmer would receive for implementing no-till practice on that field (showing full precision values) would be (2.7630 – 0.8694) t/ac × \$100/t × 3.1068 ac = \$588.30.

The unit cost of \$100/t was the amount that the expert management team decided to set as payment for each ton of sediment yield reduction. The project team estimated that it would require about \$100 per acre for farmers to convert to no-till; thus, we expected to treat about 2,700 ac with the \$270,000 project funds, which represented 16.7% of the total cropland area. With the assumption that our anticipated BMP (no-till) would achieve about 72% sediment reduction (Table 3.5) from an initial sediment yield of 4 t/ac, we anticipated to achieve a total sediment yield reduction of about 12%, which exceeded our goal of achieving 10% sediment yield reduction under the USDA Conservation Innovation Grant budget. Because contracts were signed for a five-year period, the sediment reduction being purchased averaged \$20/t/yr for the project period.

3.2.9 In-field signup sheet

An individual in-field sign-up sheet (Appendix A) was prepared in Microsoft Excel with the Visual Basic for Application computer language for each field. A database of baseline and BMP-simulated sediment yields for each field was created. On selecting the field number of interest, the values of field area (ac/field), estimated initial average annual soil loss (t/ac), estimated new average annual soil loss (t/ac) for each new BMP, and payment for each BMP (\$/field) were generated automatically from the database. The developed in-field sign-up sheets were delivered to the extension specialists, who discussed them with the owners of the targeted

fields. The sign-up sheet specified the exact payment for each BMP for each field, thus providing clear choices for the BMP selection.

3.3 Results and Discussion

3.3.1 Model evaluation

Results of the calibration runs conducted for daily, monthly, and annual measured and simulated streamflows at the watershed outlet are presented in Table 3.4. Based on the ratings proposed by Moriasi et al. (2007), the model performance was considered good for monthly streamflows when evaluation was based on NSE (> 0.65), very good when based on RSR (≤ 0.60), and excellent when based on PBIAS (< ±10%). According to these values, the SWAT model was found acceptable for streamflow simulations. The model was also calibrated at the watershed outlet for monthly and yearly average sediment yields (Table 3.4). According to Moriasi et al. (2007), the monthly performance was found satisfactory when based on NSE (> 0.50) and good when based on RSR (≤ 0.60) and PBIAS (< ±30%). The model performance of sediment was inferior to flow but was considered sufficient for estimating sediment yields in this project.

Table 3.4 Calibrated model statistics for flow and sediment

Constituent	Period	R^2	NSE	PBIAS	RMSE	RSR
Flow	Daily	0.46	0.45	4.6%	0.94	0.64
	Monthly	0.70	0.69	4.4%	0.32	0.55
	Yearly	0.96	0.89	7.5%	0.07	0.29
Sediment	Monthly	0.55	0.51	16.8%	1.44	0.53
	Yearly	0.88	0.85	17.4%	1.16	0.32

3.3.2 Field targeting

Output of the SWAT model was processed using the tools developed by Daggupati et al. (2011) to calculate average annual sediment yields for each field within the watershed. Top 20% fields with the greatest simulated soil erosion were identified in Figure 3.2 as red. Most of the identified fields were frequently close to streams. 91% of the identified fields were within 0.16 km (0.1 miles) to a stream (using the National Hydrography Dataset GIS layer) and all were

within 0.8 km (0.5 miles). In this watershed, 57% of HRUs with higher slopes (>2%) were seen closer to the stream, resulting in higher sediment yielding HRU's which further resulted in high sediment producing fields. Targeting these fields should provide more direct benefits than field's further uphill and hydrologically disconnected from the streams.

Recent studies showed that ephemeral gully erosion was considered a major source of sediment in many states, especially in Kansas (Douglas-Mankin et al., 2011) and it needs to be addressed when sediment producing fields were identified. SWAT does not simulate ephemeral-gully erosion, thus the fields with the observed ephemeral gullies were manually added to the map of targeting fields. Ephemeral gullies were present in 4% of fields (shown in black, Figure 3.2). Few ephemeral gullies were seen in No-till fields (Daggupati et al., 2010).

Accuracy of the modeled field-level predictions was validated using published measurements of sediment yields from small cropland drainage areas in Kansas (Holland, 1971). According to Holland, cropland areas in Black Kettle Creek Watershed produced sediment yields ranging from 2.8 to 5.5 Mg ha^{-1} yr^{-1} (1.24 to 2.45 t ac^{-1} yr^{-1}). Prior to 1971, typical cropland areas in this region had minimal implementation of conservation practices and few terraces. Calibrated modeling results for the top 25 fields, with no conservation practices or terraces implemented, ranged from 3.1 to 5.8 Mg ha^{-1} yr^{-1} (1.38 to 2.58 t ac^{-1} yr^{-1}), which were in good agreement with measured sediment yields. These results confirmed that the field-level targeting conducted in this study provided realistic representation of sediment yields from actual fields supporting the use of SWAT model for targeting individual fields.

3.3.3 BMP effectiveness

A database was created that included simulated baseline sediment yield and sediment yield for each BMP on every field. The effectiveness of each BMP compared to the baseline was calculated in top 250 fields. Mean BMP effectiveness of a single BMP ranged from 52% to 96% whereas mean BMP effectiveness for a combined BMP ranged from 85% to 94% (Table 3.5). The permanent grass BMP scenario produced the maximum mean BMP effectiveness among all single BMPs, whereas the No-till + Terraces (+ Contour farming) combination appeared to have greatest reductions in the combined-BMP category.

The effectiveness of each BMP spatially varied by field (Table 3.5). For example, No-till BMP had a mean effectiveness of 72% with a range of 59% to 81% among 250 fields. Similar

variability was observed for all BMPs simulated in this study. Model predictions captured the unique, variable soil, slope and landuse conditions present on each field that interacted with each BMP to produce a given sediment-reduction result. This result demonstrated the importance of using field-specific modeling results for field targeting instead of generalized percent reductions for given practices.

Table 3.5 Statistics of sediment yield reductions for simulated BMPs for top 250 fields

BMPs	Min	Mean±Stdev	Max
No-till	59%	72±5%	81%
Conservation till	42%	52±5%	67%
Contour farming	45%	53±2%	68%
Terraces (+ Contour farming)	70%	78±2%	87%
Contour grass strips	54%	61±1%	69%
Riparian vegetative buffer strip (on contour)	62%	62±0%	63%
Permanent grass	95%	96±1%	100%
No-till + Contour farming	76%	87±2%	92%
No-till + Terraces (+ Contour farming)	80%	94±3%	98%
No-till + Contour grass strips	85%	93±2%	96%
No-till + Riparian vegetative buffer	76%	87±2%	92%
Conservation till + Contour farming	75%	85±2%	90%
Conservation till + Terraces (+ Contour farming)	70%	88±3%	91%
Conservation till + Contour grass strips	85%	87±1%	91%
Conservation till + Riparian vegetative buffer	67%	85±3%	89%
Contour grass strips + Riparian vegetative buffer strip	76%	87±2%	92%

Standard deviations of mean BMP effectiveness were 5% or less for all BMPs simulated (Table 3.5). This shows that a majority of fields performed within a reasonably small range of sediment-yield reductions. However, field targeting attempts to identify the fields with the greatest benefits of implementation, not the average benefits. The differences between mean and maximum reductions for a given BMP were typically 1.5 to 4.5 times greater than the standard

deviation. Again, this demonstrates the value of using modeling results to identify these fields with the greatest potential for impact.

The modeled BMP effectiveness for selected BMPs was compared to the values reported in Devlin et al. (2003) and Merriman et al. (2009). The mean effectiveness of the selected BMPs (No-till, contour farming, terraces, riparian vegetative buffer and permanent grass) was within 10% of the mean effectiveness reported in published studies (Table 3.6). These comparison results verified that sediment-yield reductions for BMPs simulated in this study were represented reasonably well.

Table 3.6 Comparison of BMP effectiveness for selected BMPs

Selected BMPs	Mean BMP effectiveness (This study)	Mean BMP effectiveness (Literature)
No-till	72%	75%[a];78%[b]
Contour farming	53%	43%[b]
Terraces (+ Contour farming)	78%	85%[b]
Riparian vegetative buffer	62%	72%[a];76%[b]
Permanent grass	96%	95%[a]

[s]Devlin et al. (2003). [b]Merriman et al. (2009)

3.4 Conclusions

The SWAT model was used successfully to identify the agricultural fields with greatest sediment potential in the Black Kettle Creek Watershed. The model was calibrated for flow and sediment to assure and field-level sediment yields were validated with the historic local data. Fields that had ephemeral gullies were identified manually and were included for targeting, as the SWAT model cannot identify ephemeral gullies.

Various BMPs (single and combined) were simulated for each field and their effectiveness was calculated. The effectiveness of a particular BMP was different for each field based on its unique combinations of slope, soil and existing landuse. Payment to implement each BMP for a given field was calculated. An in-field signup sheet was developed to facilitate farmer signup for BMP implementation for each of the selected fields. The variability of sediment

reduction results among fields demonstrated the important influence of site-specific conditions in estimating soil-loss reductions possible with given BMPs.

Results from this study demonstrated the usability of the watershed modeling to identify cropland fields with highest sediment potential, to guide farmer support payments and quantify the important influence of BMP type and site-specific conditions for use in targeting conservation practice funding.

3.5 References

Arabi, M., J. R. Frankenberger, B. A. Engel, and J. G. Arnold. 2008. Representation of agricultural conservation practices with SWAT. *J. Hydrol. Proc.* 22(16): 3042-3055.

Arabi, M., R. S. Govindaraju, and M. M. Hantush. 2006. Cost-effective allocation of watershed management practices using a genetic algorithm. *Water Resources Res*. 42: W10429.

Arnold, J. G., and P. M. Allen. 1999. Automated methods for estimating baseflow and ground water recharge from streamflow records. *J. American Water Resour. Assoc.* 35(2): 411-424.

Arnold, J. G., R. Srinivasan, R. S. Muttiah, and J. R. Williams. 1998. Large-area hydrologic modeling and assessment: Part I. Model development. *J. American Water Resour. Assoc.* 34(1): 73-89.

Bracmort, K. S., M. Arabi, J. R. Frankenberger, B. A. Engel, and J. G. Arnold. 2006. Modeling long-term water quality impact of structural BMPs. *Trans. ASABE.* 49(2): 367-374.

Busteed, P. R., D. E. Storm, M. J. White, and S. H. Stoodley. 2009. Using SWAT to target critical source sediment and phosphorus areas in the Wister Lake Basin, USA Amer. *American J. Environ. Sci.* 5(2):156–163.

Chaubey, I., L. Chiang, M. W. Gitau, and S. Mohamed. 2010. Effectiveness of best management practices in improving water quality in a pasture-dominated watershed. *J. Soil Water Consv.* 65(6):424-446.

Daggupati, P., K. R. Douglas-Mankin, A. Y. Sheshukov, and P. L. Barnes. 2010. Monitoring and Estimating Ephemeral Gully Erosion using Field Measurements and GIS. ASABE Paper No. 10-9663. *ASABE*, St. Joseph, MI.

Daggupati, P., K. R. Douglas-Mankin, A. Y. Sheshukov, P. L. Barnes, and D. L. Devlin. 2011. Field-level targeting using SWAT: Mapping output from HRUs to fields and assessing limitations of GIS input data. *Trans. ASABE* .54(2): 501-514.

Dalzell, B. J., P. H. Gowda, and D. J. Mulla. 2004. Modeling sediment and phosphorus losses in an agricultural watershed to meet TMDLs. *J. American Water Resour. Assoc.* 40(2): 533-543.

Devlin, D., K. Dhuyvetter, K. McVay, T. Kastens, C. Rice, K. Janssen, and G. Pierzynski. 2003. Water quality best management practices, effectiveness, and cost for reducing contaminant losses from cropland. *Publication MF-2572*. Kansas State University, Manhattan, KS. 4 pp.

Douglas-Mankin, K. R., D. Maski, K. A. Janssen, P. Tuppad, and G. M. Pierzynski. 2010a. Modeling nutrient yields from combined in-field crop practices using SWAT. *Trans. ASABE.* 53(5): 1557-1568.

Douglas-Mankin, K. R., R. Srinivasan, J. G. Arnold. 2010b. Soil and Water Assessment Tool (SWAT) Model: current developments and applications. *Trans. ASABE.* 53(5): 1423-1431.

Douglas-Mankin, K., P. Daggupati, A. Sheshukov, P. Barnes, D. Devlin, and N. Nelson. 2011. Cheney Lake Watershed: Erosion from ephemeral gullies. Kansas State Research and Extension Publication. MF-3030.

Gassman, P. W., E. Osei, A. Saleh, J. Rodecap, S. Norvell, J. R. Williams. 2006. Alternative practices for sediment and nutrient loss control on livestock farms in northeast Iowa. *Agric. Ecosys. Environ.* 117: 135-144.

Gassman, P. W., M. R. Reyes, C. H. Green, and J. G. Arnold. 2007. The Soil and Water Assessment Tool: Historical development, applications, and future research directions. *Trans. ASABE.* 50(4): 1211-1250.

Gitau, M. W., T. L. Veith, and W. J. Gburek, 2004. Farm-level optimization of BMP placement for cost-effective pollution reduction. *Trans. ASABE.* 47(6): 1923-193.

Gitau, M. W., T. L. Veith, W. J. Gburek, and A. R. Jarrett. 2006. Watershed level best management practice selection and placement in the Town Brook Watershed, New York. *J. American Water Resour. Assoc.* 42(6): 1565-1581.

Holland, D. D. 1971. Sediment yields from small drainage areas in Kansas. Bulletin No. 16. Topeka, Kansas: The Kansas Water Resources Board.

Maringanti, C., I. Chaubey, and J. Popp. 2009. Development of a multiobjective optimization tool for the selection and placement of best management practices for nonpoint source pollution control. *Water Resour. Res.*45: W0640.

Maski, D., K. R. Mankin, K. A. Janssen, P. Tuppad, and G. M. Pierzynski. 2008. Modeling runoff and sediment yields from combined in-field crop practices using SWAT. *J. Soil Water Consv.* 63(4):193-203.

Merriman, K. R., M. W. Gitau, and I. Chaubey. 2009. A tool for estimating best management practice effectiveness in Arkansas. *Appl. Eng. Agr.* 25(2):199-213.

Moriasi, D. N., J. G. Arnold, M. W. Van Liew, R. L. Bingner, R. D. Harmel, and T. L. Veith. 2007. Model evaluation guidelines for systematic quantification of accuracy in watershed simulations. *Trans. ASABE.* 50(3): 885–900.

Nash, J. E., and J. V. Sutcliffe. 1970. River flow forecasting through conceptual models: Part I. A discussion of principles. *J. Hydrol.* 10(3): 282-290.

Neitsch, S. L., J. G. Arnold, J. R. Kiniry, and J. R. Williams. 2005. Soil and Water Assessment Tool (SWAT), *Theoretical documentation*. Temple, Tex.: USDA-ARS Grassland Soil and Water Research Laboratory.

Pionke, H. B., W. J. Gburek, and A. N. Sharpley. 2000. Critical source area controls on water quality in an agricultural watershed located in the Chesapeake basin. *Ecol. Eng*. 14(3): 255-265.

Santhi, C., R. Srinivasan, J. G. Arnold, and J. R. Williams. 2006. A modeling approach to evaluate the impacts of water quality management plans implemented in a watershed in Texas. *Environ. Modeling Software.* 21(8): 1141-1157.

Sheshukov, A. Y., P. Daggupati, K. R. Douglas-Mankin, and M. Lee. 2011. High Spatial Resolution Soil Data for Watershed Modeling: 1. Development of a SSURGO-ArcSWAT Utility. *J. of Natural and Environ. Sci.* 2(2): 15-24.

Steele, K. 2006. Atrazine Best Management Practices: Impacts on Water Quality. Unpublished Masters Thesis. Manhattan, Kansas: Kansas State Univ., Department of Biological and Agricultural Engineering

Strauss, P., A. Leone, M. N. Ripa, N. Turpin, J. M. Lescot, and R. Laplana. 2007. Using critical source areas for targeting cost-effective best management practices to mitigate phosphorus and sediment transfer at the watershed scale. *Soil Use Mgmt.* 23(1): 144-153.

Tripathi, M. P., R. K. Panda, and N. S. Raghuwanshi. 2003. Identification and prioritization of critical sub-watersheds for soil conservation management using the SWAT model. *Biosyst. Eng*. 85: 365-379.

Tuppad, P., K. R. Douglas-Mankin, and K. A. McVay. 2010a. Strategic targeting of cropland management using watershed modeling. J. *Agric. Eng. Intl. CIGR.* 12(3): 12-24

Tuppad, P., N. Kannan, and R. Srinivasan. 2010b. Simulation of agricultural management alternatives for watershed protection. *Water Resour. Mgmt.* 24(12): 3115-3144.

USDA-NRCS. 2005. Soil data mart. Washington, DC: USDA Natural Resources Conservation Service. Available at: http://soildatamart.nrcs.usda.gov/Default.aspx. Accessed January 2009.

USGS. 1999. National elevation dataset. Sioux Falls, S.D.: U.S. Geological Survey, EROS Data Center. Available at: www.kansasgis.org/catalog/catalog.cfm. Accessed January 2009.

Vaché, K., J. Eilers, and M. Santelmann. 2002. Water quality modeling of alternative agricultural scenarios in the US Corn Belt. *J. American Water Resour. Assoc.* 38: 773-787.

Veith, T. L., A. N. Sharpley, and J.G. Arnold. 2008. Modeling a small, northeastern watershed with detailed, field level data. *Trans. ASABE.* 51(2): 471-483.

Waidler, D., M. White, E. Steglich, X. Wang, J. R. Williams, A. Jones, R. Srinivasan, and J. G. Arnold. 2009. Conservation practice modeling for SWAT and APEX. In Proc. *2009 International SWAT conference,* University of Colorado, Boulder, CO.

White, M. J., D. E. Storm, P. R. Busteed., S. H. Stoodley, and S. J. Phillips. 2009. Evaluating nonpoint source critical source area contributions at the watershed scale. *J. Environ. Qual*. 38(4): 1654-1663.

Williams, J. R. 1975. Sediment yield prediction with universal equation using runoff energy factor. United States Department of Agriculture. Agricultural Research Service ARS-S-40.

Wischmeier, W. H., and D. D. Smith. 1978. Predicting rainfall erosion losses: A guide to conservation planning. USDA Agricultural Handbook No. 537. Washington D.C.: USDA.

Chapter 4 - Predicting Ephemeral Gully Location and Length using Topographic Index Models

Abstract

Ephemeral gullies (EGs) are channels resulting from concentrated overland flow, often forming in a similar location every year, and that add to producers' management efforts and costs. Locating EGs and implementing conservation practices is of highest importance. Predicting length of an EG is very crucial to estimate sediment load using process based models or regression equations. Topography plays an important role in the formation of EGs. This study investigates the possibility to predict EG location and length within agricultural fields according to two metrics: occurrence (presence or absence within a given area) and length (total accumulated length within a given area) using four topographic index models (Slope Area [SA], Compound Topographic Index [CTI], Slope Area Power [SAP] and Wetness Topographic Index [WTI]). Also, impacts of Digital Elevation Model (DEM) resolution, landuse and thresholds were evaluated.

Automated geospatial models were developed to locate and derive length of EGs. Results show that SA model better predicts the EG occurrence and lengths than other models tested. The SA and CTI model predictions had similar pattern in terms of locating EG trajectory, however, the CTI model had greater discontinuity along the trajectory. The method developed to derive length in this study was sensitive to discontinuity and hence the performance of CTI model was poor.

The thresholds varied among the study regions (T = 30 for S1 and T = 50 for S2) tested using SA model. No one threshold can better predict the occurrence and length of EGs. Therefore, individual calibration of model for each application site thresholds is needed. Finer resolution DEMs (e.g., 2 m) predicted EG location and lengths better compared to coarser resolution DEMs (10 m or greater). Coarser resolution DEMs can be used to locate larger classical gullies in agricultural fields or gullies in rangeland. When considering EGs only within agricultural fields, accurate landuse characterization is needed.

4.1 Introduction

Soil erosion by water is a major land degradation problem facing the world (Montgomery, 2007). It results in transporting sediments, nutrients and pesticides to surface water bodies, degrading water quality. It also results in removing organic matter, nutrients, and topsoil, decreasing soil fertility, and water holding capacity within agricultural fields. Soil erosion by water in agricultural fields occurs predominantly by three processes: interrill and rill erosion, ephemeral gully (EG) erosion and classical gully erosion. Table 4.1 describes the differences between rill erosion, EG erosion and classic gully erosion. This study focuses on EG erosion.

Table 4.1 Charecteristics of erosion (Foster, 1986)

Rill Erosion	**Ephemeral Gully Erosion**	**Classical Gully Erosion**
Rills are normally erased by tillage; they usually do not recur in the same place	Ephemeral cropland gullies are temporary features, usually obscured by tillage; recur in the same location	Gullies are not obscured by normal tillage operations
May be of any size but are usually smaller than ephemeral cropland gullies	May be of any size but are usually larger than rills and smaller than permanent gullies	Usually larger than ephemeral cropland gullies
Cross sections tend to be narrow relative to depth	Cross sections tend to be wide relative to depth; sidewalls frequently are not well defined; headcuts are usually not readily visible and are not prominent because of tillage	Cross sections of many gullies tend to be narrow relative to depth; sidewalls are steep; headcut usually prominent
Flow pattern develops as many small disconnected parallel channels ending at ephemeral cropland gullies, terrace channels, or where deposition occurs; they are generally uniformly spaced and sized	Usually forms a dendritic pattern along depressional water courses, beginning where overland flow, including rills, converge; flow patterns may be influenced by tillage, crop rows, terraces, or other unnatural features	Tend to form a dendritic pattern along natural water courses; nondendritic patterns may occur in road ditches, terraces, or diversion channels
Occurs on smooth side slopes above drainageways	Occurs along shallow drainageways upstream from incised channels or gullies	Generally occurs in well-defined drainageways

Soil is removed in shallow channels but annual tillage causes the soil profile to become thinner over the entire slope	Soil is removed along a narrow flow path, typically to the depth of the tillage layer where the untilled layer is resistant to erosion, or deeper where the untilled layer is less resistant; soil is moved into the voided area from adjacent land by mechanical action (tillage) and rill erosion, damaging an area wider than the eroded channel	Soil may be eroded to depth of the profile and can erode into soft bedrock

EG erosion is referred to as concentrated flow erosion, mega-rill erosion or shallow gully erosion. EG erosion was first comprehensively discussed by Foster (1986). Differences between EG and rills are not always very clear. EGs are larger than a rill and smaller than a classical gully. Flow in rills is usually classified as part of overland flow that occurs uniformly across a slope even though it is concentrated in rills; however, flow in EGs is clearly channelized (Foster, 1986). In some cases, the rills concentrate gradually down slope and finally form a clear EG (Figure 4.1).

Figure 4.1 Ephemeral gullies and rills.

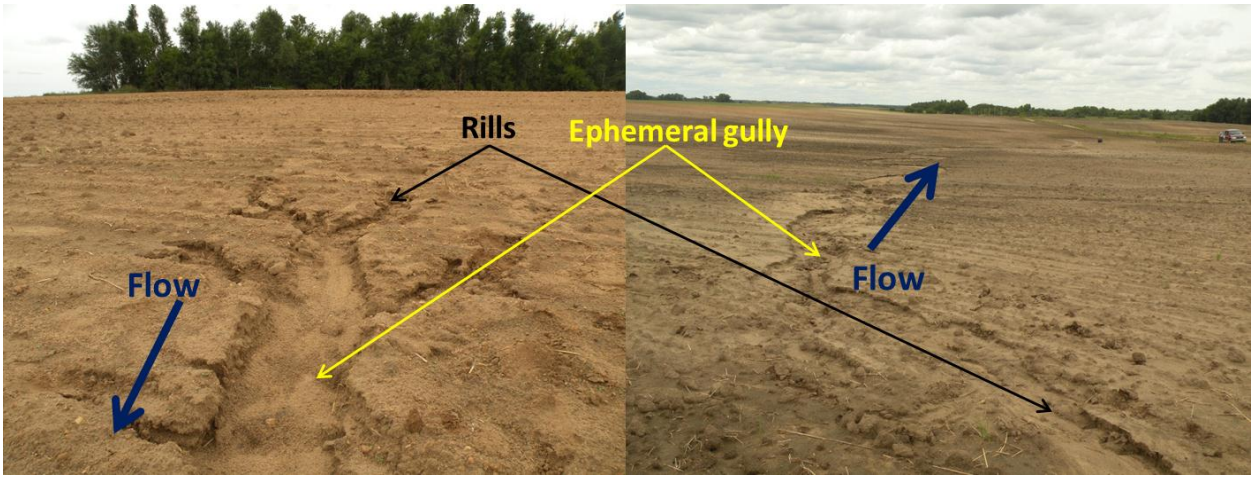

EGs are defined in literature in different ways. According to Soil Science Society of America (2001) EGs are “small channels eroded by concentrated overland flow that can be easily filled by normal tillage, only to reform again in the same location by additional runoff events”. Hauge (1977) and Poesen (1993) distinguished EGs from rills with a cross-sectional area of 929

cm^2 (i.e. 1 square foot) or greater. According to Grissinger (1996a, b), EGs are produced by concentrated flow erosion in swales or other topographically controlled locations and may be either a continuous extension of drainage network or they may be discontinuous. Smith (1993) defined EGs as small drainage channels that, if not filled in, would become permanent features of the drainage network. In this study, EGs in agricultural fields are defined as channels that tend to form during a precipitation event along natural drainage lines, when vegetation cover is minimal, and when concentrated flow of water has enough energy to detach soil. It was also observed that EGs can act as conduits to transport sediment originally detached from rills (Figure 4.2).

Figure 4.2 Ephemeral gullies as collector of sediment.

The importance of EG erosion is well established (Thorne et al., 1986; Poesen et al., 1996; Nachtergaele and Poesen, 1999; Poesen et al., 2003). Despite its importance, only few process-based erosion models have included EG subroutines. However, these models do not predict the location of EGs; location of each EG must be given as input to the model. Simple means of predicting the location of EG initiation is needed (Vandaele et al., 1996a; Vandekereckhove et al., 1998; Desmet and Govers, 1997; Knapan et al., 2010). Souchere et al. (2003) reported that the development of models that are able to predict location, length and cross-sectional area of EGs is of great importance.

The concept of a topographic threshold is widely used to predict locations in the landscape where gullies develop (Moore et al., 1988; Vandaele et al., 1996a; Vandekerckhove et al., 1998, 2000; Desmet et al., 1999; Knapan et al., 2010; Poesen et al., 2011). It was first

proposed by Horton (1945) and stated that a channel incision occurs when a threshold force is exceeded. Patton and Schumm (1975) first applied this concept to geomorphological study by examining the relationship between drainage area and valley slope for stable and unstable channel systems. Begin and Schumm (1979) combined the drainage area and valley slope by a shear stress indicator (τ) and reported that the channel initiation occurs above a threshold value of shear stress indicator (τ_{cr}) within uniform geomorphic and hydrologic conditions.

$$\tau = (c\ \gamma)\ A^{rf}\ S_v \tag{4.1}$$

where τ is a shear stress indicator (N/m^2), c is a constant, γ is the weight per unit volume of water (kg/m^3), A is drainage area (m^2), rf is an exponent, and S is valley slope gradient (m/m). Other studies used slope and drainage area to represent channel incision and have found that an inverse relationship exists between drainage area and local slope and is represented by power-type equation (Begin and Schumm, 1979; Vandaele et al., 1996a).

Another concept that is widely used to identify the location of EGs is unit stream power. The EG formation depends on "generation of concentrated surface runoff of sufficient magnitude and duration to initiate and maintain erosion, leading to channelization" (Thorne et al., 1984). Concentrated surface runoff can be represented by specific stream power, which is a function of discharge, slope and channel width. Drainage area multiplied by slope gives a parameter that can be used to represent total stream power (Desmet et al., 1999).

The importance of topographic parameters such as slope and drainage area in locating EGs is well established. Another topographic parameter, plan curvature or convergence, also contributes to EG formation as it provides the measure of the degree of flow convergence along the cross-section of a flow path (Zeverbergen and Thorne, 1987). Moore et al. (1991) indicated that slope (S), upstream drainage area (A) and plan curvature were primary topographic attributes that can be derived directly from Digital Elevation Models (DEMs) using Geographic Information System (GIS) in the form of regular raster grids. Primary topographic attributes were combined in some form (e.g., $S \cdot A_s$ or $\ln(A_s/S)$) to characterize the spatial variability of specific processes occurring in the landscape; these combinations of primary topographic attributes are commonly referred to as topographic index models, topographic indices, secondary topographic attributes, compound attributes, or compound indices (Moore et al., 1991). In this study topographic index models will be used to represent combinations of primary topographic attributes.

Several topographic index models were studied over the past few decades to predict the location of EGs. Thorne et al. (1986) used CTI (compound topographic index) model to predict EG formation:

$$t = S \cdot A \cdot PLANC \quad (4.2)$$

where t is a topographic EG index value, S is local slope (m/m), A is upstream drainage area (m^2), and PLANC is plan curvature (m/100). Parker et al. (2007) tested the CTI model to predict EG locations in a GIS environment for different sites and found out that the critical threshold for t values (T) varied from 5 to 62 depending on the study site, and the general pattern of EGs predicted did not change when T varied between 10 and 100.

Moore et al. (1988) used two methods to estimate EG location: SA (slope area index) model

$$t = S \cdot A_s \quad (4.3)$$

and WTI (wetness topographic index) model

$$t = \ln(A_s/S) \quad (4.4)$$

where t is a topographic EG index value, S is slope gradient (m/m) and A_s is unit upstream drainage area (m^2/m). Moore et al. (1988) found out that EGs were constrained to areas for which $\ln(A_s/S) > 6.8$ and $S \cdot A_s > 18$. Vandaele et al. (1996b) reported that the EG locations in a study area in south Portugal were better predicted using $\ln(A_s/S) > 9.8$ and $S \cdot A_s > 40$.

Vandaele et al. (1996a) used the SAP (slope area power index) model:

$$t = S \cdot A_s^{\,b} \quad (4.5)$$

where t is a topographic EG index value, S is slope gradient (m/m), A_s is unit contributing area (m^2/m) to locate EGs, and b is commonly assumed to be 0.4 (Vandalele et al., 1996a,b; Desmet et al., 1999). Vandaele et al. (1996a) tested the model in Kinderveld catchment in Spain and found out that $S \cdot A_s^{0.4} > 0.486$ (i.e., T = 0.486) was needed for locating initiation points of EGs. In separate studies, Desmet et al. (1999) reported that T = 0.75 and Vandaele et al. (1996b) reported that T = 1.0 performed better in predicting location of EGs in their study areas.

The topographic index models discussed above were used to locate the EGs. None of these studies used these topographic index model results to derive the length of an EG, even though the importance of length is well established (Woodward et al., 1999; Nachtergaele et al., 2001a, b; Capra et al., 2005; Gordon et al., 2007; Capra et al., 2009; Poesen et al., 2011). Length of an EG is considered to be an important parameter as it is needed as an input by process-based

models, such as EGEM and WEPP to estimate EG sediment losses (Woodward, 1999). Nachtergaele et al. (2001 a, b) reported that a strong correlation exists between EG length and volume of soil eroded. Length of an EG can also be used to estimate EG volume using simple models that relate length (L) to volume (V) (Capra et al., 2005; 2009; Poesen et al., 2011). Gordon et al. 2007 reported that topographic models are used to locate the potential EGs but there is no method currently available to predict EG length.

Therefore the goal of this study was to evaluate existing topographic index models (SA, CTI, SAP and WTI) in predicting EG location and length within agricultural fields according to two metrics: occurrence (presence or absence within a given area) and length (total accumulated length within a given area). Specific objectives were to (1) develop a GIS-based methodology to locate and derive length of EGs using existing topographic index models, (2) compare and evaluate the impacts of DEM resolution (2 m, 10 m, 30 m) and landuse data source (NASS, field reconnaissance) on EG occurrence and length predictions, and (3) evaluate the impacts of topographic index thresholds (T) on EG occurrence and length predictions.

4.2 Study Area

Two study areas where EGs are a major concern were selected. Study area 1 (S1) is located in Douglas County in north eastern Kansas, and study area 2 (S2) is located in Reno County in south central Kansas (Figure 4.3). The S1 has an area of 4,359 ha (10,771 ac) (cropland 43%) and S2 has 1,927 ha (4,762 ac) (cropland 81%). Grain sorghum and corn were the major crops in S1 whereas wheat was the major crop in S2. The EGs in S1 were smaller (mostly single EGs; average length: 210 m) and narrower whereas the EGs in S2 were larger (mostly branched EGs; average length: 408 m) and wider. Discussion on estimating length of EGs in the study areas is given in section 4.2.1.

Figure 4.3 Study areas (S1 and S2) and digitized ephemeral gullies.

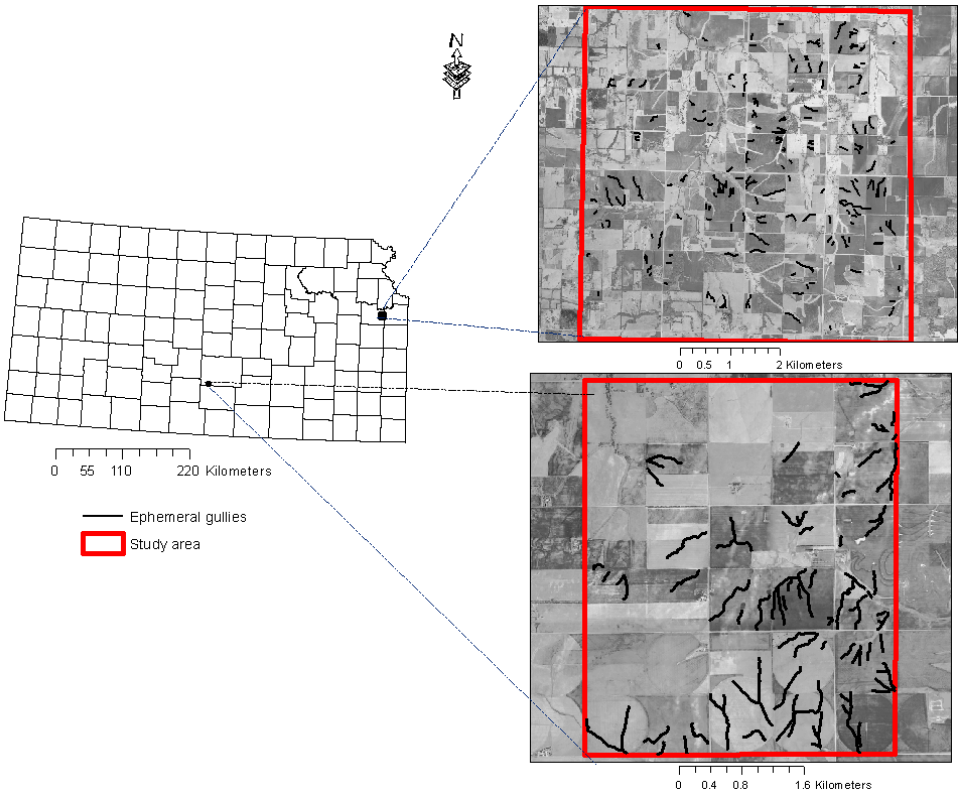

4.2 Methods

4.2.1 Digitizing EGs in study areas

EGs were seen in many agricultural fields across the study areas during field reconnaissance surveys in 2009 and 2010. Field measurements of EG characteristics (e.g., length, width, depth) were not possible because access to the agricultural fields in both study watersheds was limited, as land-owner permission was needed before entering fields. Because of this limitation, we drove on public roads in the study areas and recorded the fields that were observed to have EGs. During field visits, a Common Landuse Unit (CLU) field boundary shapefile was edited in ArcGIS on a laptop computer to record fields that had EGs. An Earthmate LT-40 GPS (Delrome, Yarmouth, ME) was used to determine the spatial location of the field. In the lab, the shapefile of fields that had EGs was overlaid on a corresponding aerial image. Various aerial images ranging from 1995 to 2011 were available in the study areas. The 2010 National Agricultural Imagery Program (NAIP) aerial image was selected for S1 and 2003 Digital Ortho Quarter Quadrangle (DOQQs) aerial image was selected for S2 because EGs were

clearly located on them; aerial images from other years were acquired during the crop growing season when a crop was fully established, and hence locating EGs on them was difficult.

EGs were manually digitized over the aerial images in the study areas in the fields where EGs were observed during field visits. Extreme care was taken in digitizing the trajectory of each EG located on the aerial image. Starting and ending points of an EG were difficult to determine precisely. Color changes on an aerial image and expert judgments of author were used to digitize accurately with an approximate 5% error. For example, the color of an EG located on an aerial image was white in a field otherwise colored green/brown/grey. The starting/ending point of an EG was chosen to be the point where color changed from green to white, and the EG digitization proceeded along the trajectory of the EG until the color changed from white back to the other color. Google Earth together with hill shade images (which enhanced the relief of the surface) were used to verify/cross check the location during digitizing process. Many EGs (69% in S1 and 38% in S2) were seen on the aerial image within the study area but were not visible from the windshield during the field visit for several reasons: (1) EGs were located far away from roads or obscured by topographic features, (2) there were established crops concealing the EGs during field visit, or (3) multiple EGs were located within one field. EGs that were located on the aerial image but were not seen during field visit were also digitized. Since this study compared model simulated EGs to observed EGs (i.e., digitized EGs on aerial image), including all EGs was considered justifiable. Finally, the digitized EGs were used as observed or reference data to evaluate performance of the topographic index models.

4.2.2 EG topographic index models and thresholds

Four widely used EG topographic index models were used to predict EG location (Table 4.2). EG topographic index models determine presence or absence of an EG at each point (i.e., in a pixel) within a given area for which topographic EG index value (t) (Eqs. 4.2 through 4.5) exceeds a threshold value (T). For each topographic index model, three T values spanning the range of thresholds reported in literature were used to predict EG location (Table 4.2).

Table 4.2 EG topographic index models and thresholds tested in S1

Model	Equation	Thresholds (T)			References
SA	$t = S \cdot A_s$ (Eq. 4.3)	5	18	40	Moore et al. (1988); Vandaele et al. (1996a)
CTI	$t = S \cdot A \cdot PLANC$ (Eq. 4.2)	12	62	100	Thorne et al. (1986); Parker et al. (2007)
SAP	$t = S \cdot A_s^{0.4}$ (Eq. 4.5)	0.3	0.5	1	Vandaele et al. (1996a,b); Desmet et al. (1999)
WTI	$t = \ln(A_s/S)$ (Eq. 4.4)	6.8	9.8	12	Moore et al. (1988); Vandaele et al. (1996b)

S – Local slope (m/m)
A – Upstream drainage area (m^2)
As – Upstream contributing area per unit contour length (m^2/m)
PLANC – Plan curvature (m/100)

4.2.3 Data inputs for topographic index models

A DEM provides key data needed for topographic index models. Topographic attributes such as slope, upstream drainage area, and plan curvature are directly derived from DEMs. The common data structure of DEM is a square grid, because this raster format has efficiency of computation and ease of processing (Tarboton et al., 1991). DEMs generally are available at different resolutions. Coarse 10 m and 30 m resolution DEMs are readily available to download for entire United States from U. S. Geological Survey (USGS) website (http://seamless.usgs.gov/). Finer resolution DEMs, such as Light Detection And Ranging (LIDAR) (e.g., 2 m resolution DEM), are available only in a few selected areas within United States. Many studies have investigated the impact of DEM resolution for evaluating model responses to change in topographic attributes and have concluded that DEM resolution substantially affects topographic attributes and thereby model results (Holmes et al., 2000; Chaubey et al., 2005; Parker et al., 2009; Momm et al., 2011).

Impacts of DEM resolution (2 m, 10 m, and 30 m) on the performance of topographic index models to correctly predict EG location were evaluated. DEMs of 2 m, 10 m and 30 m resolution for S1 were downloaded from USGS website (http://seamless.usgs.gov/website/seamless/viewer.htm) and were used as inputs to the topographic index models. Cheney Lake watershed, which includes study area S2, has 1 m LIDAR data. To maintain consistency between the study areas (only 2-m DEM was available for S1), the 2-m DEM was resampled (nearest neighbor assignment technique) from the 1-m DEM for use in this study.

In this study only EGs within agricultural fields were of interest. Therefore, landuse was used to mask out areas other than agricultural fields. Daggupati et al. (2011) reported that landuse has a major impact on modeling results for field-scale targeting. Therefore, this study evaluated the impacts of USDA National Agricultural Statistical Service (NASS) and field reconnaissance landuse (field) data sources on the performance of topographic index models to correctly predict EG location within agricultural fields . NASS 2010 landuse, which was downloaded from USDA-NASS website (http://www.nass.usda.gov/), was used. From Section 2.3.1, it is seen that NASS predicts rangeland pixels in the middle of agricultural land due to training and classification errors. However, in this study, the errors were corrected using GIS techniques, such as resampling (nearest neighbor assignment technique) and expanding, and a corrected NASS landuse was used. Field landuse was manually prepared in S1 by digitizing field boundaries over high resolution aerial image. Care was taken so that waterways were not included in the digitized landuse. In S2, field landuse was developed using CLU field boundary shapefile. In both study areas, land cover for each field was manually edited based on a field reconnaissance survey and using NASS 2010 landuse as reference.

4.2.4 Methodology to locate EGs

An automated geospatial model was built in GIS environment (ArcGIS v.10) using model builder platform (Figure 4.4) to locate EGs for each of the topographic index models. The geospatial model requires elevation (DEM), landuse and roads as inputs. Once the inputs are satisfied, the model calculates topographic attributes such as local slope, upstream drainage area, unit upstream drainage area, and plan curvature from the DEM.

Pits are small depressions within the DEM that interrupt flow networks. Generally, these small DEM depressions are filled for watershed analyses as they hinder flow-path determination and, therefore, derivation of other hydrologic parameters. But in the process of filling, many natural depressions that are important to EG formation also get filled. Therefore, the process of pit removal was not applied to the DEM. Recent studies on gullies by Kim (2007) and Bussen (2009) also did not fill DEM pits. Local slope in percent (%) was computed using deterministic eight direction (D8) algorithm (O'Callagham and Mark, 1984), and later the percent slope was divided by 100 to get local slope in m/m. The flow direction and flow accumulation grids were also computed using the D8 method. Flow accumulation for each cell, calculates the cells that

are upstream to a given cell. Drainage area (m^2) was calculated by multiplying the number of cells accumulated by the cell area (square of the cell resolution). Unit upstream drainage area (m^2/m) was calculated by dividing the drainage area (m^2) by cell resolution (m) of the DEM. The plan curvature (m/100) was calculated using a method proposed by Zeverbergen et al. (1987) and Moore et al. (1991). At a given cell, a positive value indicates that the surface is convex, negative value indicates concave, zero value indicates flat (ESRI, 2011). The plan curvature was multiplied by -1 to convert it to a more easily usable (positive) value for calculating EG topographic indices, since EGs form only in areas of negative plan curvature. Once the required topographic parameters are generated, the geospatial model calculates the topographic index value (t) for each pixel in the study area, and compares that value to the user-defined thresholds (T) for the topographic index model being used. If the pixel value of t was greater than T then the EGs were located in the form of pixels on the output raster (Figure 4.5). Since our interest was to identify EGs only in agricultural fields, the geospatial model uses landuse and roads to clip out non-agricultural areas.

Figure 4.4 Geospatial model for locating EGs using four different topographic index models.

Figure 4.5 Ephemeral gullies (EGs) located as pixels in an agricultural field in study area 1 (S1).

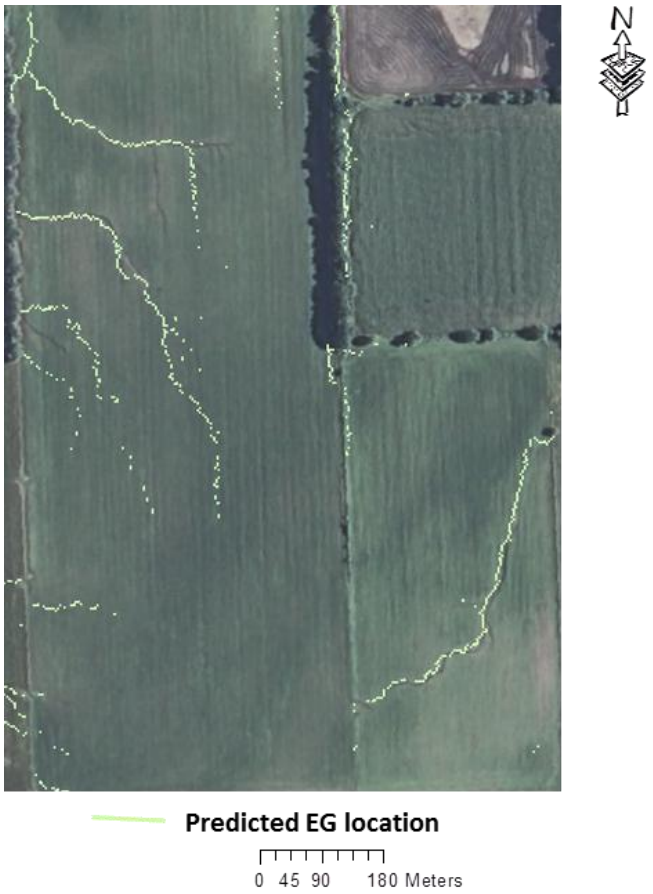

4.2.5 Methodology to estimate EG length

Several post processing techniques were developed to derive length of EGs from the output raster (generated for each topographic index model from the geospatial model discussed above) using following steps.

- Pixels that represent EGs in output raster of a topographic index model were converted into a polyline shapefile (Figure 4.6.a).
- The polylines within the trajectory of an EG were sometimes disconnected (Figure 4.6.a) (i.e., some points along an apparent EG trajectory did not meet the given threshold). To make the polylines continuous within the trajectory of an EG, the polylines were "snapped" to each other using a snapping rule of 5 m (i.e., two lines that were 5 m apart, or less, were joined) (Figure 4.6.b). Higher snapping distance (> 5 m) resulted in lines snapping to other lines that were not part of the EG trajectory

and hence distorting the shape along the trajectory (most prevalent in branched EGs). Hence, snapping distance greater than 5 m was not used in this study.

- The length of the polylines were calculated, and lengths smaller than 10 m were removed (Figure 4.6.c).
- At this point, each polyline had its own identification number, and many EGs were represented by multiple polylines. Catchments were developed separately using the DEM (blue lines Figure 4.6.d), and each individual polyline within a catchment was given a unique id (Figure 4.6.d). The size of the catchment is user defined and can be varied. In this study 1 hectare catchments were used. All individual polylines within a catchment were dissolved to one single polyline, and was considered as an EG with a unique id.
- EGs smaller than 50 m were removed.

Figure 4.6 Steps in deriving the length of ephemeral gullies (EGs): (a) EG raster converted to polyline, (b) polylines snapped, (c) length of EGs calculated and smaller lengths <10 m deleted, and (d) EGs were given unique id. Black polylines represent EGs, and blue polygons represent EG catchments.

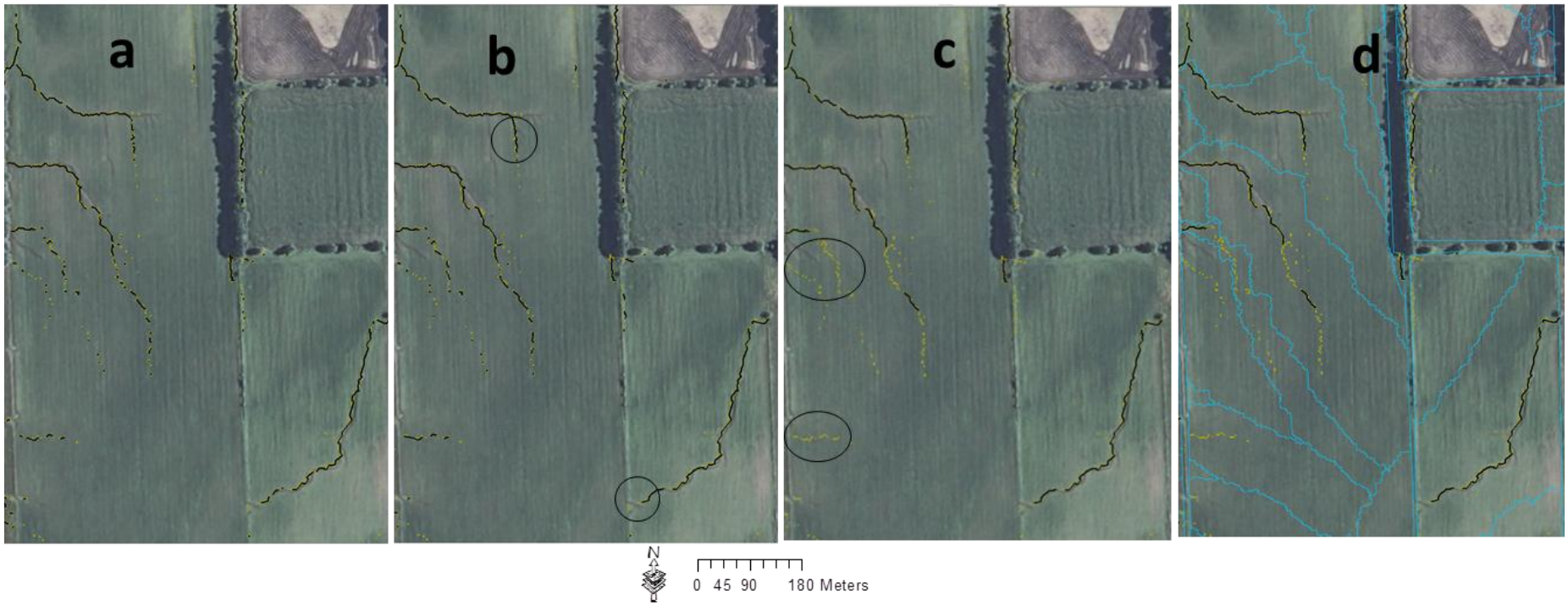

Several EGs were long and branched, as shown in the Figure 4.7. In such cases, the size of catchment can be increased (so that it includes the entire branched EG) or the catchments can be manually edited to capture branched EGs. However, in this study no changes were made to the catchment size. Thus, each segment of the branched EG in a different catchment was considered a separate EG. Currently available process-based models (e.g., EGEM, REGEM) that simulate EG erosion are capable of simulating un-branched EGs only (i.e., each branch was calculated by a separate pass through the computer program). Therefore, single EGs developed using this method can be used as direct input to those models to estimate EG erosion.

Using the above mentioned steps, EGs were given a length and a unique identification number so that they can be used either as input to the process-based model or to estimate volume using L-V relations. It should be noted that lengths obtained by this method are potential lengths derived from topographic attributes and do not consider any processes occurring during the formation of EGs. Also, it should be noted that some discontinuity within lengths may still exist along an EG trajectory. The above mention steps are tedious; therefore, an automated geospatial model was developed in ArcGIS environment using model builder platform (Figure 4.8) to derive the length of EGs.

Figure 4.7 A branched ephemeral gully (EG) in an agricultural field in study area 1 (S1).

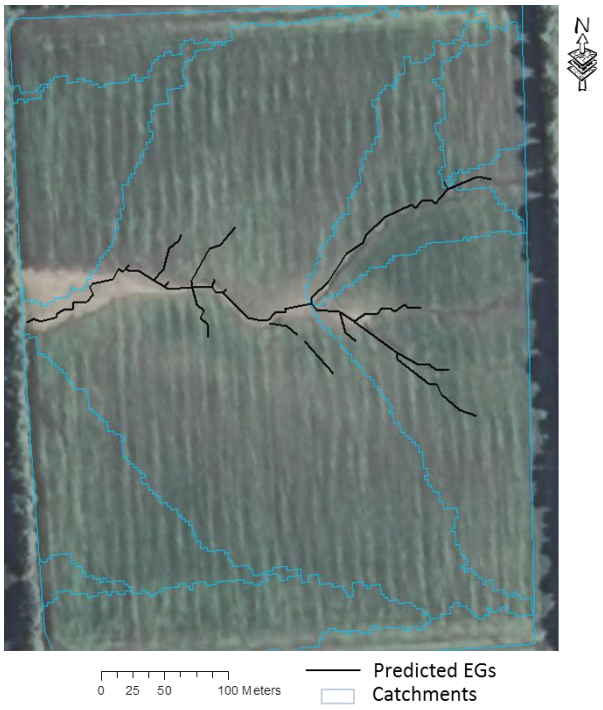

Figure 4.8 Geospatial model for estimating ephemeral gully length.

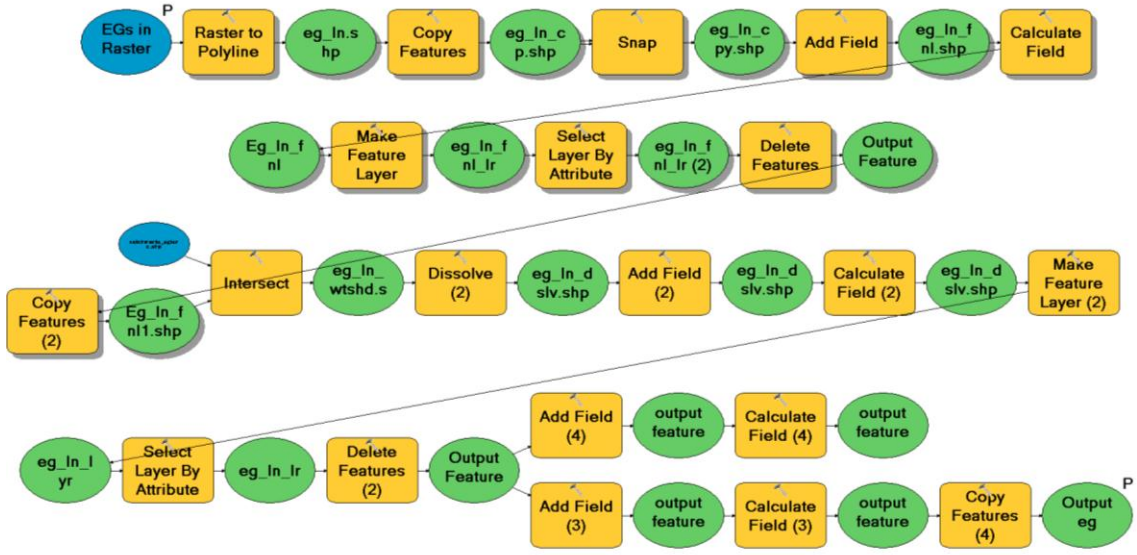

4.2.6 Evaluating the performance of topographic index models

Each of the topographic index models first identifies EGs location in the form of pixels, and later lengths were derived using several post processing techniques. Each topographic index model capability to predict location and length was assessed by three methods: 1) visual evaluation of EG trajectories, 2) error-matrix assessment of model performance in correctly identifying EG occurrence (presence or absence) within a given area, and 3) statistical assessment of model performance in correctly identifying EG length (total accumulated length) within a given area.

4.2.6.1 Visual evaluation of location and lengths

There is no established method to compare and evaluate the performance of topographic index models. Desmet et al. (1999) compared percentage of predicted EG pixels that corresponded to the location of observed EG pixels. Parker et al. (2007) used visual interpretation by comparing potential EGs pixels generated by the model to observed EGs pixels. In this study, location of EG (model predictions along the trajectory) and derived lengths was evaluated using visual interpretation. Visual interpretations gives a general understanding of each model performance.

4.2.6.2 Occurrence evaluation

Statistical analysis using an error matrix approach was carried out to evaluate the occurrence (presence or absence) of EGs in a given area. Error matrix (also called confusion matrix, correlation matrix, or covariance matrix) summarizes the relationship between two datasets: often an observed dataset and a predicted dataset. Error matrix is often used in medical and biological sciences. It is also used in reporting the accuracy of landuse data (e.g., NASS and NLCD) based on ground truth data. Error matrix approach was used by Gutierrez et al. (2009) and Meyer and Martinez-Casosnovas (1999) to predict the location of gullies in rangeland for models developed by regression analysis using observed gully data.

In this study, we used the presence-absence model of the error matrix (Table 4.3). One-hectare catchments within agricultural fields were used. Occurrence of an EG within a catchment was treated as a binary variable (1: presence and 0: absence) for each catchment based on predicted and observed EGs present within that catchment. For example, 1 and 1 were recorded in the catchment attribute table under the predicted and observed columns if both predicted and observed EGs were present in a catchment, 1 and 0 for predicted EG present and observed EG absent in a catchment, and so on. The observed EGs are the digitized EGs over an aerial image based on field reconnaissance survey, and the predicted EGs are the EGs generated by each of the topographic index models. Finally, the error matrix recorded the frequencies of the four possible types of prediction from analysis of predicted and observed EGs for each catchment (Table 4.3): (a) true positive (both predicted and observed EGs are present), (b) false positive (predicted EGs present and observed EGs absent), (c) false negative (observed EGs present and predicted EGs absent), and (d) true negative (both predicted and observed EGs absent). Frequencies are recorded in an error matrix using Table 4.3 format for each topographic index model. All the processes discussed above were automated using a geospatial model in GIS environment (ArcGIS v.10) using model builder platform (Figure 4.9) and the output of error matrix table was generated in Excel format.

Several statistics (Appendix B) can be calculated using the error matrix table. In this study, false positive rate, false negative rate, and kappa (κ) statistics (occurrence statistics) were used to evaluate the topographic index model performance. Correct classification rate is generally used to predict the accuracy of a model; however, this statistic is very simple and sometimes misleading. In this study κ was used to predict the accuracy of a model. A good

model should have higher κ with optimal (lower) false positive and false negative rates. Higher false positive rate does not necessarily indicate model error because the model may be indicating areas or catchments with high vulnerability to gullying, but the processes have not developed yet. However, high false negative rates are considered to be an error in model performance (Gutierrez et al., 2009).

Figure 4.9 Geospatial model to develop error matrix table.

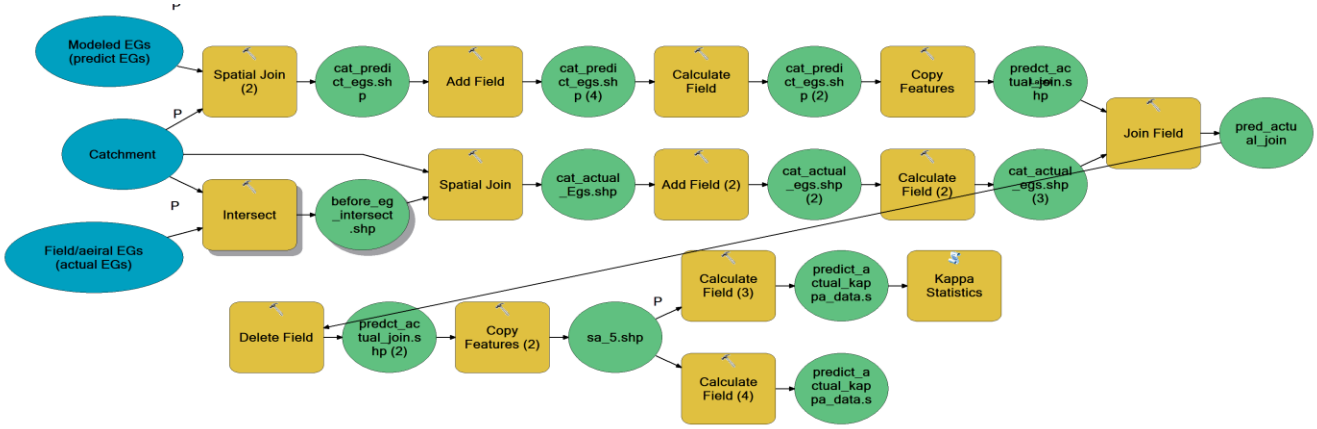

Table 4.3 Error matrix table to evaluate the occurrence (presence or absence) of EGs in a catchment

Error Matrix		Actual		Totals
		present	absent	
Predicted	present	a (true positive)	b (false positive)	a+b
	absent	c (false negative)	d (true negative)	c+d
Totals		a+c	b+d	**N**

N: Total number of catchments; a: no of catchments in which both observed and predicted EGs present; b: number of catchments where only predicted EGs present and observed EGs absent; c: number of catchments where observed EGs present and predicted EGs absent; d: number of catchments where both EGs absent.

4.2.6.3 Length evaluation

There is no standard procedure to evaluate the EG length derived from topographic index models. In this study, we compared the total cumulative predicted length of EG generated by the topographic index model to that of the observed EG length (digitized over aerial images) in each catchment for which both predicted and observed EGs were present (‘a’ column in error matrix

table). The data needed for analyzing the length are generated using an automated geospatial model (Figure 4.10).

Statistics (length statistics) used for comparison are coefficient of determination (R^2), Nash-Sutcliffe efficiency (NSE), and estimation bias (PBIAS). The above statistics are generally used to evaluate watershed model (such as SWAT, AnnAGNPS, etc.) performance based on measured and model predicted flow data (Moriasi et al., 2007) and are discussed in detail in Section 2.3.4 and 3.2.5. NSE and R^2 value of one indicates perfect model fit where predicted lengths by model are closer to the observed or digitized lengths. The optimal value of PBIAS is 0, with low-magnitude values indicating accurate model predictions. Positive values indicate model underestimation bias, and negative values indicate model overestimation bias

Figure 4.10 Geospatial model to generate data for length analysis in catchments where both observed and predicted ephemeral gullies are present.

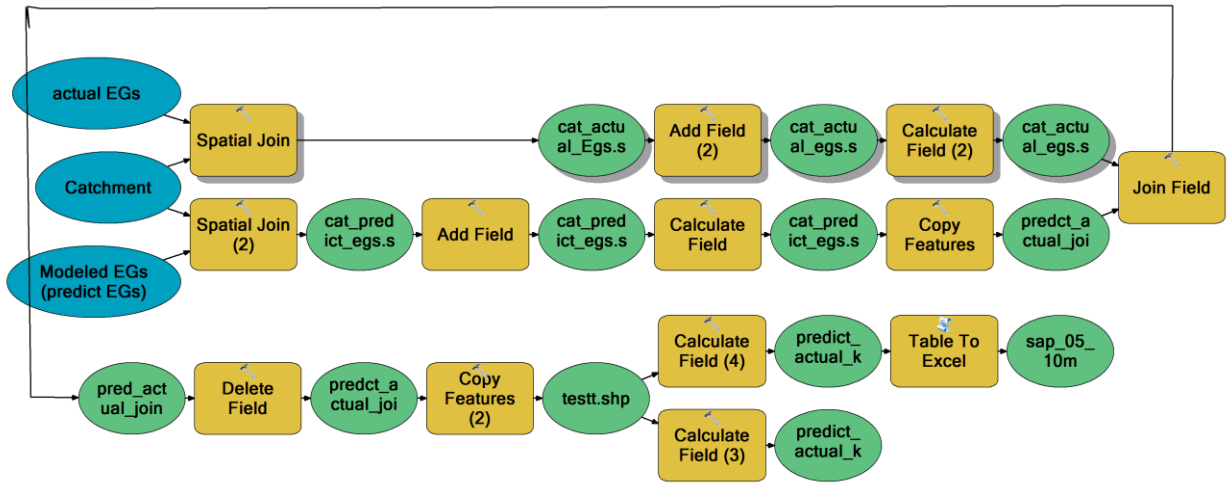

Each topographic index model along with a corresponding threshold (Table 4.2) was evaluated using the above mentioned location, occurrence and length evaluation procedures in S1. DEM resolution (2 m, 10 m, 30 m) was compared and evaluated using all topographic index models while the Landuse (NASS, Field) was compared and evaluated using SA and CTI models. The best topographic index model, DEM resolution, and landuse data source were selected and were further evaluated using a range of thresholds in S1 to understand how thresholds affected topographic index model performance in predicting occurrences and lengths of EGs. Further, the best topographic index model was applied in S2 to evaluate how the thresholds affected topographic index model performance in a different geographic location.

4.3 Results and Discussions

4.3.1 Visual interpretation of location and lengths of EGs

Figure 4.11 shows output maps of location and derived lengths for SA (Eq. 4.3, T = 18), CTI (Eq. 4.2, T = 62), SAP (Eq. 4.5, T = 0.3) and WTI (Eq. 4.4, T = 12) models using the given thresholds (T value noted for each equation) with 2 m DEM and field landuse. The visual interpretations of the output maps showed that the SA and CTI models predicted the EG location (in the form of pixels along the trajectory of the observed EGs) better than SAP and WTI models (Figure 4.11) for given thresholds.

Figure 4.11 Output maps of location and derived lengths for SA, CTI, SAP, WTI model in an agricultural field in study area 1 (S1).

(a) Aerial image (left) and digitized EGs (right)

(b) Location (left) and derived lengths (right) for SA model (Eq. 4.3, T = 18)

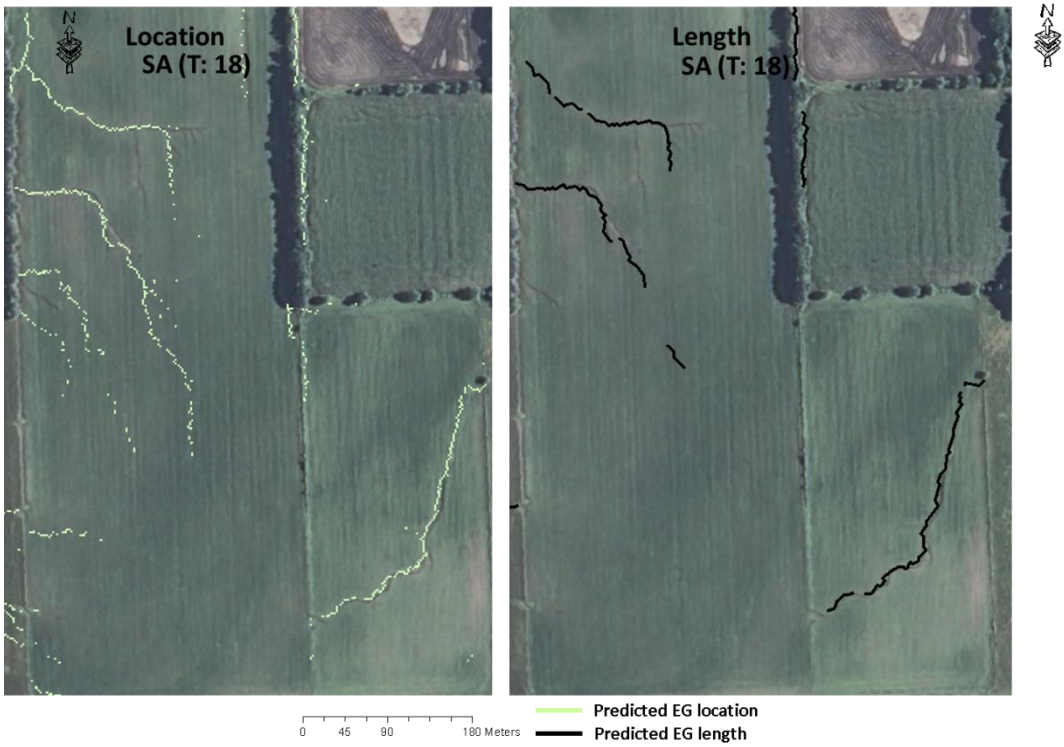

(c) Location (left) and derived lengths (right) for CTI model (Eq. 4.2, T = 62)

(d) Location (left) and derived lengths (right) for SAP model (Eq. 4.5, T = 0.3)

(e) Location (left) and derived lengths (right) for WTI model (Eq. 4.4, T = 12)

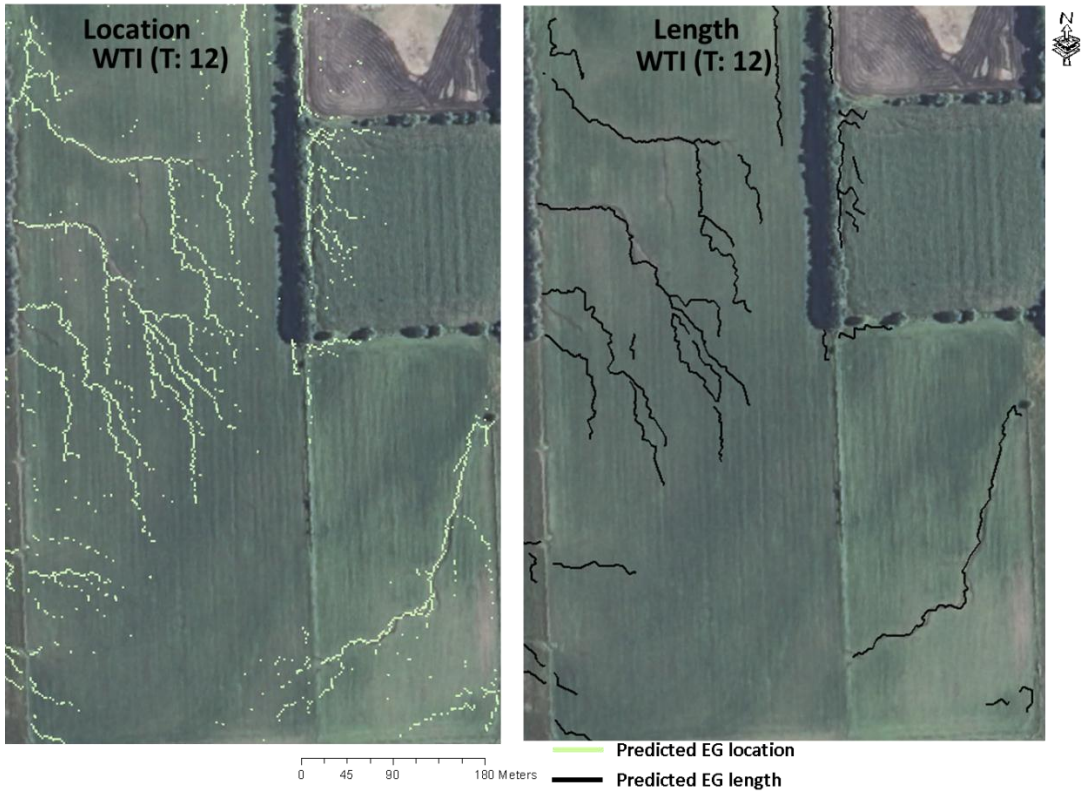

The WTI model was not able to predict the location of EGs in our study area using T = 6.8 and T = 9.8, although these thresholds successfully predicted EG location in another region (Portugal and Australia: Vandaele et al., 1996b; Moore et al., 1988). Increasing the T to 12 improved predictions of EG locations. Momm et al. (2011) also used T = 12 as threshold in a small field in Kansas for WTI model to locate EGs. However, T = 12 tends to over-predict the location of EGs. Increasing the threshold would have improved the predictive capabilities; however, such simulations were not done in this study.

The SAP model under-predicted the location of EGs for all three thresholds tested. Desmet et al. (1999) reported that lower values of b in the SAP model (Eq. 4.5) better predicted EG initiation points. In our study we used b = 0.4 in the SAP model, which may have contributed to this poor performance.

SA and CTI models have similar pattern in predictions because both models have a strong influence of slope and upstream drainage area, and a strong positive correlation exists between upstream drainage area and plan curvature (which was included in CTI only). However, closer observations revealed that the CTI model predictions were more discontinuous along the trajectory (Figure 4.12). Discontinuity using CTI model was due to the inclusion of plan curvature, which identifies the areas of reduced flow convergence in the landform topography and removes those pixels from the model predictions (Parker et al., 2007). Parker et al. (2007) reported that the CTI model is a better model to locate EGs, as this model is capable of removing areas with reduced flow convergence.

Figure 4.12 Closer observation of CTI model along the trajectory of EG (right). Light blue arrows (left) show discontinuity along the trajectory of the EG

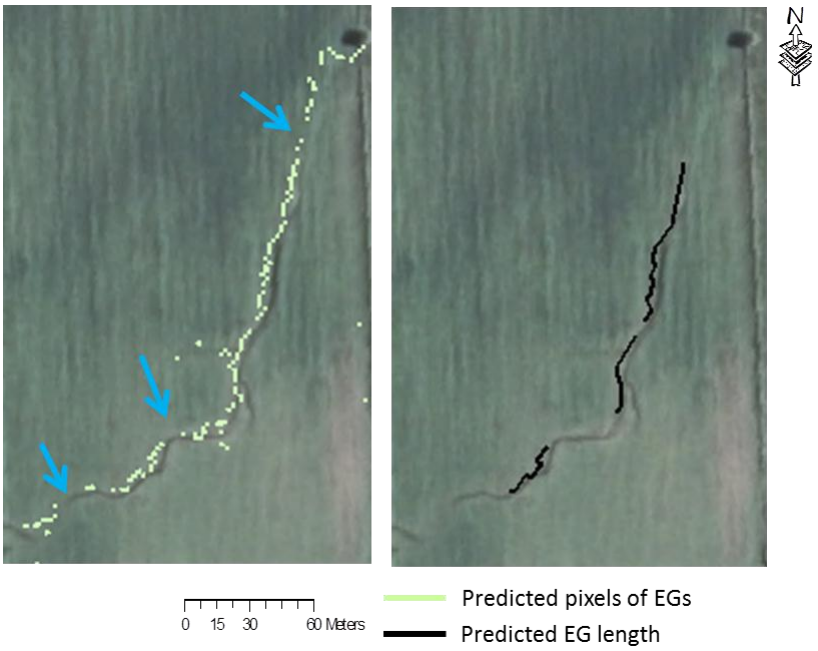

Field observation of EGs by the author during precipitation events revealed that the EGs were discontinuous initially, since flow rate was not enough to maintain concentrated flow within the areas of reduced flow-convergence along the EG trajectory; however, the EGs become continuous as the precipitation event progressed and flow rate increased. During an EG-forming precipitation event, the precipitation excess is stored as puddles along the natural drainage line (or flow-convergence line). As the precipitation event progresses, the puddles collect water from upstream rills as well as from nearby furrows. The puddles of water gradually join and a continuous stream forms along the natural drainage line. Soil erosion occurs within the drainage line, which leads to formation of an EG. This EG lengthens until the flow path intersects an area of reduced flow convergence within the natural drainage line. Similarly, EGs form along different segments of a given natural drainage line. With more precipitation excess, flow from upstream EG segments increase to the point that erosion occurs within the area of reduced flow convergence and connects upstream and downstream EG segments. The flow volume increases as it moves downstream resulting in widening and deepening of the EG. With enough flow, an EG finally becomes continuous along a drainage trajectory. The underlying processes within the formation of EG are more complex than discussed here. Several researchers around the world are still trying to understand the processes underlying the formation of these EGs.

Figure 4.11 shows the lengths derived from location predictions for each topographic index model for selected thresholds. Visual interpretations revealed that WTI (Eq. 4.4) and SAP (Eq. 4.5) models were not able to predict length correctly along the EG trajectory. The CTI (Eq. 4.2) model was also not able to predict the length due to its greater discontinuity of pixels along the trajectory (Figure 4.12), which was discussed earlier. The methodology developed in this study to derive lengths overcame small discontinuities by snapping together EGs separated by 5 m or less. The SA (Eq. 4.3) model predictions appeared to be better than other topographic index models. Similar length predictions were seen for other thresholds.

4.3.2 Occurrence analysis using error matrix

Error matrix tables were developed, and statistics of false positive rate and false negative rate were used to analyze the performance of each topographic index model and their corresponding thresholds, DEM resolution, and landuse data source in S1 (Table 4.4).

4.3.2.1 Impacts of DEM resolution

The false positive rate decreased from 54% to 1% and false negative rate increased from 21% to 97% as the DEM resolution increased from 2 m to 30 m for T = 5 in the SA model (Table 4.4). Similar trend was seen in other thresholds in SA model and also in other topographic index models (CTI, SAP, and WTI). Higher false negative rates and lower false positive rates with 10 and 30 m DEM resolutions indicated poor model performances. Comparison of 2 m vs. 10 m vs. 30 m DEM resolutions using output maps revealed that 10 m and 30 m DEM resolutions greatly underestimated EG occurrence compared to 2 m DEM resolution (Figure 4.13)

Figure 4.13 EG occurrence comparison for 2 m, 10 m, 30 m DEM resolutions.

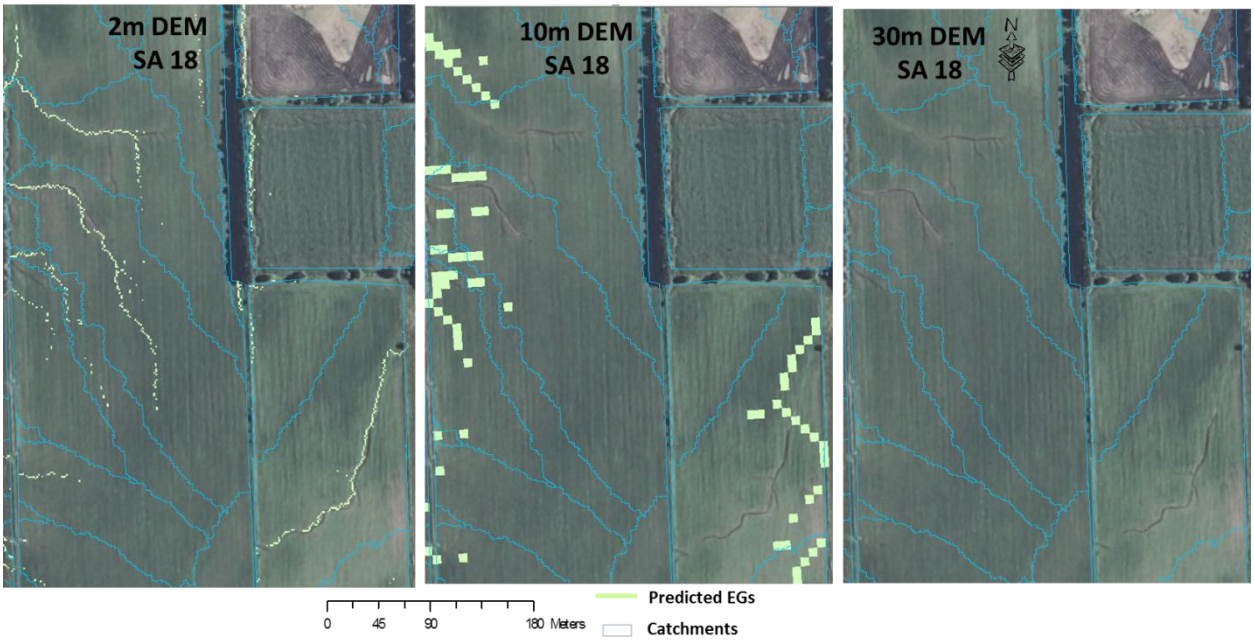

4.3.2.2 Impact of Landuse

The false positive rate either slightly decreased or remained same and the false negative rate increased as the landuse changed from field to NASS in SA and CTI models for all thresholds. The NASS landuse was rectified using GIS techniques so that pixels representing rangeland in the middle of agricultural fields were resampled with surrounding majority pixels. However, there were still a few fields that were incorrectly predicted as rangeland (i.e., were found to be agricultural fields from field reconnaissance). Because of this error, the EGs were not predicted by the model even though there were observed EGs present, which thereby slightly increased false negative rates.

In this study, the catchments within agricultural fields were used (i.e., the catchments were clipped to field landuse so that grassed waterways, forested lands etc. were not included), resulting in relatively similar false positive rates among the NASS and field landuse data sources. However, the NASS landuse data source predicted EGs in the waterways and forested areas by the side of agricultural fields (Figure 4.14). In this analysis, these EGs were not considered. Therefore, the users should be aware that NASS landuse predicts EGs when they not actually present (e.g., in waterways) and do not predict EGs when they are actually present (e.g., cropland misclassified as rangeland).

Table 4.4 Occurrence statistics for four different topographic index models

Threshold	SA Method					Threshold	CTI Method				
	Statistics	2 m		10 m	30 m		Statistics	2 m		10 m	30 m
		Field	NASS	Field	Field			Field	NASS	Field	Field
5	False positive rate	54%	52%	25%	1%	**12**	False positive rate	35%	30%	7%	0%
	False negative rate	21%	27%	37%	97%		False negative rate	18%	36%	65%	98%
18	False positive rate	27%	25%	8%	-	**62**	False positive rate	9%	9%	2%	-
	False negative rate	21%	37%	66%	-		False negative rate	32%	47%	95%	-
40	False positive rate	10%	10%	3%	-	**100**	False positive rate	5%	6%	1%	-
	False negative rate	38%	43%	83%	-		False negative rate	51%	62%	95%	-

Threshold	SAP Method				Threshold	WTI Method			
	Statistics	2 m	10 m	30 m		Statistics	2 m	10 m	30 m
		Field	Field	Field			Field	Field	Field
0.3	False positive rate	7%	6%	0%	**6.8**	False positive rate	-	-	-
	False negative rate	49%	83%	100%		False negative rate	-	-	-
0.5	False positive rate	1%	1%	-	**9.8**	False positive rate	-	-	-
	False negative rate	86%	96%	-		False negative rate	-	-	-
1.0	False positive rate	0%	0%	-	**12.0**	False positive rate	34%	10%	5%
	False negative rate	98%	100%	-		False negative rate	23%	60%	80%

Figure 4.14 EGs predictions in waterways when using NASS landuse.

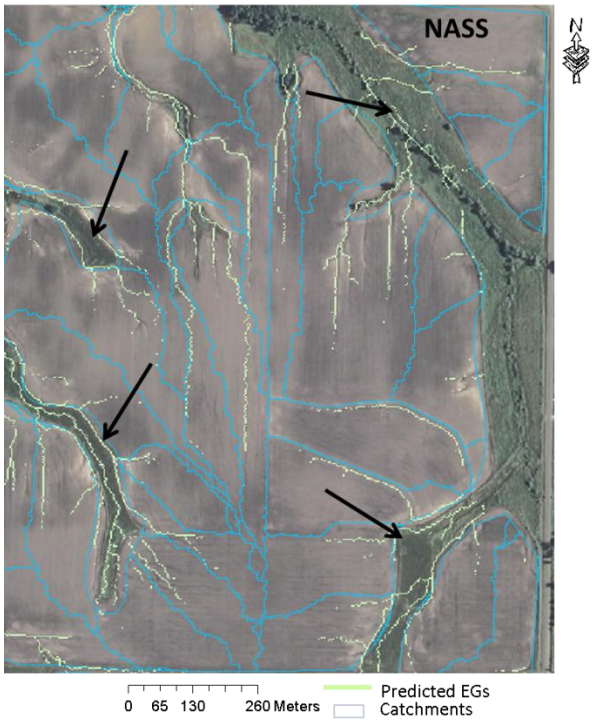

4.3.2.3 Impact of Thresholds

The false positive rate decreased from 54% to 10% and false negative rate increased from 21% to 38% as thresholds increased from 5 to 40 in the SA model using field landuse and 2 m DEM resolution (Table 4.4). Optimum false positive and false negative rates (lower values of false positives and false negatives) were seen for T = 18. However, further investigation of the role of thresholds in correctly predicting the occurrence and length of EGs is discussed below. Similar trends were also seen in the case of the CTI model, in which there was a decrease in false positive rate and increase in false negative rate as the threshold increased from 12 to 100. Optimum false positive and false negative rates were not found with the selected thresholds in case of CTI. The CTI model also resulted in higher false negative rates. Because it could not predict the location along the trajectory (seen earlier), the performance of the CTI model was considered poor.

In the case of SAP model, false positive rate decreased from 7% to 0% and false negative rate increased from 49% to 98% as thresholds increased from 0.3 to 1.0 (Table 4.4). Optimum false positive and false negative rates were difficult to obtain as this model was used to locate the

initial location of EGs not the trajectories (discussed earlier). Hence the performance of this model was also considered poor. In the case of WTI model, thresholds of 6.8 and 9.8 could not predict the locations, resulting in no statistics being calculated. However the model predicted locations using T = 12.0. The false positive rate was 34%, and false negative rate was 23% (Table 4.4). Both false positive and false negative rates were near optimum, and increasing the threshold further may have improved the model predictions (but was not done in this study).

The results show that the error matrix approach (occurrence analysis) produces a similar result as visual interpretation. Also, the importance of thresholds in EG predictions was well established. Further analysis to examine thresholds using SA model is discussed below.

4.3.3 Length Analysis

Catchments in which both observed and predicted EGs were present were extracted and compared using NSE, R^2 and PBIAS for all models and their corresponding thresholds using 2 m DEM and field landuse (Table 4.5).

SA model with T = 5 resulted in poor model agreement while T = 18 and 40 resulted in very good agreement based on R^2, NSE and PBIAS statistics (Table 4.5). In the case of CTI model, T = 12 resulted in poor model agreement while T = 62 and 100 resulted in good agreement (Table 4.5). Increase in thresholds resulted in good agreement in both model predictions. The model agreement for SA model was better compared to CTI model for higher thresholds based on statistics. The inclusion of plan curvature in the CTI model resulted in discontinuity and thereby lower EG lengths (discussed earlier), which led to the observed poor agreement compared to SA model.

In the case of the SAP model, model agreements were good despite the poor results found from occurrence statistics (Section 4.3.2). The reason for this is due to the fact that only catchments in which EGs (both predicted and observed) were present were considered for analysis, and the SAP model had very few catchments with EGs (both predicted and observed) present (103 for T = 0.3, 26 for T = 0.5 and 5 for T = 1.0). Because of this, the statistics appeared better, however, as seen earlier, the model predictions by SAP model is not capable of predicting location of EGs along the trajectory and had poor occurrence analysis results. Therefore, even though the length statistics were better, the model performance was considered poor. WTI model

with T = 6.8 and 12.8 did not yield results because no EGs were predicted at those thresholds. However, T = 12 resulted in poor model agreement.

Table 4.5 Coefficient of determination (R^2), Nash-Sutcliffe model efficiency (NSE) and percent bias (PBIAS) for all four topographic index models and their corresponding threshold (T) values in the S1 study area

Statistics	SA	CTI	SAP	WTI
	T = 5	T = 12	T = 0.3	
R^2	0.11	0.56	0.21	-
NSE	-6.14	-0.04	0.66	-
PBIAS (%)	-194.2	-79.7	20.4	-
	T = 18	T = 62	T = 0.5	
R^2	0.58	0.45	0.15	-
NSE	0.66	0.48	0.53	-
PBIAS (%)	-41.4	60.2	54.5	-
	T = 40	T = 100	T = 1.0	T = 12
R^2	0.53	0.41	0.37	0.27
NSE	0.86	0.60	0.72	-0.35
PBIAS (%)	14.6	65.3	41.3	-59.7

4.3.4 SA Model analysis using different thresholds

Occurrence and length statistics revealed that threshold values play a major role in predicting the occurrence and length of EGs. Further analysis of the SA model, which was the most promising from the above analyses (Section 4.3.1 through 4.3.3), was used to explore response to varying thresholds in study area S1 (and verified in S2).

The SA model was analyzed using thresholds of 10, 18, 25, 30, 40, 50, 70, 100, 150 and 200 in S1. For each threshold, the SA model was executed using 2 m DEM and field landuse. The model performance was evaluated using occurrence and length statistics procedures discussed earlier. Figure 4.15 shows the statistics of false positive rates, false negative rates, and κ for each of the threshold analyzed in a graphical format. The false positive rates rapidly decreased from 38% to 7% as T increased from 10 to 50 and on further increase of T from 50 to 200 resulted in gradual decrease to 1%. The false negative rates gradually increased from 20% to 25% as T increased from 10 to 30 and as T increased further from 30 to 200 there was a rapid increase from 25% to 89%. The κ rapidly increased from 0.22 to 0.46 as T increased from 0 to

30, attained a peak of 0.48 at T = 50, and gradually decreased to 0.15 as T increased to 200. Increase in T value resulted in a decreased number of pixels meeting the critical threshold value, resulting in reduced lengths predicted by the model. Because of this, number of EGs predicted decreased, resulting in lower catchments predicting the presence of EGs even though there were observed EGs present and hence resulting in higher false negative rates. Increase in thresholds (resulting in reduced length predicted by model) also results in lower number of catchments where predicted EGs present while the observed EGs were already absent resulting in lower false positive rates.

In studies related to EGs, the thresholds which results in lower false positive and false negative rates and higher κ better predict the occurrence of the EGs. False positives improved (decreased) as T increased, but the reverse trend was observed for false negatives, which became worse (increased) as T increased. Thresholds from 18 to 30 resulted in near-optimum false negatives, and T = 25 to 40 produced near-optimal κ (Figure 4.15). Higher κ was seen at T = 50, but false negatives were also higher than for lower T values. From Figure 4.16, T = 25 and 30 was close to best fit line, however, T = 30 crosses the best fit line and the statistics of NSE and PBIAS were better for T = 30 (NSE: 0.86; PBIAS: 5.2%) compared to T = 25 (NSE: 0.83; PBIAS: 13.8%).

Figure 4.15 Occurrence statistics for different thresholds using SA model in S1.

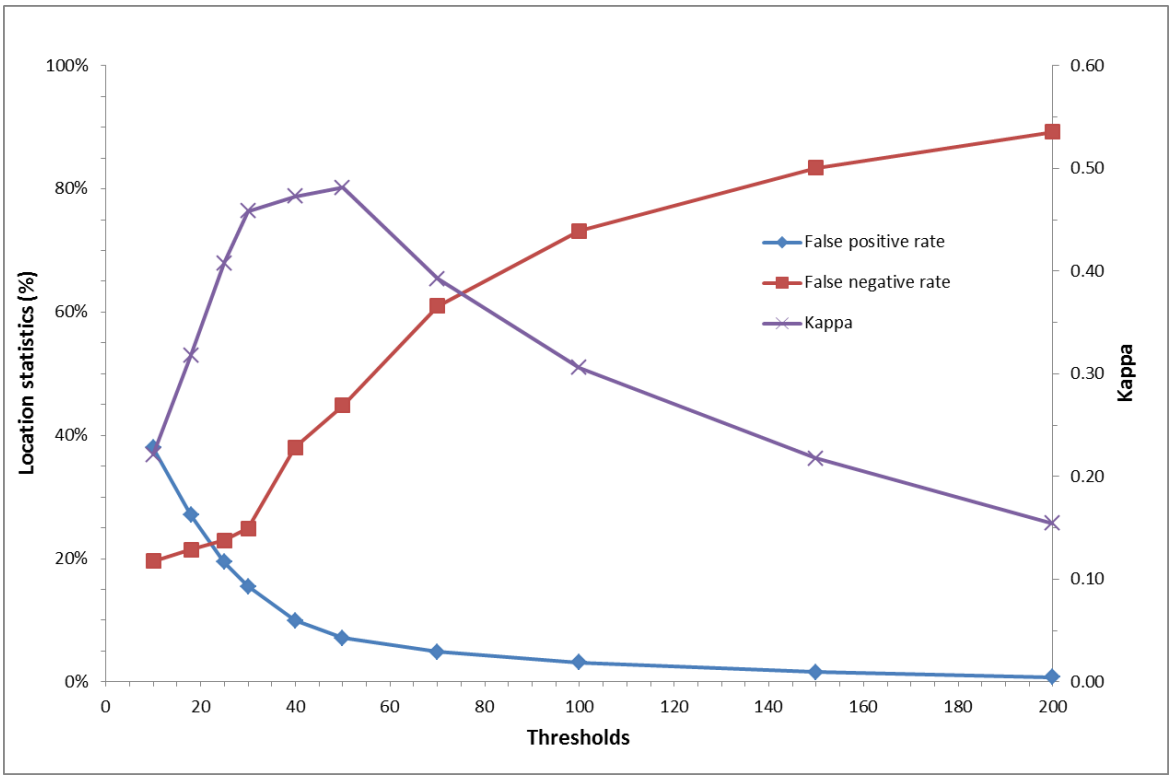

Figure 4.16 Observed and predicted lengths for different thresholds in S1.

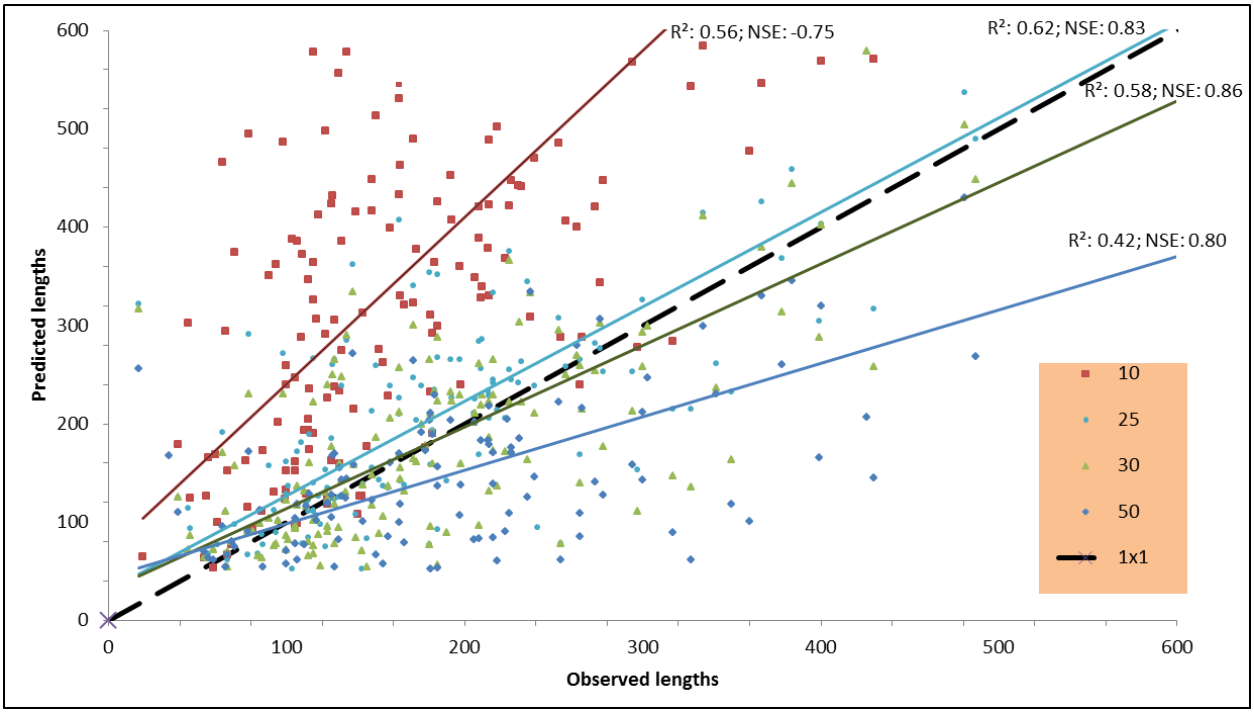

The SA model was executed in S2 (study area 2), which was of different climatological region) using above mentioned procedures. The results are shown in Figure 4.17 and Figure 4.18. The shapes of the lines that represent false positive rate, false negative rate and κ in S2 were similar to that of S1. In S2, the false positive rates were higher and false negative rates were lower for all thresholds compared to statistics in S1. The false negative rate gradually increased, unlike in S1 where there was sudden increase in false negative rate after 30. Interestingly, in S2, the κ was 0.37, false negative rate 67%, false positive rate 4% compared to κ 0.15, false positive rate 1%, false negative rate 89% in S1 at threshold 200. This shows that this model was able to predict the location of EGs along the main trajectory even at higher thresholds in S2 (Figure 4.19). Higher false positive rates in S2 were because EGs identified along the edge of terrace bounds (Figure 4.20). These EGs were not seen on the aerial images and field investigation is needed to verify their existence along the edge of terrace bounds. The optimum false positive rates, false negative rates and κ close to peak were seen for thresholds 40 and 50. Higher κ was seen at threshold 70 but false positives and false negatives were not optimum similar to S1. From Figure 4.18, it was seen that thresholds 40 and 50 crosses the best fit line, however, statistics of NSE and PBIAS were better for threshold 50 (NSE: 0.85; PBIAS: -3.9%) compared to threshold 40 (NSE: 0.84; PBIAS: -10.9%).

Threshold 50 better predicts the occurrence and length of EGs in S2, while threshold 30 better predicted in S1. Threshold that better predicted in one study area did not predict in another study area even though the study areas are within 290 kilometers (180 miles). This may indicate that every place or region is unique, and a given EG topographic index model needs to be calibrated over a range of thresholds to find the best threshold that optimally predicts the occurrence and lengths for the given region.

Figure 4.17 Occurrence statistics for different thresholds using SA model in S2.

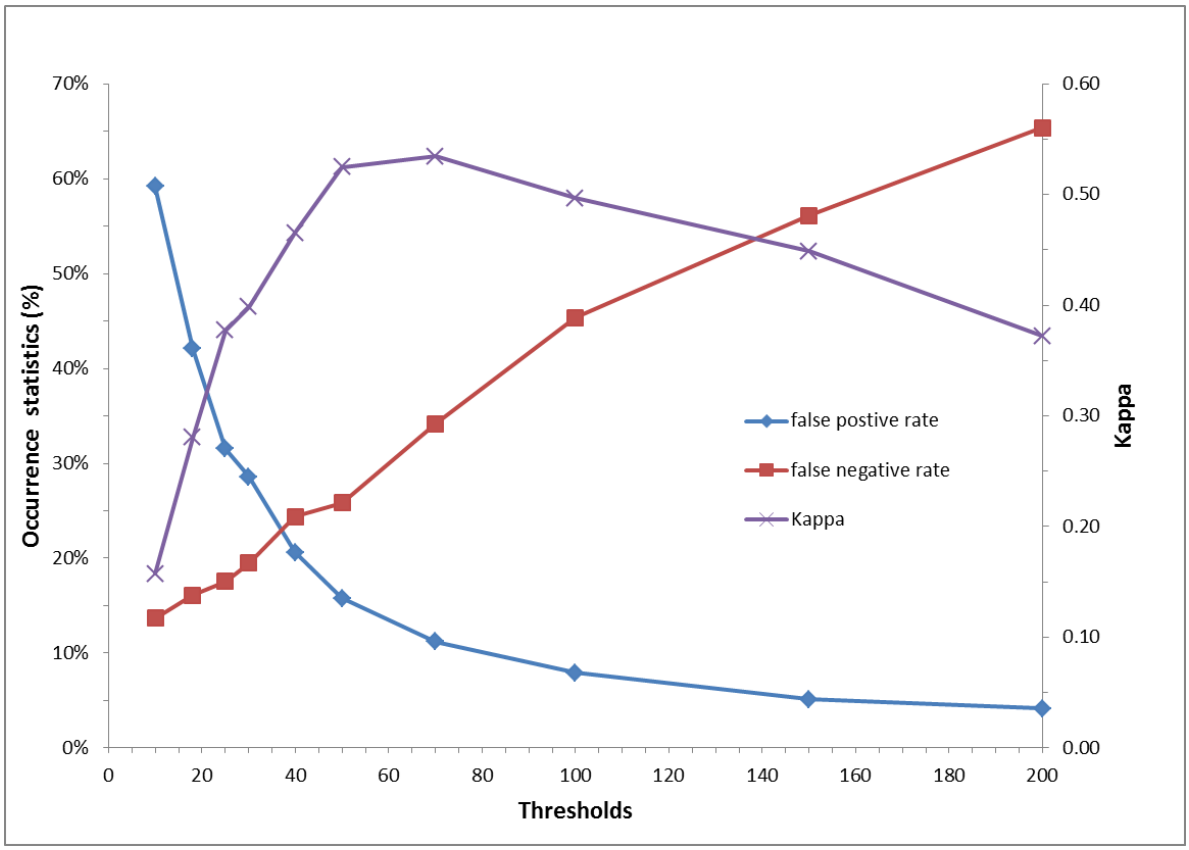

Figure 4.18 Observed and predicted lengths for different thresholds in S2.

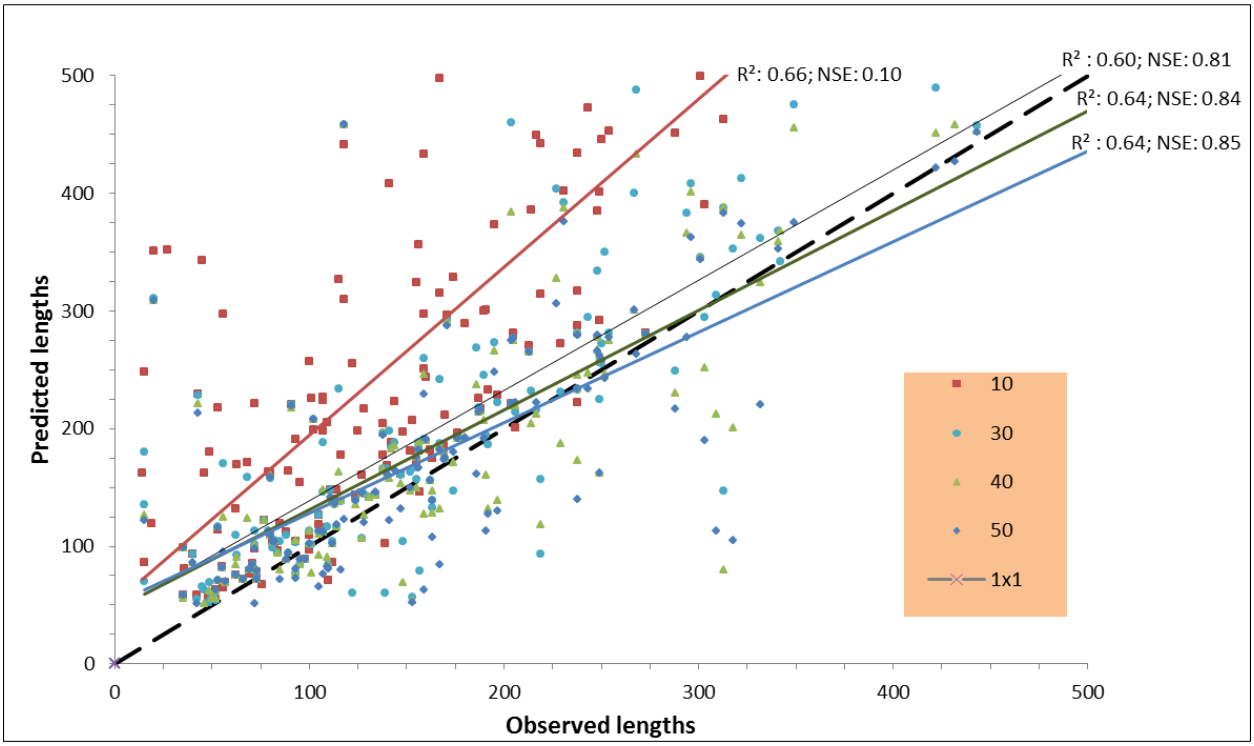

Figure 4.19 Predicted EG lengths at thresholds 25, 50 and 200 in S2.

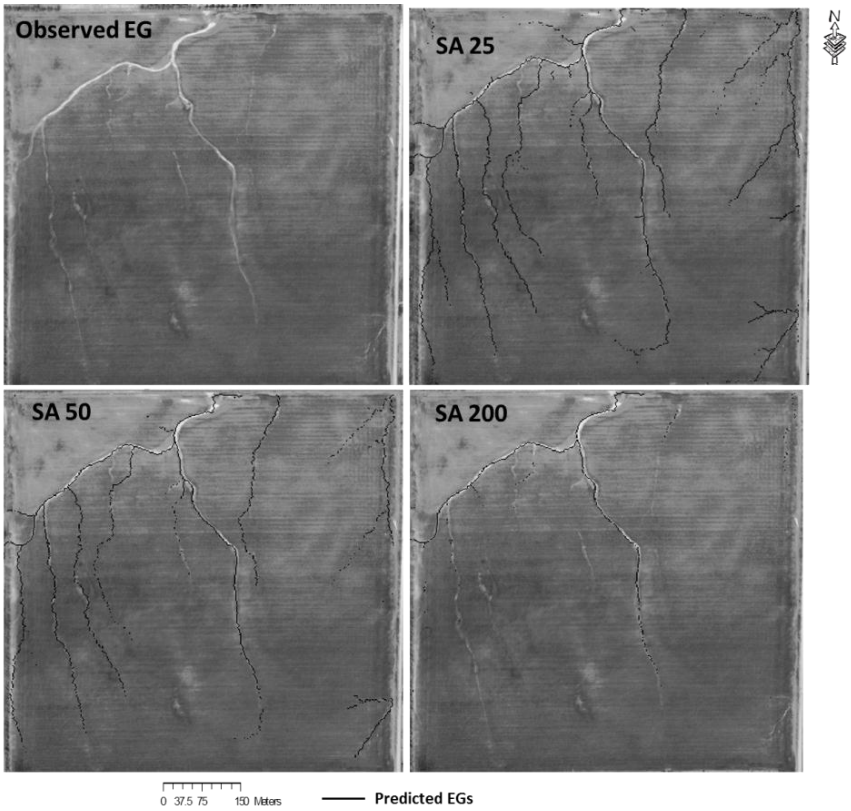

Figure 4.20 EGs along terrace channels.

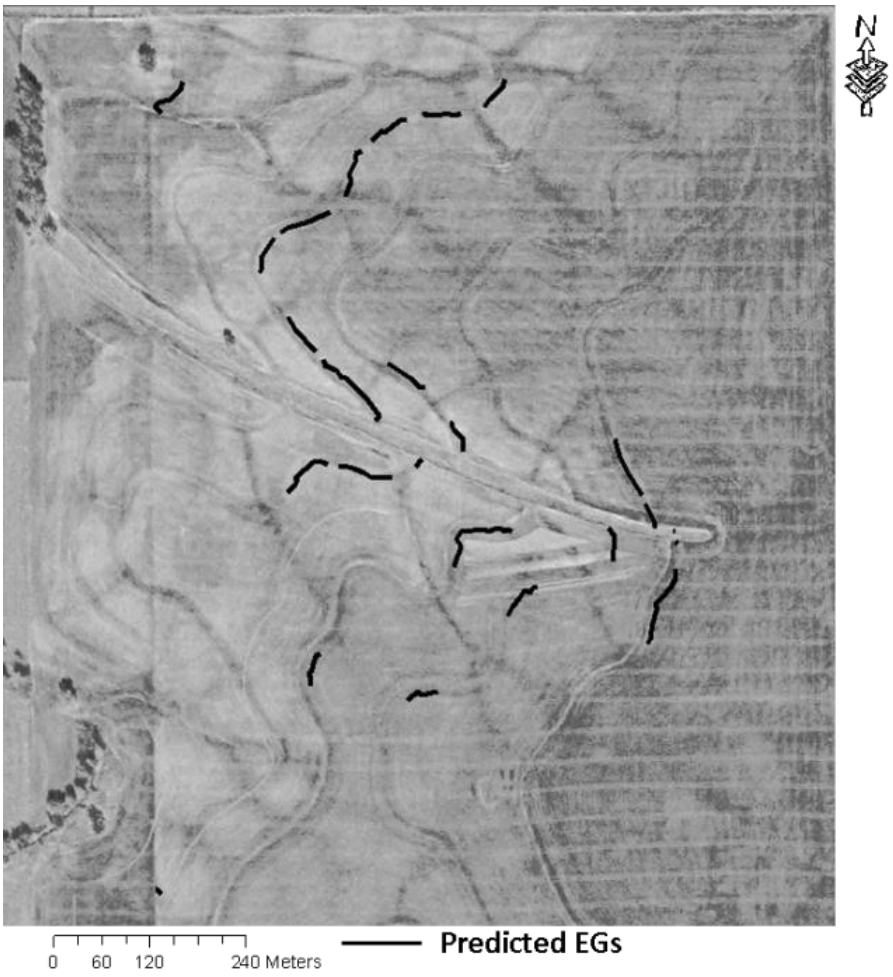

4.4 Conclusions

The performance of existing topographic index models (SA, CTI, SAP and WTI) to predict the EG locations was evaluated. Also, impacts of thresholds, DEM resolution and landuse data source were also evaluated. A methodology was developed to derive length using the topographic index models and was evaluated.

Results of visual interpretation show that the SA model better predicted the EG location and lengths than other models. The SA and CTI model predictions had similar pattern in terms of locating EG trajectory, however, the CTI model predictions had greater discontinuity along the trajectory. The method developed to derive length in this study was sensitive to discontinuity, and hence the performance of CTI model was poor. Occurrence and length statistics also show that SA model better predicted the occurrence and length of EGs than other models. The SAP

model performed poorly among all the models in predicting occurrence and lengths because this model was used to find the initiation points where EGs start. The WTI model was not able to predict the occurrence and lengths at T = 6.8 and 9.8, however it improved prediction of location and lengths at T = 12. Further testing of the model was not done in this study.

Different threshold values were required by the SA model to predict the occurrence and length of EGs in S1 (study area 1, T = 30) and S2 (study area 2, T = 50). The need for different thresholds among study regions indicated that other factors that vary among the regions and were not included in the topographic index models influence EG occurrence and length prediction. Therefore, individual calibration of topographic index model threshold for each application site is needed.

Finer resolution DEMs (e.g., 2 m) are needed to predict occurrence and length of EGs. Coarser resolution DEMs (10 m or greater) cannot locate EGs but may be useful for locating larger classical gullies in agricultural fields or gullies in rangeland. When considering EGs only within agricultural fields, field landuse is recommended over NASS landuse as NASS landuse results in either over or under predictions.

The EG locations predicted using these topographic index models were not accurate without calibration. Inclusion of other factors that vary by region, such as land management practices, precipitation characteristics, and soil properties, would likely improve EG model performance.

4.5 References

Begin, Z. B., and S. A. Schumm.1979. Instability of alluvial valley floors: a method for its assessment. *Trans. ASAE.* 22: 347-50.

Bussen, P. 2009. Analysis of a rapid soil erosion assessment tool. Unpublished Masters Thesis. Manhattan, Kansas: Kansas State Univ., Department of Biological and Agricultural Engineering

Capra, A., L. M. Mazzara, and B. Scicolone. 2005. Application of the EGEM model to predict ephemeral gully erosion in Sicily (Italy). *Catena.* 59: 133-146.

Capra, A., P. Porto, and B. Scicolone. 2009. Relationships between rainfall characteristics and ephemeral gully erosion in a cultivated catchment in Sicily (Italy). *Soil Till. Res.* 105: 77-87.

Chaubey, I., A. S. Cotter, T. A. Costello, and T. Soerens. 2005. Effect of DEM data resolution on SWAT output uncertainty. *J. Hydrol. Proc.* 19(3): 621-628.

Daggupati, P., K. R. Douglas-Mankin, A.Y. Sheshukov, P. L. Barnes, and D. L. Devlin. 2011. Field-level targeting using SWAT: Mapping output from HRUs to fields and assessing limitations of GIS input data. *Trans. ASABE.* 54(2):501-514.

Desmet, P. J. J., and G. Govers. 1997. Two-dimensional modelling of the within-field variation in rill and gully geometry and location related to topography. Catena. 29: 283-306.

Desmet, P. J. J., J. Poesen, G. Govers, and K. Vandaele. 1999. Importance of slope gradient and contributing area for optimal prediction of the initiation and trajectory of ephemeral gullies. *Catena.* 37: 377–92.

Dietrich, W. E., and T. Dunne. 1993. The channel head. In Beven, K., and M.J. Kirkby. (eds), *Channel Network Hydrol.* John Wiley and Sons, Chichester, UK.:175-219.

Foster, G. R. 1986. Understanding ephemeral gully erosion. Soil Conservation 2. National Academy of Science Press, Washington, DC.

Gordon, L. M., S. J. Bennett, R. L. Bingner, F. D. Theurer, and C. V. Alonso. 2007. Simulating ephemeral gully erosion in AnnAGNPS. *Trans. ASABE*. 50(3): 857-866.

Grissinger, E. 1996a. Rill and gullies erosion. In Agassi, M. (ed.), *Soil Erosion, Conserv. rehabilitation*. Marcel Dekker, New York: 153-67.

Grissinger, E. 1996b. Reclamation of gullies and channel erosion. In Agassi, M. (ed.), *Soil Erosion, Conserv. rehabilitation*. Marcel Dekker, New York.: 301-13.

Gutie´rrez, A. G., S. Schnabel, and A. M. Felicı´simo. 2009. Modelling the occurrence of gullies in rangelands of southwest Spain. *Earth Surf. Proc. Land*. 34: 1894-1902.

Hauge, C. 1977. Soil erosion definitions. *California Geol*. 30: 202-203.

Horton, R. E. 1945. Erosional development of streams and their drainage basins: hydrophysical approach to quantitative morphology. *Geol. Soc. America Bulletin*. 56: 275-370.

Jetten, V., J. Poesen, J. Nachtergaele, and D. van de Vlag. 2006. Spatial modelling of ephemeral gully incision: a combined empirical and physical approach. In Owens P.N. & Collins A.J. (eds), *Soil Erosion and Sediment Redistribution in River Catchments*. CAB International, Wallingford, UK: 195-206.

Kim, I. J. 2007. Identifying the roles of overland flow characteristic's and vegetated buffer systems for non-point source pollution control. Unpublished Ph.D. dissertation. Manhattan, Kansas: Kansas State Univ., Department of Biological and Agricultural Engineering

Knapen, A., and J. Poesen. 2010. Soil erosion resistance effects on rill and gully initiation points and dimensions. *Earth Surf. Process. Land.* 35: 217-28.

Meyer, A., and J. A. Martinez-Casasnovas .1999. Prediction of existing gully erosion in vineyard parcels of the NE Spain: a logistic modelling approach. *Soil Tillage Res.* 50 (3-4): 319-33.

Momm, H. G., R. L. Bingner, R. Wells, and S. D. S. Dabney.2011. Analysis of topographic attributes for identification of ephemeral gully channel initiation in agricultural watersheds. ASABE Paper No. 11-11250, St. Joseph, Mich.: ASABE.

Montgomery, D. R. 2007a. Dirt: Erosion of Civilizations. University of California Press, 296 pp.

Moore, I. D, R. B. Grayson, and A. R. Ladson. 1991. Digital terrain modelling: A review of hydrological, geomorphological, and biological applications. *Hydrol. Proc.* 5: 3-30.

Moore, I. D., G. J. Burch, and D. H. Mackenzie. 1988. Topographic effects on the distribution of surface soil water and the location of ephemeral gullies. *Trans. ASAE.* 32: 1098-1107.

Moriasi, D. N., J. G. Arnold, M. W. Van Liew, R. L. Bingner, R. D. Harmel, and T. L. Veith. 2007. Model evaluation guidelines for systematic quantification of accuracy in watershed simulations. *Trans. ASABE.* 50(3): 885-900.

Nachtergaele, J., and J. Poesen. 1999. Assessment of soil losses by ephemeral gully erosion using high-altitude (stereo) aerial photographs. *Earth Surf. Proc. Land.* 24(8): 693-706.

Nachtergaele, J., J. Poesen, L. Vandekerckhove, D. O. Wijdenes, and M. Roxo. 2001a. Testing the Ephemeral Gully Erosion Model (EGEM) for two Mediterranean environments. *Earth Surf. Proc. Land.* 26: 17-30.

Nachtergaele, J., J. Poesen, and A. Steegen. 2001b. The value of a physically based model versus an empirical approach in the prediction of ephemeral gully erosion for loess-derived soils. *Geomorphology.* 40: 237-252.

O'Callagham, J. F., and D. M. Mark. 1984. The extraction of drainage networks from digital elevation data. *Comput. Vision Graph.* 28: 323-344.

Parker, C., C. Thorne, R. Bingner, R. Wells, and D. Wilcox. 2007. Automated mapping of potential for ephemeral gully formation in agricultural watersheds laboratory. Publication, National Sedimentation Laboratory, No. 56.

Patton, P. C., and S. A. Schumm, 1975. Gully erosion, northwestern Colorado: a threshold phenomenon. *Geology.* 3(2): 88-90.

Pearson, R. G. 2007. Species' Distribution modeling for conservation educators and practitioners. Synthesis. *American Museum of Natural History*. Available at http://ncep.amnh.org.

Poesen, J. 1993. Gully typology and gully control measures in the European loess belt. In: Wicherek, S. (ed), *Farmhand Erosion in Temperate Plains Environment and Hills*, 221-239. Elsevier, Amsterdam.

Poesen, J., J. Boardman, B. Wilcox, and C. Valentin.1996. Water erosion monitoring and experimentation for global change studies. *J. Soil Water Conserv.* 51(5): 386-390.

Poesen, J., J. Nachtergaele, Verstraeten, G. and Valentin, C. 2003. Gully erosion and environmental change: importance and research needs. *Catena.* 50: 91-133.

Poesen, J., D. Torri, and T. Vanwalleghem. 2011. Ch. 19 – Gully erosion: procedures to adopt when modelling soil erosion in landscapes affected by gullying. In Morgan, R.P.C., and M.A. Nearing (eds). *Handbook of Erosion Modelling*. Blackwell-Wiley: Oxford.

Smith, L. 1993. Investigation of ephemeral gullies in loessial soils in Mississippi. Technical Report GL-93-11. U.S. Army Corps of Engineers, Waterways Experiment Station, Vicksburg, MS.

Soil Science Society of America. 2001. Glossary of soil science terms. http://www.soils.org/sssagloss/.

Souchère, V., O. Cerdan, and B. Ludwig. 2003. Modeling ephemeral gully erosion in small cultivated catchments. *Catena.* 50: 489-505.

Tarboton, D. G., R. L. Bras, and I. Rodriguez-Iturbe. 1991. On the extraction of channel networks from digital elevation data. *Hydrol. Proc.* 5(1): 81-100.

Thorne, C. R., and L. W. Zevenbergen. 1984. On-site prediction of ephemeral gully erosion. Report to the U.S. Department of Agriculture, Agricultural Research and Soil Conservation Services.

Thorne, C. R., L. W. Zevenbergen, E. H. Grissinger, and J. B. Murphey. 1986. Ephemeral gullies as sources of sediment. *Proc. Fourth Federal interagency Sed. Conf.* Las Vegas, NV, pp. 3.152-3.161.

Vandaele, K., J. Poesen, J. R. Marques da Silva, and P. Desmet. 1996b. Rates and predictability of ephemeral gully erosion in two contrasting environments. *Geomorphologie: Relief, Processus, Environ.* 2: 83-96.

Vandaele, K., J. Poesen, G. Govers, and B. van Wesemael. 1996a. Geomorphic threshold conditions for ephemeral gully incision. *Geomorphology.* 16: 161-73.

Vandekerckhove, L., J. Poesen, D. Oostwoud Wijdenes, and T. de Figueiredo. 1998. Topographical thresholds for ephemeral gully initiation in intensively cultivated areas of the Mediterranean. *Catena.* 33: 271-92.

Vandekerckhove, L., J. Poesen, and D. O. Wijdenes. 2000. Thresholds for gully initiation and sedimentation in Mediterranean Europe. *Earth Surf. Proc. Land*. 25: 1201-20.

Vrieling, A. 2006. Satellite remote sensing for water erosion assessment: A review. *Catena.* 65: 2-18.

Woodward, D. E. 1999. Method to predict cropland ephemeral gully erosion. *Catena.* 37: 393-399.

Zevenbergen, L. W., and C. R. Thorne. 1987. Quantitative analysis of land surface topography. *Earth Surf. Proc. Land.* 12: 47-56.

Chapter 5 - Predicting Ephemeral Gully Length using Physical Model

Abstract

Ephemeral gully (EG) erosion has been recognized as a major source of sediment in agricultural watersheds. Over the past few decades, soil conservation practices have been implemented to control soil erosion from sheet and rill erosion. However, excessive sediment still remains among the most prevalent water quality problems in the U.S. Major factors affecting the formation and development of EGs include precipitation, soil, topography and landuse/land management practices. Over the past few decades, models to predict location of EGs used only topography and have ignored other factors. Predicting length of an EG is also considered to be an important research need. In this study the goal was to predict the location and length of EGs in Goose Creek watershed using Overland Flow Turbulent (OFT) model, which explicitly includes topographic, precipitation, soil, and landuse/landcover factors. The precipitation excess, an input parameter in the OFT model, was derived using SWAT model and simplified Curve Number (CN)-based ArcCN-Runoff (ACR) tool in an ArcGIS environment. The performance of OFT model was also compared with Slope Area (SA) model (from Chapter 4).

Results showed that the OFT model with precipitation excess derived using SWAT model performed better that using the ACR tool. Errors in runoff estimation translated into errors in EG simulation. The OFT model with precipitation excess derived using SWAT model resulted in slightly over-predicted lengths compared to the observed data. The soil critical shear stress (τ_{cr}) values derived in this study added uncertainty that appear to have contributed to this overestimation. More accurate estimation of field-scale τ_{cr} would improve EG simulation and needs further investigation. The performance of OFT and SA models was similar. However the SA model was calibrated for a subwatershed of the tested study area while the OFT model was not calibrated. This result provides support that the physical-based model may have broader applicability than the empirical based model to predict EG lengths.

5.1 Introduction

Over the past few decades, soil conservation practices have been implemented to control soil erosion from interrill and rill erosion, but their impacts on ephemeral gully (EG) erosion is unclear. The National Resource Inventory (NRI) reported that there has been a 42% decrease in sheet and rill erosion in the United States between 1983 and 2003. However, excessive sediment remains among the most prevalent water quality problems in the U.S. (Hargrove et al., 2010). Recent studies (Foster et al., 1986; Poesen et al., 1996; Nachtergaele and Poesen, 1999; Poesen et al., 2003; Hargrove et al., 2010; Knapan and Poesen, 2010; Poesen et al., 2011) have shown that EG erosion is a major contributor of sediment and needs immediate attention.

Soil loss due to EG erosion can contribute about 10% of the total soil loss in small watersheds (Poesen et al., 1996). However, in actively eroding areas, the contribution of EG erosion can range from 30% to as high as 100% of the total soil loss (Casali et al., 1999). Contribution of EG erosion varies geographically. In the United States, EG erosion contributed from 17% of total soil loss in New York State to 73% in Washington State (Robinson et al., 2000). In central Belgium, the EG erosion accounted for 44% (Poesen et al., 1996) while in the Mediterranean and southern Portugal regions, the EG erosion contributions were as high as 83% (Vandaele et al., 1996). In the Loess Plateau of China, the contributions of EG erosion ranged from 41% to 91% (Zheng and Gao, 2000).

EGs are concentrated flow channels of various sizes which mostly form along the natural drainage lines, when vegetation cover is minimal, and when runoff energy of water (precipitation excess) exceeds critical shear stress of soil. EGs erode topsoil, but tillage fills them in, often with less-productive subsoil. If not corrected, EGs may grow into permanent gullies. As noted in the studies above, EGs may contribute more to soil loss each year than sheet and rill erosion. Factors that affect the formation and development of EGs include precipitation, soil, topography and landuse/land management practices.

EGs form only after a threshold precipitation intensity and duration are attained. Very few studies have investigated threshold precipitation events required for EG formation, and those studies typically are restricted to small areas and examined over short time periods (Carpa et al., 2009). The threshold precipitation needed for the formation and development of EGs varied geographically depending on soil conditions and initial soil moisture content. Various studies

have reported threshold precipitation of 14.5 to 22 mm (0.57 to 0.86 in) for cropland. Minimum precipitation depths of 15 mm (0.59 in) in winter and 28 mm (1.10 in) in summer were needed for the formation of EGs, based on a study spanning a 15-year period in central Belgium (Nachtergaele et al., 2001a). Casali et al. (1999) reported that a 17 mm (0.66 in) total water depth and peak precipitation intensity of 54 mm/hr (2.12 in/hr) were needed for EG formation in Navarra region (Spain). Cerdan et al. (2002) found a precipitation depth of 28.5 mm (1.10 in) and maximum 6-minute intensity of 15 mm/hr (0.59 in/hr) in December and 21.6 mm (1.12 in) depth and 98 mm/hr (3.86 in/hr) 6-minute intensity in summer resulted in the formation of rill EGs in a cropland area. Capra et al. (2009) observed EG formation for an 8-year period. They used an antecedent precipitation index, the maximum value of 3-days precipitation ($H_{max}3$-d), a simple surrogate for soil water content, and reported that a $H_{max}3$-d threshold of 51 mm (2.28 mm) was needed for EG formation.

The formation of the EGs has been described in literature as a topographic phenomenon (Patton and Schumm, 1975; Throne et al., 1986; Montgomery and Dietrich, 1994). Topographic attributes, such as upstream drainage area (used as surrogate for flow), slope, and plan of curvature, are key topographic controls in the formation process. Over the past few decades, these attributes are combined in several forms and are used to find locations of EGs (discussed in Section 4.1 and 4.2.1).

Soil (particularly top soil) resistance to concentrated flow erosion plays an important role in the formation of EGs (Poesen et al., 2003). Knapan et al. (2007) hypothesized that gully initiation at a given location in the landscape is not only hydrologically and topographically controlled, but is also controlled by erosion resistance of top soil. Knapan and Poesen (2010) proved their hypothesis using field studies on Belgium loess topsoils. The erosion resistance of top soil is commonly referred to as soil critical shear stress (τ_{cr}), threshold at which shearing forces of concentrated water flow initiate soil erosion. Soil critical shear stress is influenced by factors such as soil moisture content, bulk density, particle size distribution, random surface roughness, void space, flow resistance, soil erosivity, surface sealing and crusting, and freezing and thawing (Nearing et al., 1989). Soil critical shear stress values are difficult to define precisely because they vary considerably even for similar soil conditions (Foster, 1986). Very few studies have reported τ_{cr} values that resulted in the formation of EGs. Nachtergaele et al. (2002) and Poesen et al. (2003) reported that τ_{cr} during peak flow ranged between 3.3 and 32. 2

N/m^2 (mean = 14 N/m^2) for EGs eroded in silt loam (loess-derived) topsoils in Belgium, and between 16.8 and 74.4 N/m^2 (mean=44 N/m^2) for EGs formed in stony sandy loams in Portugal. Poesen at al. (2011) stressed for the need to collect and report τ_{cr} values leading to EG formation in a range of environment.

Landuse plays an important role in EG formation, and several recent studies have documented that a gradual or sudden shifts in landuse resulted in triggering of gullying or the increase in gully erosion rates (Poesen et al., 2011). Field observations in central Belgium showed that an increase in area under maize resulted in an increased EG erosion risk (Nachtergaele, 2001, as cited in Poesen et al., 2011). Poesen et al. (2011) stressed the need for more research on the drivers of landuse changes causing increased or decreased gully erosion risk. Landcover or vegetative biomass has a direct impact on the formation of EGs. Vandekerckhove et al. (2000) reported that landcover has greater influence than climatic conditions in explaining topographic thresholds for different areas. Landcover affects the τ_{cr} values directly; i.e., reduction in biomass (either above or below ground) results in lowering the erosion resistance of top soil (τ_{cr}), which influences EG formation. Prosser and Slade (1994) demonstrated through flume experiments that increase in vegetation cover results in decreasing susceptibility of valley floors to gully formation. Plant roots also affect the formation of EGs. De Baets et al. (2006, 2007) demonstrated that τ_{cr} increased with fibrous roots due to increase in soil cohesion compared to tap-rooted plant species.

Empirical and process-based models have been developed to quantify EG erosion at both field and watershed scales. Woodward (1999) developed a process-based EG Erosion Model (EGEM) that was tested by Nachtergaele et al. (2001a). In this model, locations of EGs and EG length were given by the user. Gordon et al. (2007) developed a Revised EGEM (REGEM) to address the limitations of EGEM. They made many improvements to the EGEM model, and also incorporated it as a subroutine within Annualized Agricultural Non-Point Source Model to predict inter-rill, rill, and EG erosion. One limitation with REGEM was that it still required users to input the location of EGs.

Considering the difficulty with use of EG process-based models, simple empirical models for EG volume estimates were developed. Nachtergaele et al. (2001 a, b) observed strong relationship between EG volume and EG length in Mediterranean environment using 112 field-measured EGs. The relation between volume and length is represented as $V = 0.048\ L^{1.29}$ with a

coefficient of determination (R^2) of 0.91. Capra and Scicole (2002) and Capra et al. (2005) confirmed similar relationships in their study area (Italy), and used data from 92 EGs to develop $V = 0.0082\ L^{1.42}$ with an R^2 of 0.64. Zhang et al. (2007) reported similar relation using 21 EGs in north eastern China, and developed $V = 0.015\ L^{1.43}$ with an R^2 of 0.67. All these models (both process-based and empirical-based) require the location and length for them to quantify sediment losses.

In the earlier chapter (Chapter 4), the potential length of EGs was derived spatially using various topographic index models and, in particular, explored the threshold sensitivity of the SA model. Models that were used in the earlier chapter were purely based on a topographic approach and did not consider precipitation, soil, and landuse/landcover parameters. Knapen et al. (2010) and Poesen et al. (2011) stressed the importance of including precipitation, soil, and landuse parameters in modeling the location of EGs.

Therefore the main goal in this study was to develop a model in a geographic information system (GIS) environment to predict length of EGs in agricultural fields utilizing a physical-based Overland Flow Turbulent (OFT) equation developed by Montgomery and Dietrich (1994), which makes use of topography, soil, landuse/landcover, and precipitation factors. The objective of this study was to compare and evaluate performance of the OFT and SA models in predicting EG length. The lengths predicted from this study can be used to estimate sediment loads from EGs using regression equations or process based models such as EGEM.

5.2 Background for OFT Model

Three processes have been identified as important in the formation of EGs (Montgomery and Dietrich 1994):

(a) EG formation by overland flow, in which flow exerts a boundary shear stress in excess of critical shear stress;

(b) EG formation by seepage, in which seepage gradients entrain surficial material as a result of water flowing through and emerging from the soil;

(c) EG formation by land sliding.

Most of the EGs observed during the field surveys across the state of Kansas were formed due to overland flow (Daggupati et al., 2010). According to Montgomery and Dietrich (1994), gully formation by overland flow occurs either in laminar or turbulent flow regimes.

Flow over bare or less-vegetated soils often is considered turbulent, and flow over grassy or well vegetated surfaces generally is laminar (Prosser and Abernethy, 1996). Since our interest was on EGs forming in agricultural fields as a result of tillage, the turbulent flow regime was considered as the flow regime for overland flow.

Montgomery and Dietrich (1994) derived discharge per unit contour length (q, m^3/m) assuming steady-state precipitation intensity (P, mm/hr) over a surface with uniform infiltration capacity (I, mm/hr):

$$q = (P - I)a \tag{5.1}$$

where a is drainage area per unit contour length (m^2/m) and (R – I) is precipitation excess (mm/hr). Contour length is defined as length along the contour (line of constant elevation). Discharge per unit contour length can also be expressed by the product of flow velocity (v) and flow depth (h) (Montgomery and Dietrich, 1994; Anderson and Anderson, 2010). Flow velocity can be expressed using Manning's equation:

$$v = \frac{1}{n} R^{2/3} S^{1/2} \tag{5.2}$$

where n is Manning's resistance coefficient ($second/m^{1/3}$), R is hydraulic radius (m), and S is water surface slope (m/m). In open channel hydraulics, hydraulic radius is approximate to flow depth (Montgomery and Dietrich, 1994). Therefore, discharge per unit contour length can be expressed as

$$q = \frac{1}{n} h^{5/3} S^{1/2} \tag{5.3}$$

where n is Manning's resistance coefficient ($second/m^{1/3}$), h is flow depth (m), and S is water surface slope (m/m). The critical shear stress of gully formation is determined by soil properties. A basal shear stress (depth–slope product) greater than the critical shear stress is required for sediment transport. Therefore,

$$\tau_{cr} = \rho_w g (hS)_{cr} \tag{5.4}$$

where τ_{cr} is critical shear stress of soil (N/m^2), ρ_w is density of water (kg/m^3), and g is acceleration due to gravity (m/s^2). Rearranging Eq. 5.3 to solve for h_{cr}, and substituting in Eq. 5.2 gives critical discharge (q_{cr}):

$$q_{cr} = \frac{{\tau_{cr}}^{5/3}}{(\rho_w g)^{5/3} n S^{7/6}} \tag{5.5}$$

Critical drainage area per unit contour length (a_{cr}) necessary for overland flow erosion by turbulent flow is obtained by equating Eq. 5.5 and Eq. 5.1

$$a_{cr} = \frac{3{,}600{,}000\ {\tau_{cr}}^{5/3}}{(R-I)(\rho_w g)^{5/3} n S^{7/6}} \tag{5.6}$$

The right side of the Eq. 5.6 was multiplied by 3,600,000 so that units were balanced. Eq. 5.6 has a well-established physical meaning to it. However, most of the processes are simplifications of complex hydraulic processes. In Eq. 5.6, the upstream unit drainage area is inversely proportional to local slope, surface roughness and precipitation excess, and is a function of critical shear stress. An EG is simulated to be present at a given location when its specific drainage area is greater than or equal to a_{cr} (Eq. 5.6). In this study, Eq. 5.6 was developed in a GIS environment utilizing the model builder platform, and was coupled with methodology to derive length (as discussed in Section 4.2.3) to predict length of EGs.

5.3 Study Area

Goose Creek watershed is a 13,306 ha (32,880 ac) subwatershed within Cheney Lake watershed that drains into North Fork River (Figure 5.1).

Figure 5.1 Goose Creek watershed. Black lines are digitized ephemeral gullies.

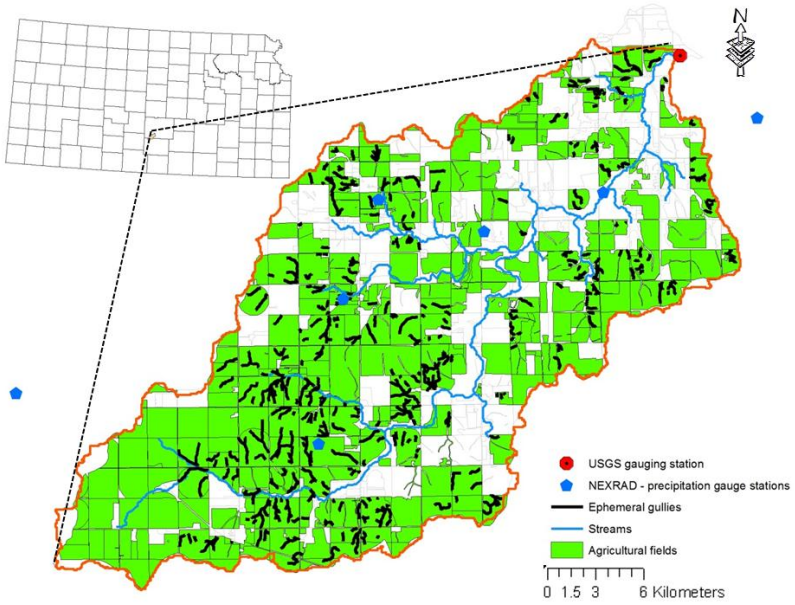

The watershed is located within Reno and Kingman counties of Kansas. Primary landuse in the watershed is cropland (64%), followed by rangeland (29%), and 1% others (water, urban). Fine loamy textured soils highly susceptible to EG erosion are predominant in this subwatershed (KDHE, 2000; Parajuli et al., 2009). Winter wheat is a major crop in the watershed while grain sorghum, corn and soybeans are warm-season crops. Most of the fields in the watershed are conventionally tilled, and typical planting dates for wheat was in the last week of September (Lisa French, Cheney Lake Watershed Inc., 2010, personal communication). Erosion from EGs is a major concern in the watershed (Daggupati et al., 2010; Douglas-Mankin et al., 2011). The preliminary monitoring results in the watershed as part of a USDA Conservation Effects Assessment Project (CEAP) showed that EGs contribute roughly 2.46 Mg/ha (1.1 t/ac) (Douglas-Mankin et al., 2011) while average EG contribution for Kansas was 2.92 Mg/ha (1.3 t/ac) as compared to 8.06 Mg/ha (3.6 t/ac) from sheet and rill erosion (USDA-NRCS, 1997).

5.4 Study Setting

Several aerial images from the recent past (images taken in different years ranging from 1995 to 2011) in continental U.S. have been made available to the public through Google Earth (Google Earth Version 6.1, Mountain View, CA) as well as through National Agriculture Imagery Program (NAIP) and Digital Ortho Quarter Quadrangles (DOQQ). Most of the images were taken during the crop growing season when a crop was fully established, and hence locating the EGs on them was difficult. However, on the 2003 DOQQ aerial image, EGs were located in the study area (Goose Creek watershed) because it was acquired in the study area on 22 March (verified using Google earth timeline) when the crop (wheat) was not fully established.

Daily and hourly records of precipitation showed that the EGs on the 22 March 2003 aerial image likely resulted from precipitation events on October 2 (3 mm (0.11 in)), 3 (85 mm (3.31 in)) and 4 (13 mm (0.50 in)) of 2002 (Figure 5.2).

Figure 5.2 Time line of precipitation, landuse/landcover and management practices in Goose Creek watershed

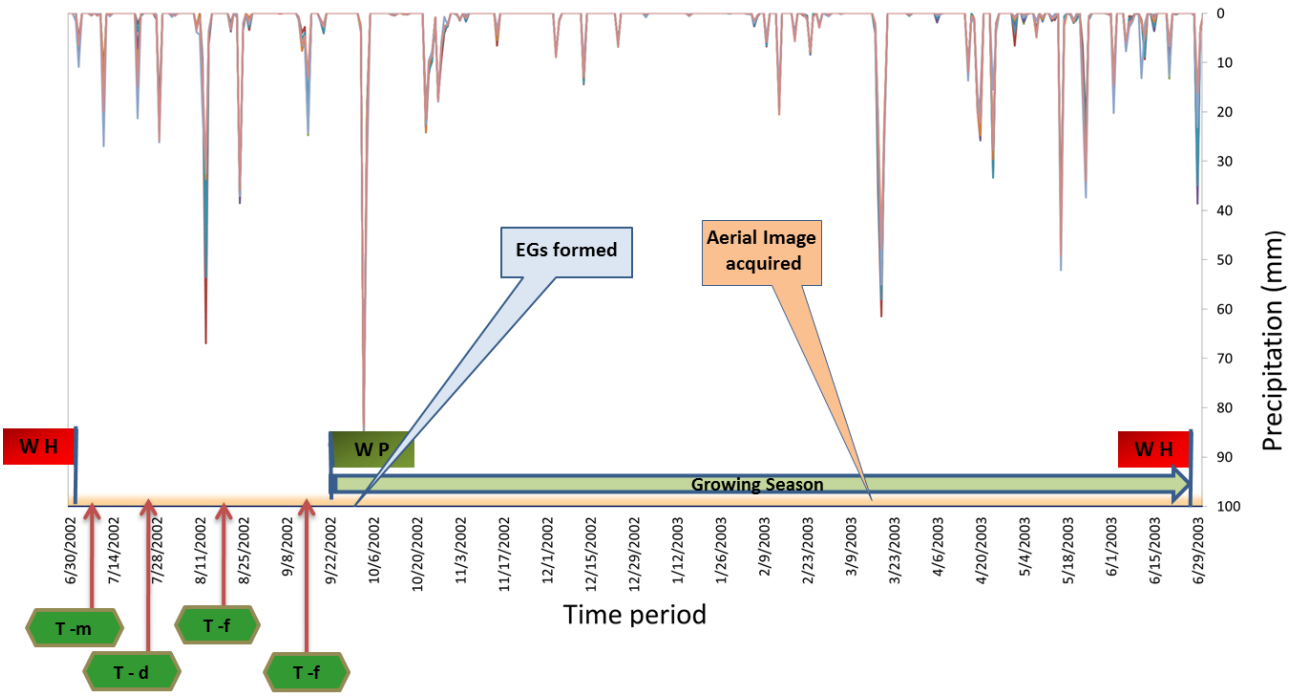

WH- Wheat harvested; WP- Wheat planted; T-m – Tillage (disc primary); T-d – Tillage (disc); T-f – Tillage (field cultivator)

A majority of the cropland in the watershed was wheat, and the wheat fields were tilled in mid-September and were planted in late September. Several precipitation events prior to planting would have resulted in increased soil moisture, and the precipitation of 85 mm (3.31 in) on October 3 likely resulted in the formation of EGs. Since the crop was planted, the farmers could not till the fields to "remove" the EGs. Further precipitation events would have resulted in increasing the dimensions of EGs based the antecedent soil moisture, soil and crop cover conditions. Therefore, in this study, EGs resultant from the precipitation on October 3 was modeled and analyzed using the OFT model.

5.5 Methods

5.5.1 Digitizing EGs

EGs on the 2003 aerial image within agricultural fields in Goose Creek watershed were carefully digitized manually. Extreme care was taken such that each EG was digitized along the trajectory of the EG located on the aerial image. Starting and ending of an EG was difficult to

determine, therefore, color changes on an aerial image and expert judgments of author was used to digitize accurately with a 5% error. For example, the color of an EG located on an aerial image was white in a field colored green/brown/grey. Digitizing of EG was started when the color changed from green to white and proceeded along the trajectory of EG until the color changed from white to other color. Google Earth as well as hill shade images (enhances the relief of the surface) was used to verify/cross check the location during digitizing process. Finally, the digitized EGs were used as observed or reference data to evaluate model performance. This study was considered as a first attempt to model EGs lengths that were resultant based on an actual precipitation event.

5.5.2 OFT model

The OFT model was built in a GIS environment using model builder platform based on Eq. 5.6 to predict length of EGs in Goose Creek watershed (Figure 5.3). The geospatial model requires data on topography, soils, landuse and management, and weather to derive local slope, drainage pattern, manning's resistance coefficient (n), and precipitation excess (runoff) as OFT model (Eq. 5.6) inputs.

Topographic parameters such as upslope drainage area per unit contour length (a) and slope (S) were calculated using a digital elevation model (DEM). Local slope in percent (%) was computed using deterministic eight direction (D8) algorithm (O'Callagham and Mark, 1984), and the percent slope was divided by 100 to get local slope in m/m. The flow direction and flow accumulation grids were also computed using D8 method. The drainage area in m^2 was calculated by multiplying the accumulation in cells by the square of the cell size.

The OFT model uses a term that characterizes the drainage area per unit contour length, a. Tarboton (2003) describes this term in the following way:

> "Hydrologic processes are fundamentally different on hillslopes and in channels. In channels flow is concentrated. The drainage area, A, (e.g. in m^2) contributing to each point in a channel may be quantified. On hillslopes flow is dispersed. The "area" draining to a point is zero because the width of a flow path to a point disappears. On hillslopes flow and drainage area need to be characterized per unit width (e.g. $m^3/s/m = m^2/s$ for flow). The specific catchment area, a, is defined as the upslope drainage area per unit contour width, b (a = A/b) (Moore et al., 1991) and has units of length (e.g. $m^2/m = m$)."

Figure 5.3 Geospatial model for predicting location and length of EGs using OFT model

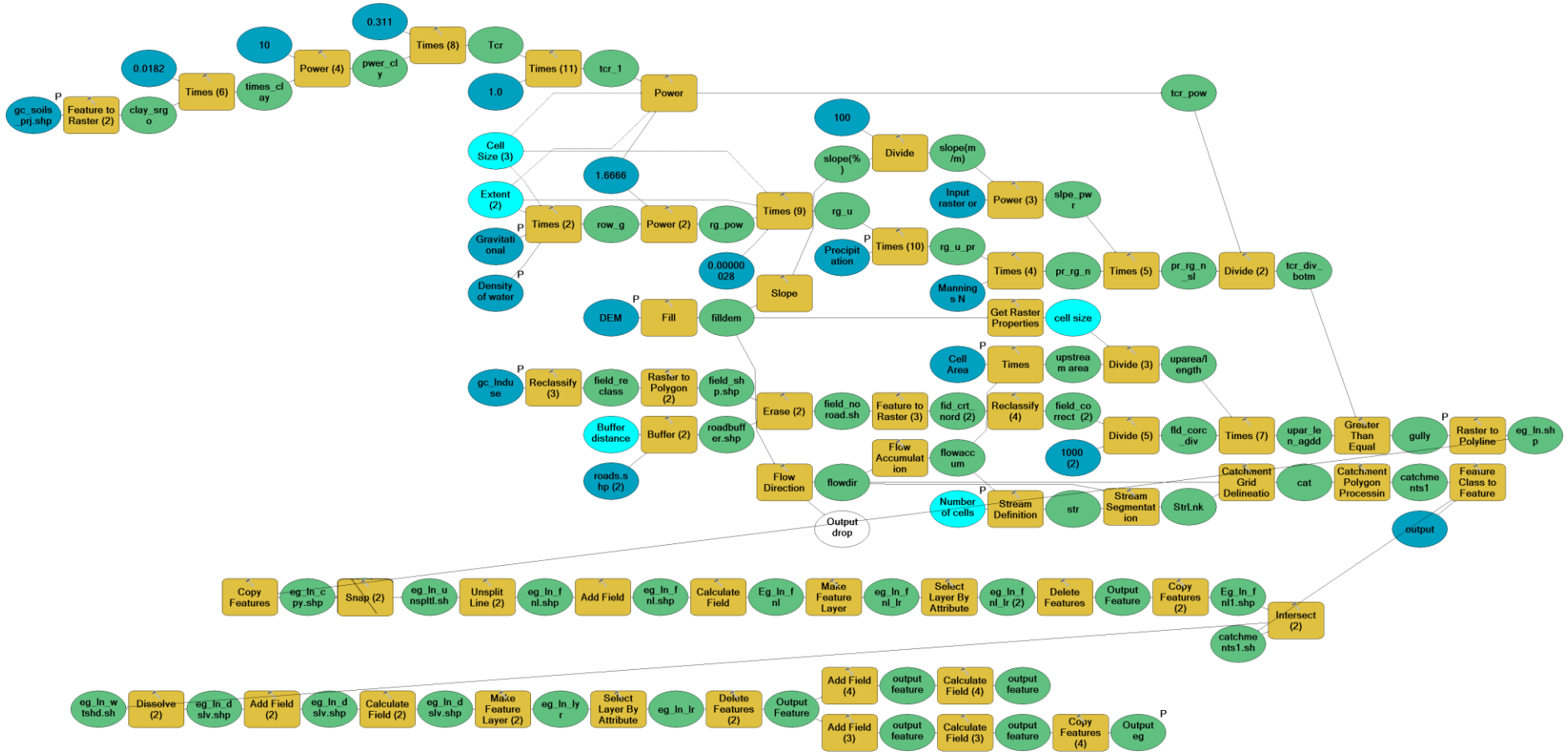

Pack et al. (2001) and Classens et al. (2005) stated that in a grid-based approach, grid resolution (m) can be taken as the effective contour length. Desmet et al. (1999), however, used the grid resolution times $(2)^{0.5}$ (= 1.414) to estimate effective contour length. In this study specific catchment area, or upstream drainage area per unit contour length (m^2/m), was calculated by dividing the drainage area by resolution of the DEM.

The soil data from SSURGO database (USDA-NRCS, 2005) was processed using a SSURGO processing tool (Sheshukov et al., 2012) and was used as shapefile into the model. The processed soil has more than 20 soil related parameters (e.g., hydrologic group, texture, sand, silt and clay content). In this study, clay percent of topsoil was used to calculate the soil critical shear stress (τ_{cr}) using the following equation (Smerdon and Beasley, 1961):

$$\tau_{cr} = 0.311 \times 10^{0.00182Pc} \quad (5.7)$$

where Pc is percent clay content (%). Equation 5.7 is used in many watershed models and is also currently used in EGEM and REGEM to calculate τ_{cr} (Gordon et al., 2007).

Landuse was used to clip out non-agricultural areas within the GIS, as this study was focused on modeling EGs in agricultural fields. Landcover was represented in the model by adjusting τ_{cr}. Knapan et al. (2007) and Souchere et al. (2003) reported that landcover and τ_{cr} are related to each other, and an increase in land cover increases τ_{cr}, and vice versa. Gordon et al. (2007) reported that no till can be represented in REGEM model by doubling τ_{cr} values. In this study, the crop was planted a week prior to the formation of the EGs, therefore τ_{cr} was multiplied by 1.0 (i.e., unadjusted), assuming crop cover was insignificant at this point. Other inputs used were overland flow resistance coefficient n (0.03), acceleration due to gravity (9.8 m^2/sec), and density of water (1000 kg/m^3).

Another important input parameter needed by the model was precipitation excess (runoff). This parameter is highly variable over space and time and is difficult to obtain. Prosser and Abernethy (1996) used 22 mm/hr (0.85 in/hr) as precipitation excess in a model similar to OFT model, which was used to locate gullies in rangeland. They observed a peak hourly precipitation of 42 mm/hr (1.63 in/hr) responsible for gully formations in rangeland, and have used 20 mm/hr (0.78 in/hr) as steady state infiltration rate for that soil in the study area (verified using soil texture and precipitation simulator studies). Very few studies have made attempts to derive individual-storm-based precipitation excess for EG-prediction purposes.

Precipitation excess on 3 October 2002 was of interest in this study, as it was deduced to be the storm responsible for forming the EGs observed in the 22 March 2003 aerial image of the study area and being modeled in this study. Precipitation excess on a particular day depends on many factors, such as landuse/landcover/management, soil, topography, antecedent soil moisture content, and also varies spatially. Therefore, an attempt was made in this study to derive precipitation excess (discussed below) from SWAT watershed model and from simple ArcGIS-based ArcCN-Runoff (ACR) tool. In both cases the spatially varied precipitation excess was developed for the whole watershed and was given as input to the OFT model.

5.5.2.1 Precipitation excess using SWAT watershed model

This study used the SWAT model, version 2009 (ArcSWAT 93.7b), a widely used, watershed-scale, process-based model (Gassman et al., 2007; Douglas-Mankin et al., 2010) developed by the USDA Agricultural Research Service (ARS) (Arnold et al., 1998; Neitsch et al., 2005). The SWAT model divides the watershed into a number of subwatersheds based on topography. Each subwatershed was further divided into hydrologic response units (HRUs), which are the smallest landscape component of SWAT used for computing hydrologic processes. Flow, sediment, nutrients, and other constituent yields are simulated at the HRU level, summed to the subwatershed level, and then routed through the channels, ponds, reservoirs and wetlands to the watershed outlet.

SWAT calculates surface runoff for each HRU based on USDA NRCS Curve Number (CN) method (USDA-SCS, 1972). SWAT modifies a user-input CN_2, which is a function of hydrologic soil group, landuse and land management, on a daily basis using root-zone soil moisture. SWAT assumes CN_1 at wilting point, CN_3 at field capacity, and a CN of 100 at saturation point (Arnold et al., 2000).

Watershed conditions were defined by several inputs to the SWAT model. Topographic dataset was prepared from the U.S. Geological Survey (USGS) 10 m × 10 m Digital Elevation Model (USGS, 1999). The soil dataset was developed from the Soil Survey Geographic (SSURGO) database (USDA-NRCS, 2005) with a processing utility (Sheshukov et al., 2012) that converted the SSURGO dataset into an ArcSWAT compatible format. Landuse/landcover (LULC) data were derived manually using the CLU (Common Landuse Unit) field boundary shapefile. Each field landcover in the LULC data was manually edited based on field survey data

available for the Goose Creek watershed. Farming operations such as planting, harvesting, and manure application were derived by consulting extension specialists working in that watershed.

Daily precipitation data for the watershed was obtained using Next Generation Radar (NEXRAD) Process 3 (P3) data. NEXRAD contains hourly rainfall data in the form of grid cells with a grid spatial resolution of approximately 4 km x 4 km. Daily precipitation data for each grid cell was obtained by summing hourly P3 data for the same 24-hour data collection period of precipitation gauge stations in the watershed. A previous study by Gali (2010) in Cheney Lake watershed developed P3 data in SWAT format (Gali et al., 2012). Precipitation data were created for each SWAT subwatershed (subwatersheds delineated by Gali (2010) for Cheney Lake watershed) using an area-weighted-average of NEXRAD grid cells that represented each subwatershed. In this study, a total of 7 precipitation gauge stations which covered Goose Creek watershed (Figure 5.1), with a daily precipitation data from 1 January 1994 to 31 December 2006, were extracted and used as weather input into SWAT model.

Once the inputs of topography, soil, landuse, land management, and weather were satisfied, the model delineated the watershed into 29 subwatersheds and 1520 HRUs. The HRUs in SWAT do not have spatial reference, but this limitation was overcome by redefining the topographic, soil, and landuse thresholds to 0%, 0%, 0% (Gitau et al., 2006; Busteed et al., 2009; Daggupati et al., 2011). Farming operations were simulated by modifying SWAT management files for each HRU that represent individual farm fields within the watershed.

Flow was calibrated to daily measured streamflow recorded at the outlet of the watershed from 1 January 1997 to 31 July 2000. An automated baseflow filter program (Arnold and Allen, 1999) was used to determine the baseflow recession constant. During calibration, the model parameters were either increased or decreased from their respective baseline values (Table 5.1) based on the hydrographs (Figure 5.4) and model statistics. Watershed outlet stream discharge from the SWAT model was evaluated statistically using coefficient of determination (R^2), Nash-Sutcliffe model efficiency (NSE) (Nash and Sutcliffe, 1970), and percent bias (PBIAS) (Moriasi et al. 2007).

The model agreement with the observed flow data was satisfactory to very good for daily values (NSE: 0.47; R^2: 0.53; PBIAS: 26.6%), and agreement for monthly values was good to very good (NSE: 0.65; R^2: 0.58; PBIAS: 26.9%). Daily comparison of observed and modeled stream flow (Figure 5.4) showed that the model captured peaks during the summer months with

greater accuracy. Since we are interested in EG formation, which generally result from higher flow rate events, further detailed calibration was not done in this study. The calibrated model was run again on daily basis from 2001 to 2005. The model output of surface runoff was extracted for October 2 (day 275), 3 (276), 4 (277) for each HRU within the watershed.

Figure 5.4 Daily simulated and observed stream flow at the outlet of the watershed

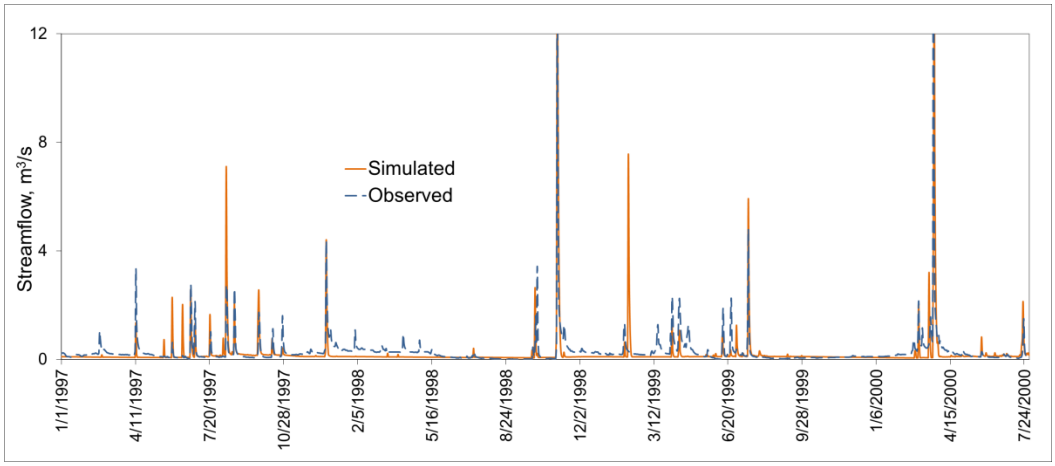

Hourly precipitation using a local weather station (Pretty Prairie weather station located 19 km east of watershed) revealed that precipitation on October 2 lasted for one hour, on October 3 precipitation lasted 18 hours (started at 6:00 AM and ended at 12:00 PM), and on October 4 precipitation lasted 3 hours. The precipitation on October 3 was assumed to have resulted in the formation of EGs because the precipitation on that day was 85 mm, which was greater than the precipitation depths reported in literature that resulted in the formation of EGs (discussed earlier). It was also seen from Figure 5.6 that stream flow at the outlet of watershed was 0.24 m^3/s on October 2, while on October 3 flow was 17.7 m^3/s. This suggests that the precipitation on October 3 resulted in surface runoff on the same day and would have led to the formation of EGs. The OFT model needs steady-state precipitation excess (runoff) in mm/hr; therefore, total surface runoff (mm) for each HRU was divided by the total time the precipitation lasted on October 3. Typical watershed contribution area for an EG is small, and therefore the time of concentration (T_c) will be low. T_c calculated using TR -55 for the EG shown in Figure 5.9 was 21 minutes for the precipitation amount of 85 mm. According to rational method hydrograph (discussed as in Wanielista et al., 1996, Figure 6.16), when precipitation (of a constant rate) continues past the time of concentration then a constant runoff rate is produced for the remaining

duration of rainfall. From Figure 5.5, it can be seen that for the rainfall on October 2, which lasted for 18 hours, the runoff was assumed to take about 20 minutes to reach constant rate (or steady state) and continued at this rate until the duration of the rainfall. There was a constant runoff rate for around 17.6 hours. Therefore, dividing the surface runoff with duration of precipitation to get steady state precipitation excess in mm/hr was considered to be justifiable for this study. Therefore the surface runoff (mm) for each HRU was divided by 18 hours (duration of the storm event) to get precipitation excess in mm/hr.

Figure 5.5 Runoff, precipitation, time of concentration for a typical ephemeral gully watershed.

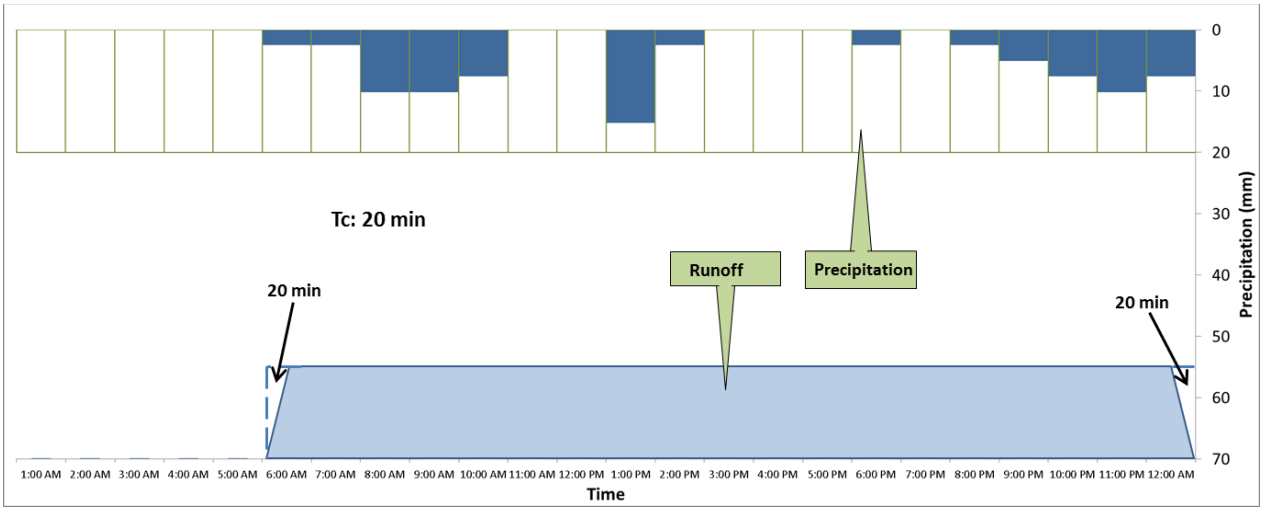

The modeled HRU output along with precipitation excess was joined to fullHRU shapefile (generated during SWAT model input processing), and was area-weighted to each field within the watershed, so that precipitation excess was represented spatially. The spatially varied precipitation excess was converted to a raster format and was used in the OFT model.

Figure 5.6 Precipitation and stream flow before during and after EG formations

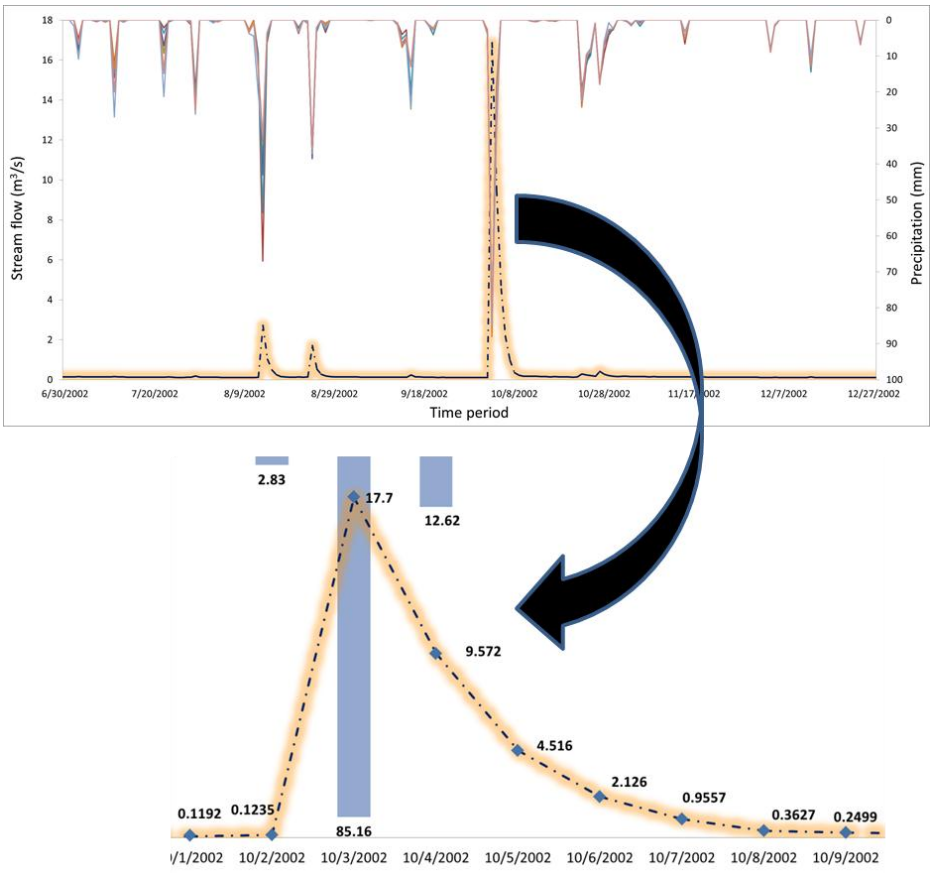

5.5.2.2 Precipitation excess using ACR tool

Deriving spatially varied precipitation excess using SWAT model is very tedious and time consuming and involves many inputs and a skilled technician. Hence a modified ArcGIS-based ArcCN-Runoff (ACR) tool (Zhan and Huang, 2004) was also tested for generating spatially varied precipitation excess in Goose Creek watershed. Soil and landuse are the only inputs needed by the ACR tool. SSURGO soil and manually prepared field landuse were modified to suit the tool requirements and were used as inputs. Once the inputs were satisfied, the tool intersected landuse and soil layers to extract landcover and soil group attributes, and a new layer was prepared. The landcover was edited to represent the actual landcover conditions on October 3 using index table in the CN database (Figure 5.7) (e.g., cropland land represented as fallow poor condition because the crop was just planted in the watershed and the soil had little crop residue). The CN database was built based on similar CN databases that are being used by SWAT, AnnAGNPS and BASINs watershed models. The CN_2 for each parcel/polygon in the

layer was calculated using the soil group and landcover attributes provided. A spatially varied CN layer was generated, and was used to calculate spatially varied surface runoff using USDA NRCS CN method (USDA-SCS, 1972) for daily precipitation amount on October 3. Unlike in the SWAT model, the CN in the ACR tool cannot be changed daily (i.e., CN_2 was used). The surface runoff was then divided by 18 hours, as discussed above, was area-weighted to each field to obtain spatially varied precipitation excess (mm/hr), and was used as input to the OFT model.

Figure 5.7 ArcGIS based ArcCN-Runoff (ACR) tool

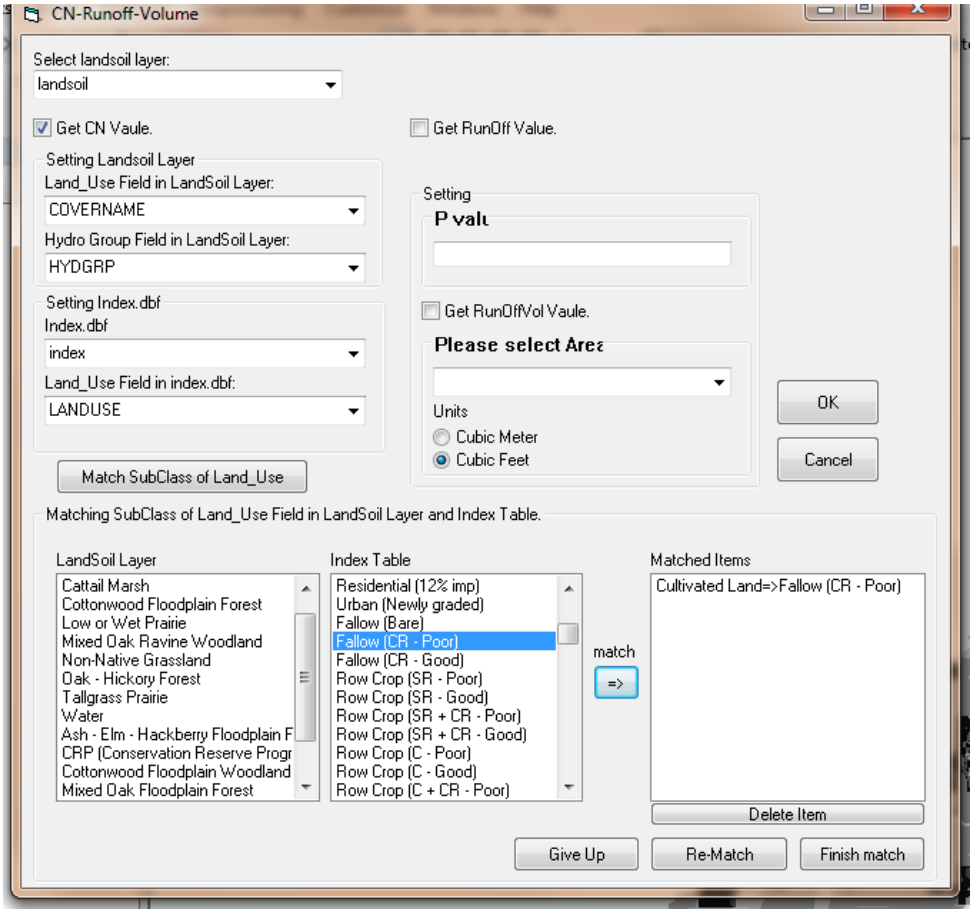

5.5.3 SA model

The SA model as described in the earlier chapter (Section 4.1 and 4.2.1) was modified to calculate EG lengths automatically once the inputs were satisfied. The automated geospatial model is presented in Figure 5.8. In this study a threshold of 50 was used because threshold 50 performed better in identifying location and lengths compared to other thresholds in a small

study area (S2: 1,927 ha (4,761 ac)) within the Goose Creek watershed (13,306 ha (32,880 ac)) (Chapter 4).

5.5.4 Assessment of Models

Three scenarios were developed using the OFT and SA models to predict lengths of EGs. Two scenarios were developed using the OFT model by changing spatially varied precipitation excess calculated using the SWAT model (Scenario 1) and ACR tool (Scenario 2). Scenario 3 was developed directly using the SA model. Each scenario's performance in predicting EG occurrence (presence or absence within a given area) and EG length (total accumulated length within a given area) was evaluated, as described in Chapter 4. Visual interpretation was used to evaluate length predictions along the trajectory of digitized or observed EG (Section 4.2.5.1). Occurrence statistical analysis using error matrix approach (Section 4.2.5.2) was carried out to evaluate the occurrence (presence or absence) of EG in a given location. One-ha catchments were used to construct error matrix table, and false positive, false negative and Kappa (κ) statistics were used for analysis. The performance of each scenario in correctly predicting lengths was evaluated using length statistical analysis techniques (Section 4.2.5.3). Length of observed and predicted EGs were compared by extracting EGs in catchments where both observed and predicted EGs were present, and NSE, R^2 and PBIAS were used for comparison.

5.6 Results and Discussions

5.6.1 Visual interpretation

Figure 5.9 shows the output maps of lengths for scenarios 1, 2 and 3 in an agricultural field where an EG has formed as a result of the 3 October 2002 precipitation event, and was seen on aerial image taken on 22 March 2003. Scenario 2 (OFT model with precipitation excess from ACR tool) over-predicted lengths compared to scenario 1 (OFT model with precipitation excess from SWAT model) and scenario 3 (SA model).

Figure 5.8 Geospatial model for predicting location and length of EGs using SA model

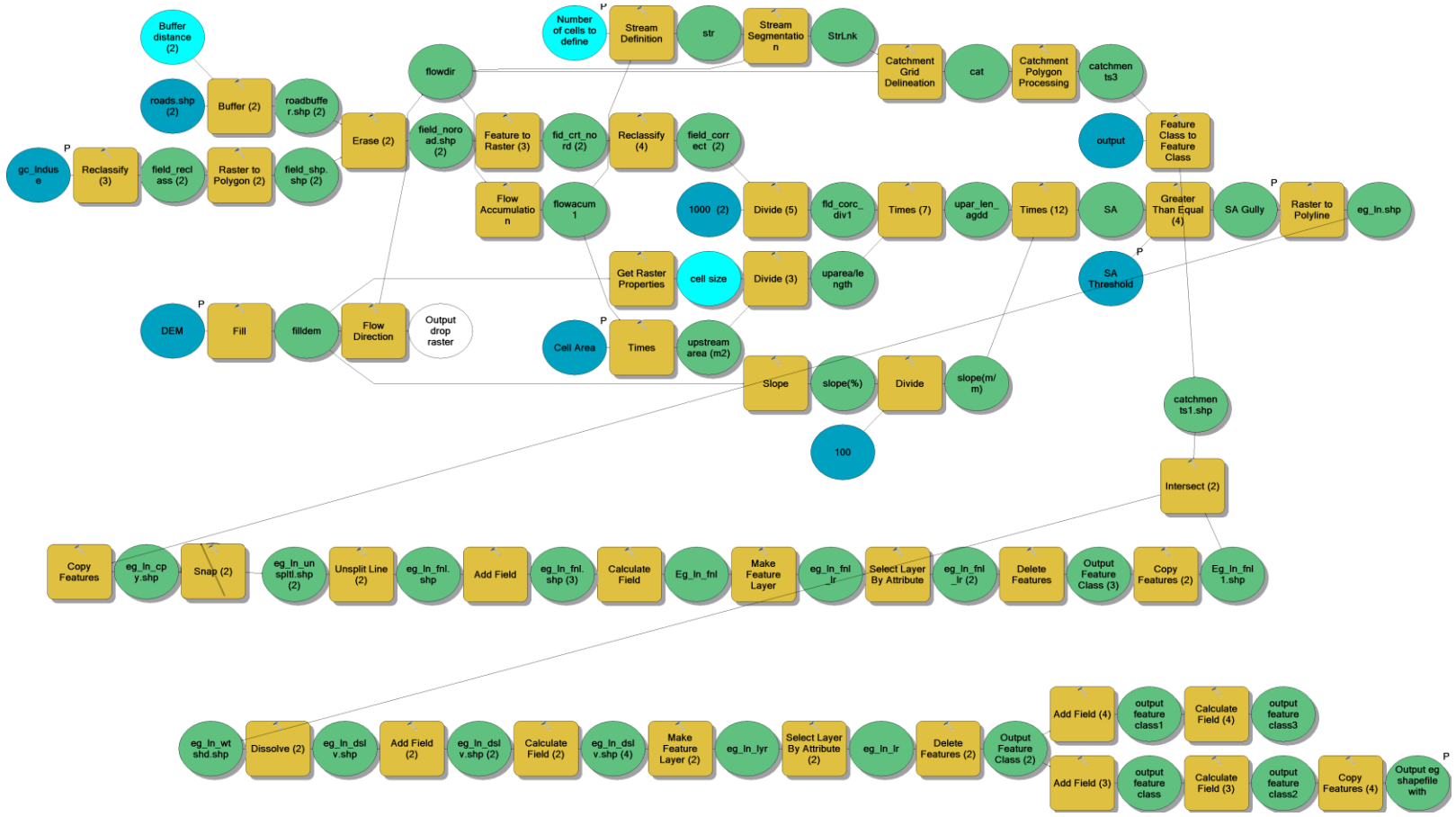

Figure 5.9 Observed EG length digitized from an aerial image, and predicted EG lengths for scenarios 1, 2 and 3 in an agricultural field.

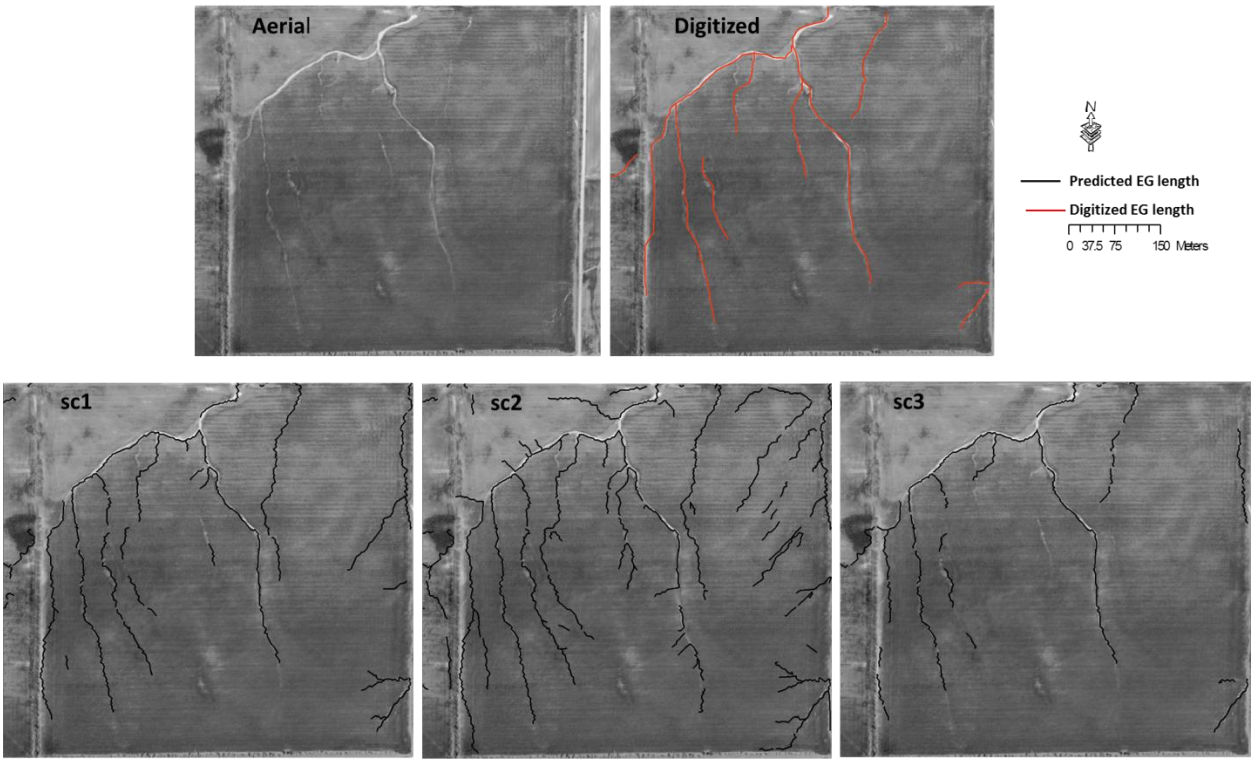

Scenarios 1 and 2 were generated using the OFT model with all inputs constant except for the precipitation excess, which resulted in different length predictions of EGs. The agricultural field shown in Figure 5.9 was used as an example field to demonstrate the differences among precipitation excess using SWAT model and ACR tool. The agricultural field was planted in wheat, soil was fine loam (9.5% clay, 27% silt, 63.5% sand) with hydrologic soil group B, precipitation on October 3 was 85 mm (3.3 in), area-weighted surface runoff generated on that day using SWAT model was 29.3 mm (1.15 in), and the resultant precipitation excess was 1.62 mm/hr (0.06 in/hr). The area-weighted surface runoff generated by ACR tool was 47.5 mm (1.85 in), and the resultant precipitation excess was 2.63 mm/hr (0.10 in/hr). The surface runoff and precipitation excess using ACR tool (scenario 2) was approximately 1.5 times greater than those using the SWAT model (scenario 1). The SWAT model was run on daily basis, and varied antecedent moisture conditions on daily basis to calculate daily CN and thereby the daily surface runoff. In the case of the ACR tool, even though it used actual land cover (discussed earlier) and the same soil data as in the SWAT model, use of a constant CN_2 resulted in greater

surface runoff. This shows the advantage of using process-based watershed models in predicting surface runoff for a given day compared to other simple means of estimating surface runoff using different methods. The OFT model, which uses Eq. 5.6 to generate length, is sensitive to precipitation excess. Increase in precipitation excess results in an inverse-proportional decrease of critical drainage area needed for an EG to form, resulting in increased EG length predictions. Therefore, greater precipitation excess using ACR tool resulted in larger lengths compared to lengths generated using SWAT model precipitation excess.

Visual interpretation revealed that scenario 1, developed using the OFT model, slightly over-predicted lengths compared observed lengths. The reasons are explained below.

Soil critical shear stress (τ_{cr}) is an important parameter in predicting the length of EGs. Knapan and Poesen (2010) reported that EG initiation and lengths are controlled by τ_{cr}. Findings of Knapan and Poesen (2010) are confirmed in this study using Eq. 5.6, where τ_{cr} and critical drainage area are directly proportional, and an increase in τ_{cr} results in an increase of critical drainage area needed for EG formation, resulting in reduced lengths of EG. Poesen et al. (1992) and Knapan et al. (2007) reported that soil shear strength values at saturation appeared to be a good indicator of τ_{cr}. Knapan and Poesen (2010) measured soil shear strength in locations where EGs were formed during winter in silt loam soils using Torvane (4.8 cm diameter, with the shear plane at 0.6 cm depth) after precipitation events and derived τ_{cr} using

$$\tau_{cr} = 1.36\tau_s + 3.6 \quad (5.8)$$

where τ_s is soil shear strength. The values of τ_{cr} ranged from 5 to 15 N/m^2 in their study area. The τ_{cr} values in our watershed ranged from 0.31 to 0.71 N/m^2 and were derived using Eq. 5.7. The τ_{cr} values were smaller compared to literature because Eq. 5.7 calculates τ_{cr} from clay content of generalized SSURGO soils. At this time the values of τ_{cr} used in this study are uncertain, and therefore we assume that this would have contributed to the slight over predictions of lengths.

Interestingly, visual interpretations reveal that scenario 3 (SA model) predictions closely matched the observed lengths (Figure 5.9) even though scenario 3 was a simple topographic approach. Visual interpretation is not sufficient for analyzing results; therefore, occurrence and length statistics were developed to statistically analyze results and are discussed below.

5.6.2 Occurrence and length analysis

Error matrix tables were developed using 1-ha catchments, and statistics of false positive rate, false negative rate and κ were used to analyze the performance of each scenario (Table 5.1). Scenario 2 had greater false positive rate (53%), lower false negative rate (12%), and lower κ (0.17) compared to scenario 1 (false positive = 34%, false negative = 18%, and κ = 0.29). Better false positive and false negative rates were seen for scenario 1compared to scenario 2, resulting in better overall performance of scenario 1 compared to scenario 2. The reason for scenario 2 performing poorly is due to the use of greater precipitation excess values from the ACR method, as discussed earlier, resulting in greater number of EGs predictions in catchments where observed EGs were not present and hence higher false positive rates and lower κ.

Table 5.1 False positive rate, false negative rate, Kappa (κ) for each scenario

Statistics	Scenarios		
	1	2	3
False positive rate	34%	53%	26%
False negative rate	18%	12%	30%
Kappa (κ)	29%	17%	30%

Scenario 1 had greater false positive rate (34%), lower false negative rate (18%), and similar κ (0.29) compared to scenario 3 (false positive = 26%, false negative = 30%, and κ = 0.30). Better false positive and false negative rates were seen for scenario 3 compared to scenario 1, resulting in slightly better overall performance of scenario 3 compared to scenario 1.

The reason for better performance of SA model (scenario 1) was because the SA model used a threshold 50 based on calibration in a small study area (S2) that was within the Goose Creek watershed (Figure 5.10). The results of each threshold and their effects on model performance in S2 was discussed in Section 4.3.4. Comparison of occurrence statistics from the S2 area used in calibration (Figure 4.17) to those found by applying the same threshold (T = 50) in the Goose Creek watershed showed in an increase in false positive rate from 16% to 26%, increase in false negative rate from 26% to 30% and reduction in κ from 0.52 to 0.30. This shows that calibrating a topographic index model and selecting a best threshold in one small area and applying it to a larger area within the same geographical region results in decreased model performance. Also, from Chapter 4, it was also found that using a best threshold from one area

in another geographical region resulted in sub-optimal model performance. Therefore, using topographic model has its limitation.

Figure 5.10 Study areas (S1 and S2). S2 is a part of Goose Creek watershed. Threshold for S1 was 30 and Threshold for S2 was 50.

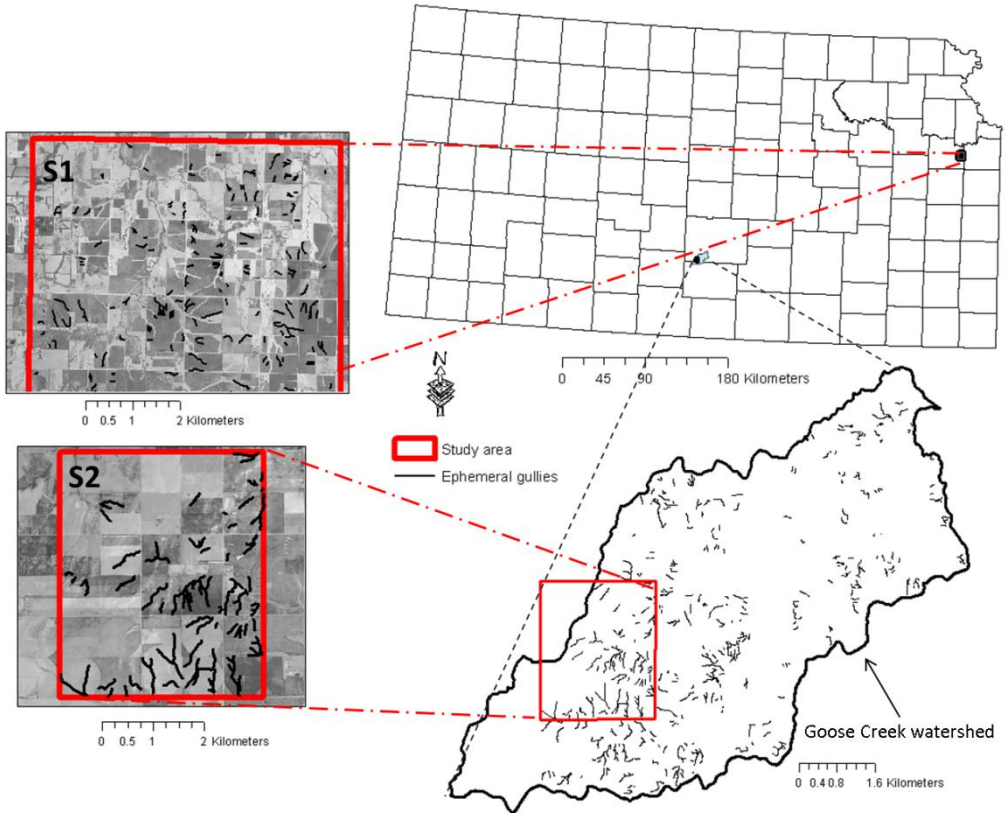

On the other hand, the OFT model was un-calibrated (unlike the SA model). Major factors that result in the formation of EGs, such as precipitation, soil, topography and landuse/land management practices, were incorporated in the OFT model, which utilizes a physical based equation developed by Montgomery and Dietrich (1994). Extreme care was taken to input detailed field-level data into the model. The τ_{cr} values derived using Eq. 5.6 were uncertain because only a simple empirical relationship (Eq. 5.6) using SSURGO clay-content data were used. The occurrence statistics of false positive = 34%, false negative = 18%, and κ = 0.29 were considered to represent reasonably good model performance, particularly since the model was uncalibrated, even though this performance was slightly lower than using the

calibrated SA model. Further investigation is needed to reduce uncertainties associated with definition of τ_{cr} to more adequately evaluate the OFT model predictive capabilities.

Terracing is the dominant best management practice implemented in the watershed. Around 36% of the agricultural fields in Goose Creek watershed were terraced. Both OFT model and SA model predicts gullies along terrace channels. It was interesting to see that OFT model also predicted EGs along terrace channels because of greater influence of upstream drainage area and slope. At this time, a model predicting the EGs along terrace channels was considered to be an error by the model, because the EGs along terrace channels were not visible during digitizing EGs on 2003 aerial image, and further field investigation would be needed to verify their existence along terrace channels.

EGs lengths (predicted and observed) present in catchments were extracted and compared using R^2, NSE and PBIAS for each scenario (Table 5.2). The performance was worse for scenario 2 (NSE: -0.39, PBIAS: -94.5%) and better for scenario 3 (NSE: 0.67, PBIAS: -18.4%) compared to scenario 1 (NSE: 0.55, PBIAS: -40.7%). The NSE and PBIAS for scenario 2 was very poor compared to scenario 1 and scenario 3. The reason for poor statistics by scenario 2 was because of over prediction of EG lengths, due to poor runoff estimation. Slightly better statistics of scenario 3 compared to scenario 1 was also discussed earlier.

The statistics of NSE: 0.55 and PBIAS: -40.7% for OFT model were considered to demonstrate good model performance in predicting EG length. PBIAS of -40.7% show that the model over-estimated EG length, i.e., the simulated lengths were larger than the observed length. This was mainly due to uncertainty with the τ_{cr}. Also, the length statistics of NSE and PBIAS demonstrated poorer model performance for Goose Creek watershed (NSE: 0.67, PBIAS: -18.4%) compared to S2 (NSE: 0.85, PBIAS: -4.0%), which again shows the limitation of applying a threshold calibrated in one region to a larger region. The results of the occurrence and length statistical analysis were similar to visual interpretation results. However occurrence and length statistics helped better analyze the model performances.

Table 5.2 Coefficient of determination (R^2), Nash-Sutcliffe model efficiency (NSE) and percent bias (PBIAS) for three scenarios to evaluate model performances

Statistics	Scenarios		
	1	2	3
R^2	0.50	0.46	0.39
NSE	0.55	-0.39	0.67
PBIAS (%)	-40.7	-94.5	-18.4

5.7 Conclusions

The OFT model, which utilizes topography, precipitation, soil and landuse/landcover, was developed in a GIS environment to predict location and length of EGs. The precipitation excess, an input parameter in the OFT model, was derived using processed based SWAT model and ACR tool. OFT model and SA model performances were compared and evaluated.

Visual interpretation, occurrence and length statistics reveal that OFT model with precipitation excess derived using SWAT model (scenario 1) performed better compared to precipitation excess derived using ACR tool (scenario 2). Fixed CN in ACR tool resulted in higher precipitation excess and thereby larger EG length predictions. OFT model with precipitation excess derived using SWAT model slightly over-predicted the EG lengths compared to observed EG lengths, probably because of uncertainties in estimating τ_{cr}. Therefore, an accurate determination of τ_{cr} is needed to derive length of EGs. Future research to derive τ_{cr} using readily available or readily obtainable data is needed.

The occurrence and length statistics showed that performance of calibrated SA model and uncalibrated OFT-SWAT model was similar. The SA model requires calibration of threshold for the site being tested, whereas the OFT model did not need calibration, as it considered site specific topography, precipitation, soils and landuse/landcover. Hence usage of the physical based OFT-SWAT model was demonstrated to provide similar performance to the best-performing, calibrated topographic index model (SA model) for the study area without requiring extensive field-based EG length data and model calibration, and thus provides a preferred method to predict EG lengths.

5.8 References

Anderson, R. S., and S. P. Anderson. 2010. Geomorphology: The Mechanics and Chemistry of Landscapes. Cambridge University Press, 368 p.

Arabi, M., J. R. Frankenberger, B. A. Engel, and J. G. Arnold. 2008. Representation of agricultural conservation practices with SWAT. *J. Hydrol. Proc.* 22(16): 3042-3055.

Arnold, J. G., R. S. Muttiah, R. Srinivasan, and P. M. Allen. 2000. Regional estimation of base flow and groundwater recharge in the Upper Mississippi River Basin. *J. Hydrol.* 227: 21-40.

Arnold, J. G., and P. M. Allen. 1999. Automated methods for estimating baseflow and ground water recharge from streamflow records. *J. American Water Resour. Assoc.* 35(2): 411–424.

Arnold, J. G., R. Srinivasan, R.S. Muttiah, and J. R. Williams. 1998. Large area hydrologic modeling and assessment Part I: Model development. *J. American Water Resour. Assoc.* 34(1): 73–89.

Busteed, P. R., D. E. Storm, M. J. White, and S. H. Stoodley. 2009. Using SWAT to target critical source sediment and phosphorus areas in the Wister Lake basin, USA. *American J. Environ. Sci.* 5(2): 156-163.

Capra, A., and B. Scicolone. 2002. Ephemeral gully erosion in a wheat-cultivated area in Sicily, Italy. *Biosyst. Eng.* 83(1): 119-126.

Capra, A., L. M. Mazzara, and B. Scicolone. 2005. Application of the EGEM model to predict ephemeral gully erosion in Sicily (Italy). *Catena.* 59: 133–146.

Capra, A., P. Porto, and B. Scicolone. 2009. Relationships between rainfall characteristics and ephemeral gully erosion in a cultivated catchment in Sicily (Italy). *Soil Tillage Res.* 105: 77-87.

Casali, J., J. J. Lopez, and J. V. Giraldez.1999. Ephemeral gully erosion in southern Navarra (Spain). *Catena.* 36: 65– 84.

Cerdan, O., Y. Le Bissonnai, A. Couturier, H. Bourennane, and V. Souchere. 2002. Rill erosion on cultivated hillslopes during two extreme rainfall events in Normandy, France. *Soil Tillage Res.* 67: 99–108.

Classens, L., G. B. M. Heuvelink, J. M. Shoorl, and A. Veldkamp. 2005. DEM resolution effects on shallow landslide hazard and soil redistribution modeling. *Earth surf. Process. Landforms.* 30: 461- 477

Daggupati, P., K. R. Douglas-Mankin, A. Y. Sheshukov, and P. L. Barnes. 2010. Monitoring and Estimating Ephemeral Gully Erosion using Field Measurements and GIS. ASABE Paper No. 10-9663. ASABE, St. Joseph, MI.

Daggupati, P., K. R. Douglas-Mankin, A. Y. Sheshukov, P. L. Barnes, and D. L. Devlin. 2011. Field-level targeting using SWAT: Mapping output from HRUs to fields and assessing limitations of GIS input data. *Trans. ASABE.* 54(2):501-514.

De Baets, S., J. Poesen, G. Gyssels, and A. Knapen. 2006. Effects of grass roots on the erodibility of topsoils during concentrated flow. *Geomorphology.* 76: 54-67.

De Baets, S., J. Poesen, A. Knapen, and P. Galindo. 2007. Impact of root architecture on the erosion-reducing potential of roots during concentrated flow. *Earth Surf. Proc. Land.* 32: 1323–45. DOI: 10.1002/esp.1470.

Douglas-Mankin, K., P. Daggupati, A. Sheshukov, P. Barnes, D. Devlin, and N. Nelson. 2011. Cheney Lake Watershed: Erosion from ephemeral gullies. Kansas State Research and Extension Publication. MF-3030.

Douglas-Mankin, K. R., R. Srinivasan, and J. G. Arnold. 2010. Soil and Water Assessment Tool (SWAT) model: current developments and applications. *Trans. ASABE* 53(5):1423-1431.

Foster, G. R., 1986. Understanding ephemeral gully erosion. Soil Conservation, vol. 2. National academy of science Press, Washington, DC, pp. 90-125.

Gali, R. K. 2010. Assessment of NEXRAD P3 data on streamflow simulation using SWAT. M.S. Thesis, Department of Biological and Agricultural Engineering, Kansas State University, Manhattan, KS.

Gali, R. K., K. R. Douglas-Mankin, X. Li, and T. Xu. 2012. Assessing NEXRAD P3 data effects on Stream-flow Simulation using SWAT Model in an Agricultural Watershed. *J. Hydrol. Eng.* (submitted 7/15/2001)

Gassman, P.W., M. R. Reyes, C. H. Green, and J. G. Arnold. 2007. The Soil and Water Assessment Tool: historical development, applications, and future research directions. *Trans. ASABE.* 50(4): 1211-1250.

Gitau, M. W., T. L. Veith, W. J. Gburek, and A. R. Jarrett. 2006. Watershed-level best management practice selection and placement in the Town Brook watershed, New York. *J. American Water Resour. Assoc.* 42(6): 1565-1581.

Gordon, L. M., S. J. Bennett, R. L. Bingner, F. D. Theurer, and C. V. Alonso. 2007. Simulating ephemeral gully erosion in AnnAGNPS. *Trans. ASABE*. 50(3): 857-866.

Hargrove, W. L., D. Johnson, D. Snethen, and J. Middendorf. 2010. From dust bowl to mud bowl: sedimentation, conservation measures, and the future of reservoirs. *J. Soil Water Cons.* 65(1): 14A-17A.

KDHE. 2000. A Watershed Conditions Report for the State of Kansas HUC 11030014 (North Fork Ninnescah). Kansas Department of Health and Environment: Topeka, KS. Available at: http://www.kdheks.gov/nps/wc_reports/11030014.pdf.

Knapen, A., and J. Poesen. 2010. Soil erosion resistance effects on rill and gully initiation points and dimensions. *Earth Surf. Proc. Land.* 35: 217-28.

Knapen, A., J. Poesen, and G. Govers . 2007. Resistance of soils to concentrated flow erosion: A review. *Earth-Sci. Rev.* 80: 75-109.

Montgomery, D. R., and W.E. Dietrich. 1994. Landscape Dissection and Drainage Area-Slope Thresholds. Process Models and Theoretical Geomorphology, M. J. Kirby (ed.). Wiley, New York, 221-246.

Moriasi, D. N., J. G. Arnold, M.W. Van Liew, R. L. Bingner, R. D. Harmel, and T. L. Veith. 2007. Model evaluation guidelines for systematic quantification of accuracy in watershed simulations. *Trans. ASABE.* 50(3): 885-900.

Moore, I. D, R. B. Grayson, and A. R. Ladson. 1991. Digital terrain modelling: a review of hydrological, geomorphological, and biological applications. *Hydrol. Proc.* 5: 3-30.

Nachtergaele, J., and J. Poesen. 2002. Spatial and temporal variations in resistance of loess-derived soils to ephemeral gully erosion. *Eur. J. Soil Sci.* 53: 449-63.

Nachtergaele, J., J. Poesen, L. Vandekerckhove, D. O. Wijdenes, and M. Roxo. 2001a. Testing the Ephemeral Gully Erosion Model (EGEM) for two Mediterranean environments. *Earth Surf. Proc. Land*. 26(1): 17.

Nachtergaele, J., and J. Poesen. 1999. Assessment of soil losses by ephemeral gully erosion using high-altitude (stereo) aerial photographs. *Earth Surf. Proc. Land.* 24: 693- 706.

Nachtergaele, J., J. Poesen, and A. Steegen. 2001b. The value of a physically based model versus an empirical approach in the prediction of ephemeral gully erosion for loess-derived soils. *Geomorphology.* 40: 237-52.

Nash, J. E., and J. V. Sutcliffe. 1970. River flow forecasting through conceptual models: Part I. A discussion of principles. *J. Hydrol.* 10(3): 282-290.

Nearing, M. A., G. R. Foster, L. J. Lane, and S. C. Finkner. 1989. A process-based soil erosion model for USDA-Water Erosion Project technology. *Trans. ASAE.* 32: 1587-159.

Neitsch, S. L., J. G. Arnold, J. R. Kiniry, and J. R. Williams. 2005. Soil and Water Assessment Tool (SWAT), Theoretical documentation. Temple, Tex.: USDA-ARS Grassland Soil and Water Research Laboratory.

O'Callagham, J. F., and D. M. Mark. 1984. The extraction of drainage networks from digital elevation data. *Comput. Vision Graph.* 28: 323-344.

Pack, R. T., D. G. Tarboton, and C. N. Goodwin. 2001. Assessing Terrain Stability in a GIS using SINMAP. 15th Annual GIS Conference, GIS 2001, Vancouver, British Columbia, February 19 – 22

Parajuli, P. B., N. O. Nelson, L. D. Frees, and K. R. Mankin. 2009. Comparison of AnnAGNPS and SWAT model simulation results in USDA-CEAP agricultural watersheds in south-central Kansas. *Hydrol. Process*. 23: 748-763.

Parker, C., C. Thorne, R. Bingner, R. Wells, and D. Wilcox. 2007. Automated Mapping of Potential for ephemeral gully formation in agricultural watersheds. National Sedimentation Laboratory Technical Research Report No 56, Oxford, Mississippi, USA.

Patton, P. C., and S. A. Schumm. 1975. Gully erosion, Northwestern Colorado: a threshold phenomenon. *Geology*. 3: 88–90.

Poesen, J., 1992. Mechanisms of overland flow generation and sediment production on loamy and sandy soils with and without rock fragments. In: Parsons, A.J., Abrahams, A.D. (Eds.), *Overland Flow Hydraulics and Erosion Mechanics*. UCL Press, London, UK, pp. 275–305.

Poesen, J., J. Boardman, B. Wilcox, and C. Valentin.1996. Water erosion monitoring and experimentation for global change studies. *J. Soil Water Conserv.* 51(5): 386-390.

Poesen, J., J. Nachtergaele, G. Verstraeten, and C. Valentin. 2003. Gully erosion and environmental change: importance and research needs. *Catena* 50: 91-133.

Poesen, J., D. Torri, and T. Vanwalleghem. 2011. Ch. 19 – Gully erosion: procedures to adopt when modelling soil erosion in landscapes affected by gullying. In: Morgan, R.P.C., and M.A. Nearing (eds). *Handbook of Erosion Modelling*, Blackwell-Wiley: Oxford.

Prosser, I. P., and B. Abernathy. 1996. Predicting the topographic limits to a gully network using a digital terrain model and process thresholds. *Water Resour. Res.* 23(7): 2289-2298.

Prosser, I. P., and C. J. Slade. 1994. Gully formation and the role of valley-floor vegetation, southeastern Australia. *Geology*. 22: 1127-30.

Robinson, K. M., S. J. Bennett., J. Casali and G. J. Hanson. 2000. Processes of headcut growth and migration in rills and gullies. *Intl. J. Sediment Res.* 15: 69-82.

Sheshukov, A.Y., P. Daggupati, K. R. Douglas-Mankin, and M. Lee. 2012. High Spatial Resolution Soil Data for Watershed Modeling: 1. Development of a SSURGO-ArcSWAT Utility. *J. Natural & Environ. Sci.* 2(2): 15-24.

Smerdon, E. T., and R. P. Beasley. 1961. Critical tractive forces in cohesive soils. *Agr. Eng.* 42(1): 26-29.

Souchère, V., O. Cerdan and B. Ludwig. 2003. Modeling ephemeral gully erosion in small cultivated catchments. *Catena* 50: 489-505.

Tarboton, D.G., 2003. Terrain analysis using digital elevation models in hydrology. *In Proc. 23rd ESRI international User Conf.* San Diego, CA. July 7-11

Thome, C. R., L.W. Zevenbergen, E. H. Grissinger and J. B. Murphey. 1986. Ephemeral gullies as sources of sediments. *In Proc. Federal Interagency Sedimentation Conf*. 3-152 - 3-161.

USDA-NRCS. 1997. America's private land, a geography of hope. USDA-NRCS. Washington, D.C.

USDA-NRCS. 2005. Soil Survey Geographic (SSURGO) database. Washington, D.C.: USDA Natural Resources Conservation Service. Available at: http://soildatamart.nrcs.usda.gov/Default.aspx. Accessed November 2011.

USDA-SCS. 1972. National Engineering Handbook, Hydrology Chapter 4. Washington, D.C.: U.S. Department of Agriculture, Soil Conserv. Service.

USGS. 1999. DASC data catalog. Lawrence, Kans.: Kansas Data Access and Support Center. Available at: www.kansasgis.org/catalog/catalog.cfm. Accessed November 2011.

Vandaele, K., J. Poesen, J. R. Marques da Silva, and P. Desmet. 1996. Rates and predictability of ephemeral gully erosion in two contrasting environments. *Geomorphologie: Relief, Processus, Environment.* 2: 83-96.

Vandekerckhove, L., J. Poesen, and D. W. Oostwoud. 2000. Thresholds for gully initiation and sedimentation in Mediterranean Europe. *Earth Surf. Proc. Land.* 25: 1201-20.

Wanielista, M., R. Kersten, and R. Eaglin. 1997. Hydrology, Water Quality and Quality Control, 2nd Ed. New York: John Wiley & Sons, Inc.

Woodward, D. E. 1999. Method to predict cropland ephemeral gully erosion. *Catena* 37: 393-9.

Zhan, X., and M. N. Huang. 2004. ArcCN-Runoff: an ArcGIS tool for generating curve number and runoff maps. *Environ. Modell. Softw.* 875-879.

Zhang, Y., Y. Wu, and B. Liu. 2007. Characteristics and factors controlling the development of ephemeral gullies in cultivated catchments of black soil region, Northeast China. *Soil Tillage Res.* 96: 28-41.

Zheng, F., and X. Gao. 2000. Process and modeling of soil erosion on loess slope. Shaanxi Peoples Press, Xian, pp. 96-119.

Chapter 6 - Conclusions and Recommendations

6.1 Conclusions

The overall goal of this study was to address the concern that excess sediment continues to enter water bodies (e.g., lakes, streams, reservoirs) from agricultural fields despite the widespread implementation of conservation practices on for the past few decades. Researchers must identify the main causes (sources) of sediment and prevent or mitigate future sediment contributions so that the current as well as the future generations will benefit. Therefore, this research focused on developing various methods and tools that help in identifying and quantifying sources of sediment.

An ArcGIS toolbar was developed to aggregate SWAT HRU output by field and prepare maps of high-priority fields by sediment, total nitrogen, and total phosphorus yields. The developed toolbar was applied in Black Kettle Creek watershed which was the focus of an innovative project to target conservation practice funding and pay directly for modeled sediment reduction. The SWAT model was calibrated for flow and sediment to assure and field-level sediment yields were validated with the historic local data, and was used to identify agricultural fields with greatest sediment yields in the watershed. Various BMPs (single and combined) were simulated for each field, and effectiveness of a particular BMP was different for each field based on its unique combinations of slope, soil and existing landuse. The variability of sediment reduction results among fields demonstrated the important influence of site-specific conditions in estimating soil-loss reductions possible with given BMPs. The mean BMP effectiveness for top 250 fields ranged from 52% to 96% for single BMPs and 85% to 94% for selected combinations of BMPs. Permanent grass produced the greatest average single-BMP effectiveness (96%) followed by Terraces (with contour farming) (78%) and No-till (72%). No-till + Terrace (with contour farming) had the greatest combined-BMP effectiveness (94%).

Payments to implement each BMP for a given field within the watershed were calculated from field-scale sediment-reduction estimates. An in-field signup sheet was developed to facilitate farmer signup for BMP implementation for each field. Results from this study helped in targeting conservation practices in highest sediment producing fields using modeling approach that allowed flexibility for both adaptor (farmers) and funders (project staff) based on payments

scaled directly by project outcome (in this case, dollars per ton of sediment reduction) while assuring the project objective (i.e., sediment reduction) was met. It is to be noted that the fields with ephemeral gullies were not identified and added separately to the SWAT-generated targeting map because SWAT does not explicitly simulate ephemeral gully (EG) erosion.

Research findings also showed that the fields with high sediment-yield density in this study appeared to be most sensitive to differences in land use data source (field reconnaissance, NASS, or NLCD) followed closely by land management practices (terraces, contour farming and no-till). Differences in DEM (10 m or 30 m) and soil (SSURGO or STATSGO) data source also were very important, though to a lesser extent than other inputs in the watershed tested. Results of this study clearly demonstrated that extreme care should be used in selecting the source of spatial model input data when using SWAT for field-level targeting.

EGs are considered to be a major source of sediment and have gained attention recently. Spatially locating and deriving length of EGs using several topographic index models (SA, CTI, SAP, and WTI) and a physical based model (OFT model) were explored in this study. Automated geospatial models within GIS environment were developed to locate and derive length of EGs. Results show that the SA model predictions were better compared to other topographic models tested. The SA and CTI model predictions had similar pattern in terms of locating EG trajectory, however, the CTI model had greater discontinuity along the trajectory. The method developed to derive length in this study was sensitive to discontinuity and hence the performance of CTI model was poor.

The EG predictions using topographic index models were not accurate without calibrating a range of thresholds to select best threshold for each individual site tested. Applying a calibrated threshold from one site to another site within similar geographical conditions results in slightly poor predictions. However, using a threshold in another geographical location is not recommended (T = 30 for S1 and T = 50 for S2). Hence limitations of topographic index models in well established.

In order to overcome the limitation of topographic index models, an OFT model (physical based model) which utilizes topography, precipitation, soil and landuse/landcover was developed and tested. The precipitation excess an input parameter in the OFT model was derived using SWAT model and ACR tool. The main advantage of OFT model over topographic index models is that no calibration was required by the OFT model because it accounts for site specific

conditions. The OFT model with precipitation excess derived using SWAT model performed better compared to ACR tool. OFT model resulted in slight over predictions compared to observed data because of uncertainties involved with τ_{cr}. The τ_{cr} was derived using clay content of generalized SSURGO data added uncertainty that appear to have contributed to this overestimation. This study result demonstrates the advantage of using physical-based models over simple empirical based models to predict EGs.

Results from this study show that finer resolution DEMs (e.g., 2 m) are needed to locate EGs. Coarser resolution DEMs (10 m or greater) cannot locate EGs but may be useful for locating larger classical gullies in agricultural fields or gullies in rangeland. When considering EGs only within agricultural fields, field landuse is recommended over NASS landuse as NASS landuse results in either over or under predictions.

6.2 Recommendations

1. Field reconnaissance landuse showed good results compared to NASS landuse in both Field targeting and ephemeral gully (EG) studies. Manually preparing field reconnaissance landuse for bigger watersheds is tedious. On the other hand, the NASS landuse can be readily downloadable for many states in US. Therefore, refining methods to improve NASS landuse to better suit the need of the study needs to be explored.
2. In this study, baseline sediment yield and various BMP sediment yield reductions were simulated for each field within the watershed and results show that the effectiveness of a particular BMP was different for each field. It would be interesting to compare the spatially varied BMP reduction with a generalized BMP reduction for given practice. If the comparison is close, then we can use the baseline sediment yield for each field and a generalized BMP reduction for a given BMP and calculate payments instead of simulating site specific BMPs in a watershed model.
3. A big research need to derive length has led to developing a methodology to derive length using topographic index models. The methodology as it is developed converts the pixels that represent EGs into polylines and uses a snapping distance of 5 m to snap lines within a given area (catchments were used in this study). The method is very sensitive to discontinuity among the pixels. Also, this method does not consider any processing that occur during the EG formation. This is the first time such a methodology was developed

to derive length and it needs further exploration and refinements to suit different research needs.

4. In this study, catchments of 1-ha were used as a mask so that the polylines that represent EGs within that catchment were dissolved to get unique id and thereby length can be derived. The method as it is developed captures single EGs however, in the case of branched EGs, each segment of the branched EG in a different catchment was considered a separate EG. Increasing the size of catchment captures the entire branched EG. Increasing the size of the catchment and their impacts on EG predictions needs to be explored.
5. The physical based model used in this study performed better close to topographic index model without the need for calibration. Therefore usage of physical based model is encouraging. The soil critical shear stress (τ_{cr}) was calculated using percent clay of generalized SSURGO soils based Eq. 5.6. Further methods or equations needs to be explored to generate τ_{cr} so that overall model performances can be improved.
6. Testing the OFT model in another watershed in different geographic and climatic region to evaluate the model predictions of EG lengths needs to be explored.
7. The SWAT model used to calculated precipitation excess in the OFT model. NEXRAD data was used as rainfall input and a detailed calibration based on stream gauge data was done in this study. Not all watersheds have NEXRAD data and stream gauge data. Therefore, OFT model performance with precipitation excess derived from un-calibrated SWAT model and weather data from rain gauge needs to be compared.
8. In this study, the OFT model was developed and tested in only one watershed. It needs to be evaluated in another watershed of different geological and climatological region.

Appendix A - Field-specific sign-up sheet developed using SWAT output

Black Kettle Watershed Field Sign Up Sheet
Conservation Innovation Project

Field # 525 Field area (acres) 3.11 Estimated initial soil loss (tons/ac) 2.76

New Best Management Practice(s) to be Established	Est. New Soil Loss (tons/ac)	Soil Loss Payment for this	(pick one) √
Single New BMPs			
No-till	0.87	$588.30	
Conservation till	1.50	$392.98	
Contour farming	1.31	$452.70	
Terraces (+ Contour farming)	0.59	$673.90	
Contour grass strips	1.06	$529.33	
Riparian vegetative buffer strip (on contour)	1.04	$536.30	
Permanent grass	0.08	$834.85	
Other*:			
Combinations of New BMPs			
No-till + Contour farming	0.25	$781.88	
No-till + Terraces (+ Contour farming)	0.09	$830.50	
No-till + Contour grass strips	0.18	$801.03	
No-till + Riparian vegetative buffer	0.37	$744.00	
Conservation till + Contour farming	0.48	$708.30	
Conservation till + Terraces (+ Contour farming)	0.34	$752.45	
Conservation till + Contour grass strips	0.37	$744.85	
Conservation till + Riparian vegetative buffer	0.42	$728.55	
Contour grass strips + Riparian vegetatve buffer strip	0.37	$744.00	
Other*:			

New Ephemeral Gully BMP (alone or added to any BMP above, except Terraces)		√
Grassed waterways (to repair ephemeral gullies)*	*field assessment*	

*Soil loss reductions & payments for other BMPs or combinations of BMPs must be approved by the project team.

Field Legal Description: _____

Land Operator/Manager: _____

Address and Telephone Number: _____

_____

Total Payment = $ _____ (½ paid the first year, other ½ paid the second year)

I agree to implement this practice(s) and maintain it (them) for 5 years:

Land Manager/Operator: _____ Date: _____

Conservation District Personnel: _____

Appendix B - Error matrix table and statistics

Error Matrix		Actual		Totals
		present	absent	
Predicted	present	a	b	a+b
	absent	c	d	c+d
Totals		a+c	b+d	**N**

Measure	*Calculation*
Prevalence	(a + c)/N
Overall diagnostic power	(b + d)/N
Correct classification rate	(a + d)/N
Sensitivity	a/(a + c)
Specificity	d/(b + d)
False positive rate	b/(b + d)
False negative rate	c/(a + c)
Positive predictive power (PPP)	a/(a + b)
Negative predictive power (NPP)	d/(c + d)
Misclassification rate	(b + c)/N
Odds-ratio	(ad)/(cb)
Kappa	[(a + d) − (((a + c)(a + b) + (b + d)(c + d))/N)]/[N − (((a + c)(a + b) + (b + d)(c + d))/N)]

Appendix C - Granted permission to reprint Transactions of ASABE journal article

American Society of
Agricultural and Biological Engineers

1/22/2012

Prasad Daggupati

Graduate Research Assistant

Watershed Modeling Laboratory

Department of Biological & Agricultural Engineering

Kansas State University

Manhattan, KS

Dear Prasad,

We are pleased to grant permission for you to use the following document in your dissertation. We understand that it will be made available online through the K-State Research Exchange and via UMI/ProQuest Information and Learning, and that copies of the dissertation will be available for purchase. *Transactions of ASABE*, Field-Level Targeting Using SWAT: Mapping Output from HRUs to Fields and Assessing Limitations of GIS Input Data, Vol. 54(2): 501-514.

Regards,

Donna M Hull

Director Publications

American Society of Agricultural Engineers

2950 Niles Rd.

St. Joseph, MI 49085

269-428-6326